THE SOFT/HARD WET ANODIZATION

OF ALUMINUM OXIDE AND

ITS USE IN A THIN FILM

MULTILAYERED CAPACITOR

John Reed Dickey

Certificate of Approval:

Richard C. Jaeger
Alumni Professor
Electrical Engineering

Jim L. Davidson, Chairman
Associate Professor
Electrical Engineering

Yonhua Tzeng
Assistant Professor
Electrical Engineering

Leo L. Grigsby
Georgia Power Distinguished
Professor
Electrical Engineering

Norman J. Doorenbos
Associate Vice President for
Academic Affairs/Dean

REPORT DOCUMENTATION PAGE		READ INSTRUCTIONS BEFORE COMPLETING FORM
1. REPORT NUMBER AFIT/CI/NR 87-90T	2. GOVT ACCESSION NO.	3. RECIPIENT'S CATALOG NUMBER
4. TITLE *(and Subtitle)* The Soft/Hard Wet Anodization of Aluminum Oxide And Its Use In A Thin Film Multilayered Capacitor		5. TYPE OF REPORT & PERIOD COVERED THESIS/DISSERTATION
		6. PERFORMING ORG. REPORT NUMBER
7. AUTHOR(s) John Reed Dickey		8. CONTRACT OR GRANT NUMBER(s)
9. PERFORMING ORGANIZATION NAME AND ADDRESS AFIT STUDENT AT: Auburn University		10. PROGRAM ELEMENT, PROJECT, TASK AREA & WORK UNIT NUMBERS
11. CONTROLLING OFFICE NAME AND ADDRESS AFIT/NR WPAFB OH 45433-6583		12. REPORT DATE 1986
		13. NUMBER OF PAGES 136
14. MONITORING AGENCY NAME & ADDRESS(*If different from Controlling Office*)		15. SECURITY CLASS. *(of this report)* UNCLASSIFIED
		15a. DECLASSIFICATION. DOWNGRADING SCHEDULE

16. DISTRIBUTION STATEMENT *(of this Report)*

APPROVED FOR PUBLIC RELEASE; DISTRIBUTION UNLIMITED

17. DISTRIBUTION STATEMENT *(of the abstract entered in Block 20, if different from Report)*

18. SUPPLEMENTARY NOTES
APPROVED FOR PUBLIC RELEASE: IAW AFR 190-1
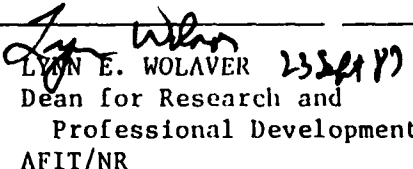
LYNN E. WOLAVER 23 SEP 87
Dean for Research and
Professional Development
AFIT/NR

19. KEY WORDS *(Continue on reverse side if necessary and identify by block number)*

20. ABSTRACT *(Continue on reverse side if necessary and identify by block number)*
ATTACHED

DD ₁ FORM ₇₃ 1473   EDITION OF 1 NOV 65 IS OBSOLETE

THESIS ABSTRACT

THE SOFT/HARD WET ANODIZATION

OF ALUMINUM OXIDE AND

ITS USE IN A THIN FILM

MULTILAYERED CAPACITOR

John Reed Dickey

Master of Science, March 19, 1987

(B.S.E.E., Auburn University, 1986)

(B.S., Southern Oregon State College, 1983)

(B.A. Southern Oregon State College, 1983)

151 pages

Directed by Jim L. Davidson

Literature has identified and characterized the existence of

barrier and porous alumina formed by the electrolytic anodiza-

tion of aluminum. Barrier films are limited in thickness by the

v

THE SOFT/HARD WET ANODIZATION

OF ALUMINUM OXIDE AND

ITS USE IN A THIN FILM

MULTILAYERED CAPACITOR

John Reed Dickey

A Thesis

Submitted to

the Graduate Faculty of

Auburn University

in Partial Fulfillment of the

Requirements for the

Degree of

Master of Science

Auburn, Alabama

March 19, 1986

THE SOFT/HARD WET ANODIZATION

OF ALUMINUM OXIDE AND

ITS USE IN A THIN FILM

MULTILAYERED CAPACITOR

John Reed Dickey

_____
Signature of Author

_____2 FEB 87_____
Date

Copy sent to:

Name   Date

VITA

John Reed Dickey, son of Otis M. Dickey and Faye Garten Dickey, was born on July 20, 1952 in Denver, Colorado. He attended Southfield High School and graduated in June, 1970. He earned a Bachelor of Science in Math/Chemistry Interdisciplinary Studies and a Bachelor of Arts in Humanities concurrently from Southern Oregon State College in Ashland, Oregon in June, 1983. He also earned a Bachelor of Science in Electrical Engineering in March, 1986 from Auburn University in Auburn, Alabama. John was admitted to the graduate school at Auburn University in March, 1986 to work toward a Master of Science degree in Electrical Engineering.

formation voltage, found to be typically 12 to 15 Å/volt. Porous layers may be formed thicker without such limitation.

In this work, anodization was performed on vacuum or sputter deposited aluminum films typical of those used for interconnect metal for integrated circuits. Substrates were thermally oxidized silicon wafers. The anodization consisted of a two step operation. A layer of soft anodized aluminum was first formed using sulfuric acid electrolyte. This anodized layer was then subjected to a boric acid hard anodization. Single level and multilevel capacitor structures were formed and dielectric evaluation performed. Effective dielectric contants of up to approximately 70 ,volume resistivities of up to 1.2×10^{18} ohm-cm and breakdown voltages up to 2.38 times that of the hard anodization forming voltage were observed. Cleaved SEM cross sections were examined and indicated a dense amorphous alumina layer was formed. This is in agreement with reported observations that amorphous alumina has better dielectric properties than crystalline layers.

TABLE OF CONTENTS

LIST OF TABLES

LIST OF FIGURES

I. INTRODUCTION

The study of thin film oxides has increased greatly in the last ten years because of their wide and diversified applications in the fabrication of microelectronic devices. The performance of these devices is highly dependent on the quality of the insulating films used in them. This thesis will deal with the dielectric properties of a novel type of aluminum oxide and will examine its potential for use in a multilayered capacitor with a high density energy storage capability.

While dielectric properties of barrier anodic thin films of aluminum oxide have been investigated by several groups of researchers, most studies have centered on films under 1000Å thick. A few isolated tests have been performed on films up to one micron, but generally, the focus of attention has been on how these films behave in a microelectronic environment at voltages not exceeding 15-20 volts.

Storage of electrical energy in thin, solid dielectrics has,

to this point, received much less investigation. Most of these studies have centered around conventional electrolytic or ceramic capacitors. Aluminum oxide has an excellent thermal conductivity which is the primary concern for high frequency pulse-discharge devices.[1] It is also light weight and inexpensive to fabricate. Though the dielectric properties of both the 'soft' and the 'hard' oxides have been well documented, little has been written on what will be referred to as 'soft/hard' anodization. In order to properly present the advantages and disadvantages of this two step process, it is necessary to give some background on each of the two former one step processes and their dielectric properties.

Conventional Wet Anodization of Aluminum

Porous or 'soft' oxides have been used for protective coatings in the metal industry since 1923 and the barrier type or 'hard' aluminum oxide has been used for electrolytic capacitors since the early 1900's.[2] Wet anodization is the well known process of electrolytic (electric field induced) oxidation of a metal. When aluminum is made the positive electrode (anode),

and is placed in an electrolyte (current conducting medium) with a cathode, a current will pass through the cell. As the current is passed through the cell, the aluminum is converted to aluminum oxide (Al_2O_3) layer by layer. Since the oxide grows atomistically, its adherence to the bulk metal or substrate is excellent.[3,4] The wet anodization technique for dielectric film growth is superior to other techniques (i.e. plasma anodization or reactive sputtering) because precise control of the thickness of the film can be achieved and because there are fewer defects owing to the self-healing nature of the process.[5]

In a normal, dry oxygen ambient, aluminum will quite quickly acquire a 10Å - 50Å thick layer of native oxide. Two different types of oxide (nine different phases) can be formed by anodization depending on the type of electrolyte, the current density, and the bias conditions used during the anodization.

A non-porous hard oxide will be formed initially in either the hard or soft anodization. Under the influence of the applied potential, oxygen and hydroxide ions which both have a negative ionic charge are driven toward the anode. These anions penetrate the existing oxide layer and combine with positively

charged aluminum ions from the metal substrate to form an oxide/hydrate coating at the metal/oxide interface.[6] If the electric field is strong enough and the electrolyte can dissolve the metal, aluminum ions will be torn away from the oxide layer. In the H_2SO_4 electrolyte, this produces an aluminum salt solution, aluminum sulfate.[7,8]

When the electrolyte is weak, the oxide film being formed is inhomogeneous in composition; the oxide layer contacting the electrolyte contains a surplus of oxygen while the one next to the metal has a surplus of aluminum. These two layers are interspaced by a region with a more stoichiometric composition. The dimensions of the oxygen ions exceed by a factor of 2.6 those of the aluminum ions (1.3Å and 0.5Å respectively). For this reason, the aluminum ions diffuse much easier through the oxide layer than the oxygen ions and the region of more stoichiometric composition is displaced closer to the surface of the electrolyte.[9]

An aluminum oxide with a surplus of oxygen is a p-semiconductor and with a deficiency of oxygen, an n-semiconductor. Therefore a p-n junction with an intermediate layer of a dielec-

tric is formed in the oxide film obtained.[9] Figure 1 illustrates this point.
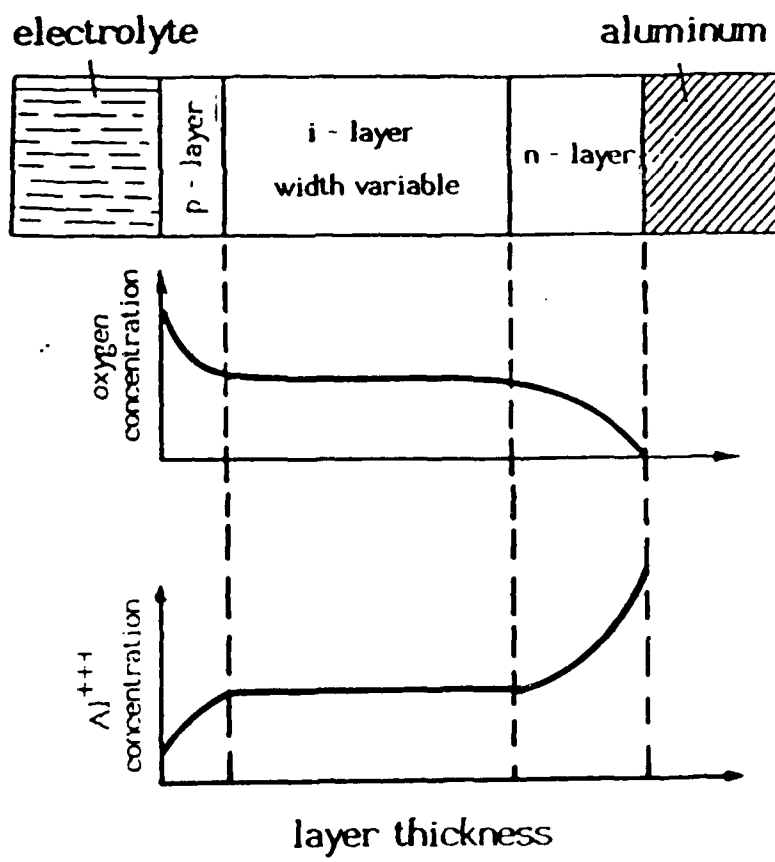
Figure 1 Qualitative structural diagram of wet anodized aluminum oxide. I - layer is of variable width but is closer to electrolyte/ oxide interface.

Porous Aluminum Oxide

Sulfuric and chromic acids are the two most common electrolytes for soft oxide growth. The use of sulfuric acid as an electrolyte was patented in 1927 in England by Gower and O'Brian. Chromic acid does not promote corrosion of aluminum so unintentional trapping of the solution in pores, cracks, or crevices is not a problem; however, only three microns of growth can be achieved with its use. Chromic acid also costs more than sulfuric acid and presents pollution and waste problems. Therefore, sulfuric is the preferred electrolyte.[10]

In solution, the H_2SO_4 dissociates to form SO_4^{--} ions. These ions drift toward the anode under the influence of the applied potential. At the oxide/electrolyte interface, two oxygen atoms may be pulled from the negative ion and the remaining SO_2^{++} can combine with two nearby H_2O molecules to reform H_2SO_4. The two displaced protons will find their way to the cathode via the proton switching mechanism and the two oxygen atoms can combine with Al^{+++} ions to form Al_2O_3.

Some water is needed for the proton switching mechanism but too much water will tend to increase the number of Al^{+++}

ions that pass through the oxide and into the solution. In sulfuric solution, much of the water is tied up in acid hydrate as opposed to being 'free' water. The addition of glycol to electrolytes is a good method to reduce the amount of free water and is often used. However, this will tend to lower the pH of the bath which also lowers the current density during the anodization. The desired pH level can be raised by titration with a base such as NH_4OH.

After the initial hard oxide layer has formed, the growth proceeds as an advancing front with most of the new soft oxide forming at the hard oxide/soft oxide interface.[6] The porous structure appears as densely packed, hexagonal columns with each column containing a tiny central pore. See Figure Two. Billions of pores are formed in each square inch of aluminum oxide. See Table One. The pores allow anodizing electrolyte to be carried to the advancing barrier front where the new growth is occurring. The oxide will continue to thicken until equilibrium between new oxide growth and dissolution of the existing oxide is established.[6] Thicknesses of up to 500 microns have been obtained in soft anodization.
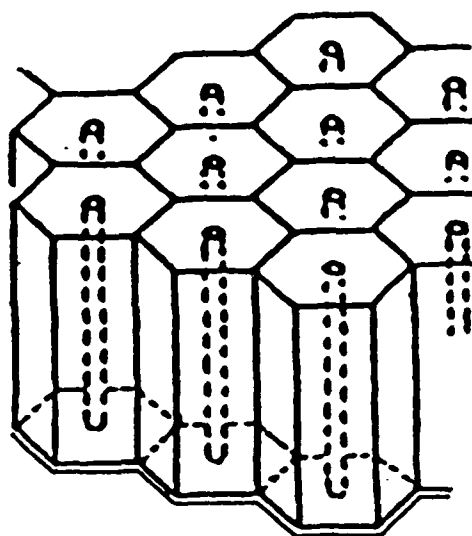
Figure 2   Structural diagram of porous
aluminum oxide. Pores provide the electrolyte
with access to the region of primary growth --
the thin, initial barrier layer at the oxide/al-
uminum interface.[3]

The porous nature of soft oxide detracts from the ideal
dielectric since it allows contaminants and moisture to pene-
trate. The pores can be sealed by boiling the oxide for 15 to 25
minutes. During the sealing process, the oxide lining of the
pores is converted from amorphous oxide to a monohydrate
(boemite and/or bayerite) which results in an increase in
volume and the pores close to seal the surface.[11]

Electrolyte	Voltage	Pores/in² (x 10⁹)
H_2SO_4	15	498
	20	334
	30	179
CrO_3	20	140
	40	52
	60	27

Table 1 Number of pores in soft or porous Al_2O_3 film. [3]

Polymer sealing has been used in thin film aluminum passivation instead of 'vapor' sealing to reduc; the dielectric constant and increase the electrical resistance to current flow. Vapor sealing creates water of crystallization which lowers resistance and raises the dielectric constant of the layer.[12]

Generally, soft alumina has not been utilized to a large extent as a dielectric but has seen a great deal of service in corrosion protection.

The anodization set-up is illustrated in Figure Three while the typical voltage characteristic is given in Figure Four; the current density is constant.

Platinum, wire-mesh cathode

Aluminum coated wafer as anode

cathode

anode
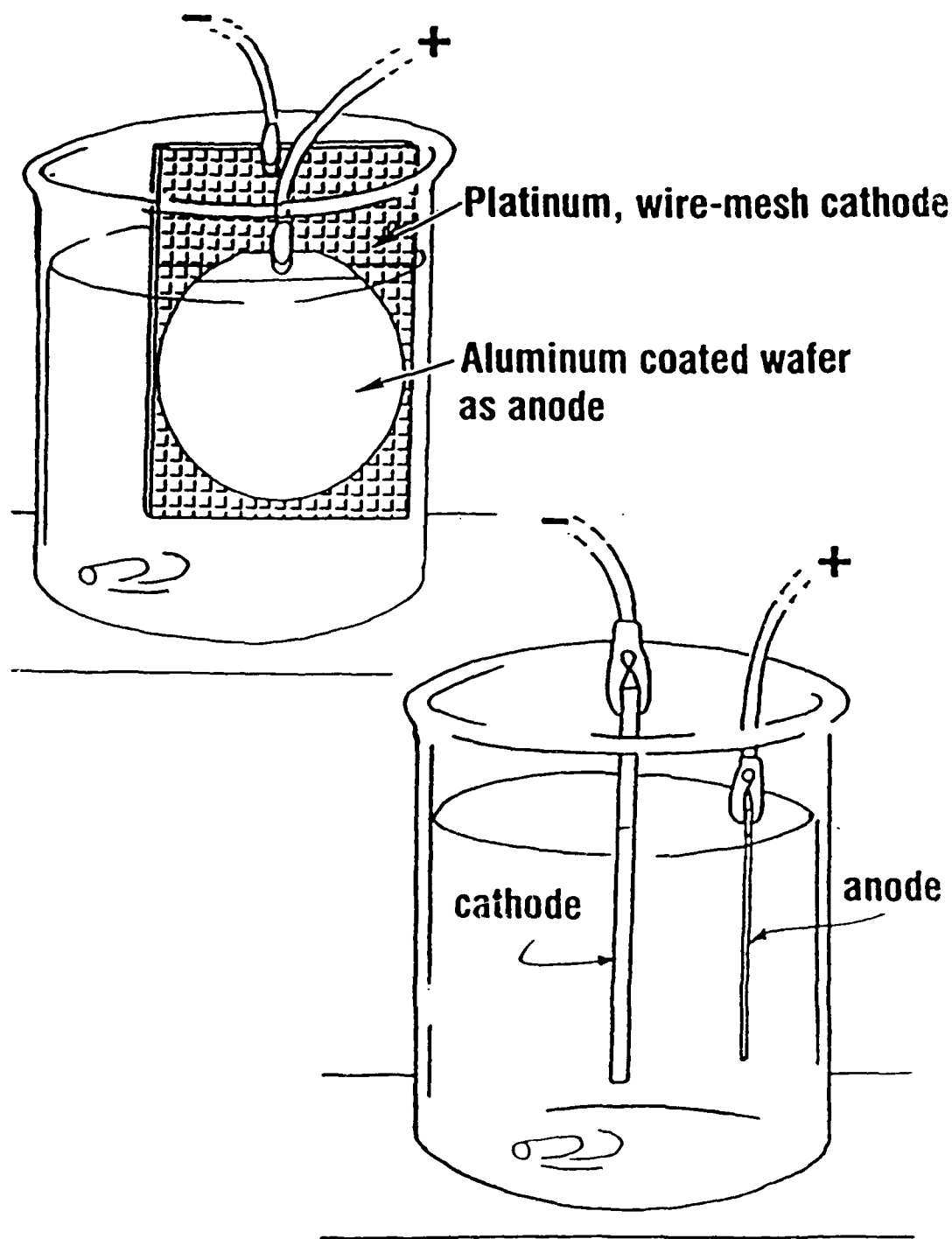
Figure 3 Wet anodization set-up showing front and side views.
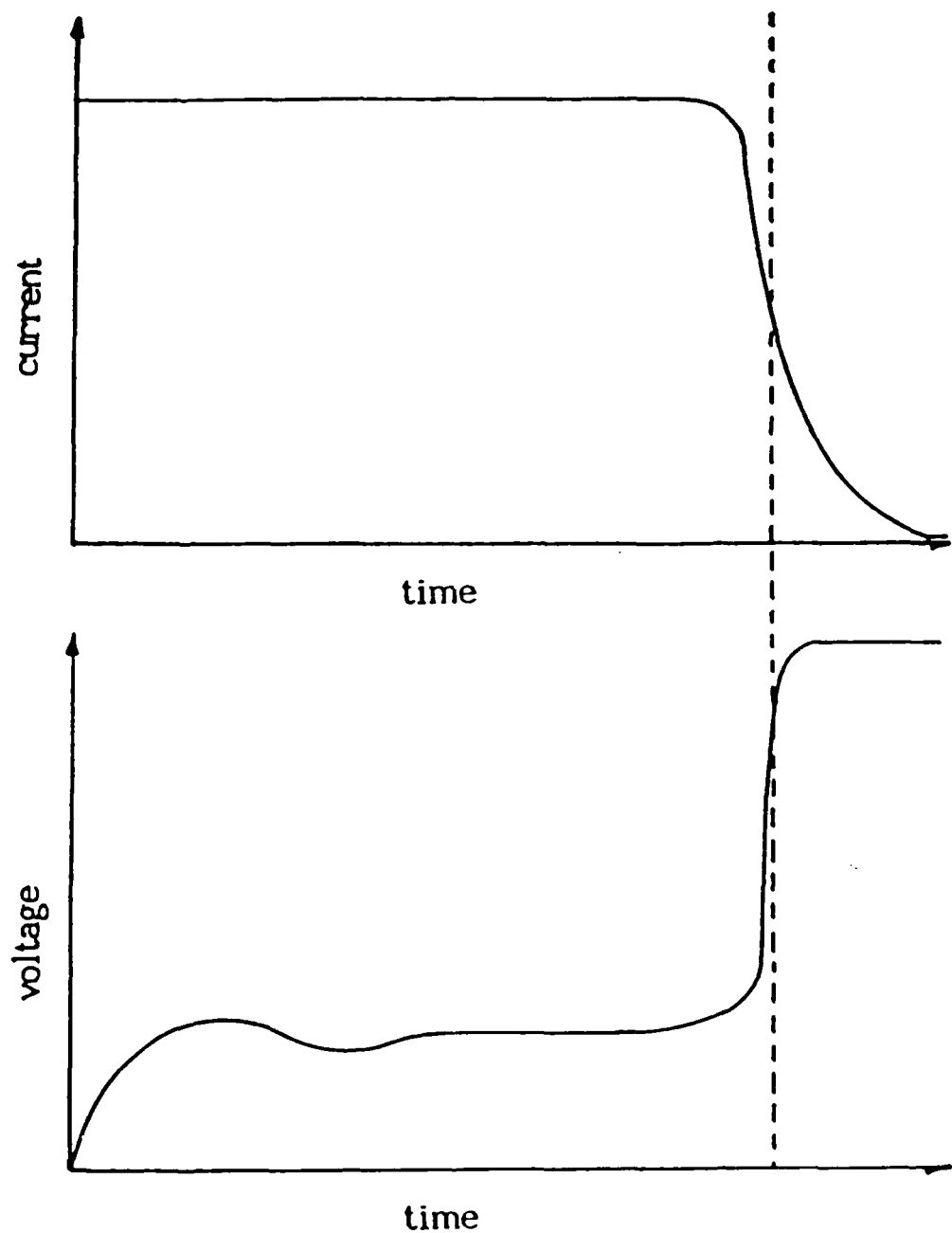
Figure 4 Typical current and voltage charac-
teristics for a soft or porous anodization
cycle. Dotted line shows the point at which
nearly all of the film of aluminum has been
anodized.

Barrier Oxide Anodization

Barrier or hard anodization has been the focus of a great deal of research. Although it has dielectric properties that are generally better than those of the soft oxide, its growth is limited and purely hard oxides are generally not produced thicker than 6000Å. The oxide's dielectric properties tend to degrade with increasing thickness when processed with the conventional wet anodization method. Since there are at least nine different phases of aluminum oxide, not counting hydrates, listed in the ASTM powder diffraction file, it is not unreasonable to expect different phases to occur when different deposition techniques are used.[13]

Except for the change of electrolyte, the anodization set-up is the same as for the soft anodization. Conventionally, the process proceeds as follows:

1. The current density is maintained at a set value (e.g. 1mA cm^{-2}) by means of a variable series resistance with the desired anodization voltage set on the power supply.

2. Initially, the anodization is carried out at a constant current density by reducing the series resistance from

maximum to zero.

3. The process is then allowed to continue at constant voltage until the anodization current density decreases to an ultimate minimum limit (e.g. $1 \mu A \ cm^{-2}$) at which point the anodization is terminated.

4. The oxide film is washed thoroughly with DI water and baked in air with time and temperature varying considerably among researchers.

The total amount of time in the bath varies from only a few minutes to several hours. Figure Five shows typical anodizing cycles for different anodization voltages.

Although many weak electrolytes have been utilized in the hard anodization process, boric acid and tartaric acid have been used most extensively. As Table Two shows, boric acid solutions have been found to be better overall than tartaric acid.

It has been shown that when glycol is used with boric acid, the current efficiency is unity, i.e., that all the charge passed is used for oxide formation.[14,15]

Polycrystalline alumina has poorer dielectric properties than the amorphous film. Forming at current densities below
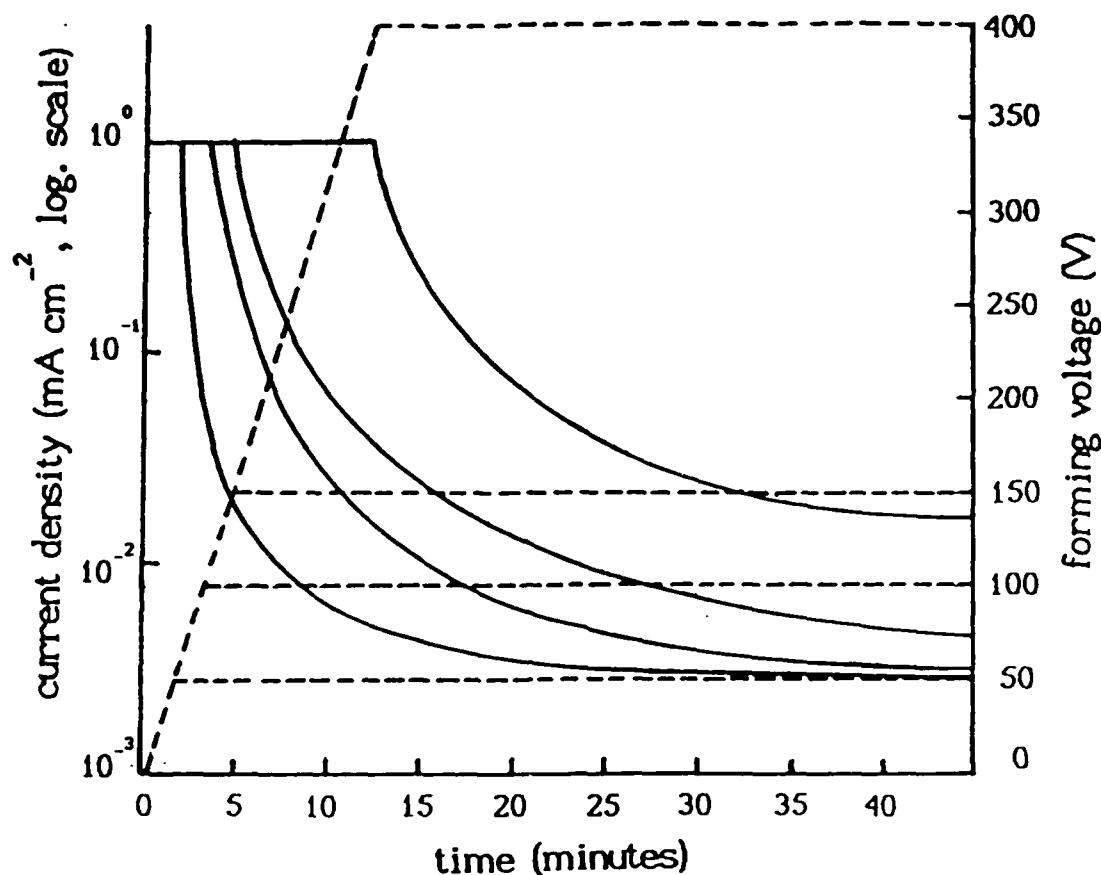
Figure 5 Current and voltage characteristics for several conventional anodization cycles producing hard or barrier aluminum oxide. [5]

0.25mA cm^{-2} promotes crystalline oxide growth. The crystalline oxides grown at high current densities are of the $\gamma\text{-Al}_2\text{O}_3$ phase and those grown at lower current densities are of the $\gamma'\text{-Al}_2\text{O}_3$ phase.[16] However, as will be shown, the rate of change of the current density is more important to the crystalline formation than the level of the current density.

Anodizing voltage (V)	Capacitance density at 100 kHz (pF/mm²)	Loss tangent at 100 kHz (x .001)	Breakdown voltage (V)	Leakage current density at 5V (A/cm²)
Boric acid electrolyte				
50	920	15.7	40	3.5×10^{11}
100	500	15.2	82	2.0×10^{11}
150	320	14.5	120	1.4×10^{11}
400	114	9.25	315	0.5×10^{11}
Tartaric acid electrolyte				
50	902	18.4	33	4.8×10^{11}
100	493	16.8	60	3.2×10^{11}
150	309	15.3	75	2.1×10^{11}
400	104	14.1	190	1.0×10^{11}

Table 2 Properties of aluminum oxide films grown in boric acid and tartaric acid electrolytes under similar environmental conditions.[5]

The films grown in a bath with a higher anion concentration contain more electrolyte byproducts and exhibit better dielectric properties. This suggests that the presence of electrolyte byproducts in barrier anodic films can be beneficial with regard to their performance as dielectrics because the byproducts tend to retard the formation of partially polycrystalline Al_2O_3.[17]

It has also been shown that wet anodizations taking place in colder temperature electrolytes produce superior dielectric films. The low loss in an oxide layer formed by low temperature anodization can be explained as follows. As is well known, non-porous Al_2O_3 films are obtained by aluminum anodization only over a limited pH range. At low temperature, the reduction in number of ions in the electrolyte makes the pH value favorable for such a process. This is even more effective because Al_2O_3 formation is an exothermic reaction which should be favored at low temperatures. For these reasons, films formed by low temperature anodization should have low porosity as well as a low dielectric loss. Research done with halide ions has shown that these ions inhibit the growth of the oxide in the following decreasing order: chloride > bromide > iodide > fluoride.[18]

Physical Properties of Hard Alumina

It must be noted that both the physical and dielectric properties reported in the literature vary substantially, therefore, care should be taken to observe the differences in experimental methods and conditions. It should also be noted that in regards

to the reported rates of growth of the oxide, most estimates of actual oxide thickness are based upon previously reported growth rates as opposed to measurement.

Researchers who have actually measured oxide thickness have reported growth limits based upon the forming voltage of between 12.0 Å/V to 15.0 Å/V depending primarily upon the choice of electrolyte and the temperature.

From the anodization cycles, it is evident that the film acquires its maximum resistance during the first few minutes of the constant-current mode, indicating that most of the thickness of the film is accumulated during this short period and that during the period of the constant-voltage mode the density of the oxide film is increased as the holes and depressions in the film are filled in.[5]

Once a certain phase of the oxide has formed, it is not necessarily a permanent condition. On the contrary, research has shown that many different transformations can take place in which one phase is actually converted to another phase or phases. If the aluminum substrate has any hillocks or other

topological pr~rusions, islands of polycrystalline alumina can form as Figure Six below illustrates.

region of excess
oxygen   void

$\gamma' - Al_2O_3$

region of excess
Al^{+++} Al substate
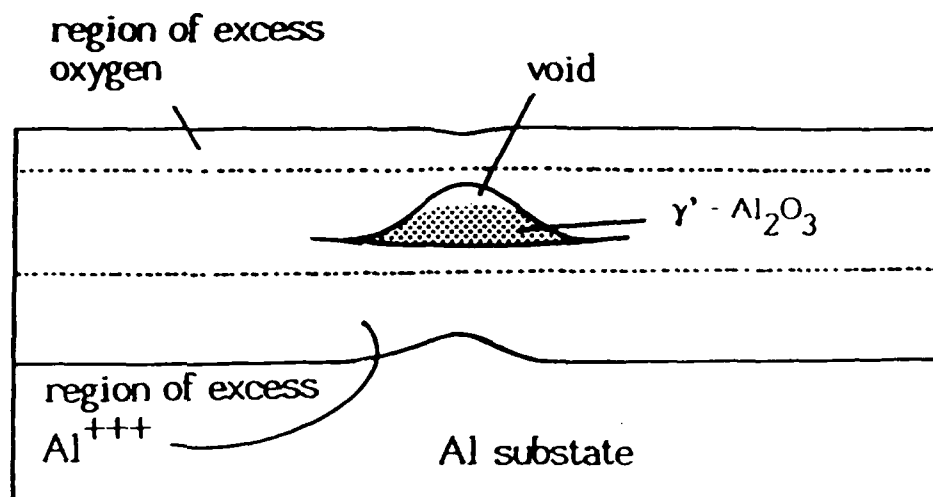
Figure 6   Schematic of a cross section of an alumina film.   The polycrystalline island forms first in the region of fewest excess ions and spreads laterally. [19]

From the shape and location of the crystalline γ'-alumina islands, it is evident that the islands nucleate near the middle of the carrier oxide layer and develop relatively rapidly in the lateral direction during the growth of the hard oxide layer. [19]

This is possibly due to the location of the most stoichiometric Al_2O_3 and would support the previously stated hypothesis that anodization by-products as well as excess ions tend to suppress the formation of polycrystalline Al_2O_3.

Bernard and Russel[20] have shown that cracks and voids in the hard oxide can contain O_2 which acts as a dielectric but can cause instability of the dielectric properties of the film as a whole.

Chen and Hutchins[14] have shown that the number of crystalline growth sites and hence the extent of crystallinity varies with the crystallographic orientation of the aluminum substrate as well as with the current density. Their reported data suggests that the crystalline anodic oxide grows by transformation rather than by direct deposition. Hard oxide that was grown on (100) oriented grains of the aluminum substrate was thicker and less crystalline than oxide grown on other surface orientations. The rate of growth of the crystalline sites increases markedly with anodization temperature.

Diffraction patterns of these islands correspond to the γ'-Al_2O_3 structure which is a less ordered form of γ-Al_2O_3[14]. Each crystalline area is surrounded by a transition layer approximately 50nm wide which varies according the formation voltage. These transition layers represent intermediate stages between the amorphous and fully crystalline oxide and indicate

that the amorphous to crystalline transformation may be a fairly complex multistage process.[14] Alwitt[21,22] has shown that amorphous thermal oxide formed during a heat treatment prior to the anodization results in highly crystalline anodic oxide films and postulated that the thermal oxide transforms more readily because it is more ordered. Post anodic heat treatments at 800°C of amorphous oxide also shows a transformation to the $\gamma'-Al_2O_3$ phase.[16]

Hard oxide films that are subjected to a prolonged anodization (e.g. 1000 min or more) at the formation potential thicken into a porous structure similar to that of porous films formed in aggressive electrolytes. Pore colonies are observed to form at both the oxide/electrolyte and oxide/metal interfaces.[23]

Dielectric Properties of Hard Oxide

In addition to the parameters of the wet anodization process there are other factors which influence the dielectric behaviour of hard (and soft) anodic alumina. The purity of the aluminum, the post-anodization bake, and the ambient humidity all affect how the oxide behaves electrically.

Merrill and West demonstrated that the purity of the

aluminum substrate had a dramatic impact on the dielectric strength of the oxide with an increase from 6KV/mil with a foil purity of 99.99 to nearly 9KV/mil with a foil purity of 99.999.[24]

Gubanski and Krowinski[25] noted that conduction in the hard films is unstable with time, independent of the electrolyte used. The instability is eliminated by a prolonged post anodization heat treatment and is possibly due to further film formation and adsorbed water expulsion.

Odynets et al. reported that humidity in the air gave rise to a large spread in their results though it should be noted that their samples were anodized in an aqueous electrolyte.[26]

Generally, the capacitance density decreases with increasing frequency but the change is small. Figure Seven is from data obtained by Ahmad and Singh[5] and shows this dependency.

Capacitance density also varies according to the formation voltage is illustrated in Figure Eight. Notice that the relationship is not linear as would be expected.

Figure Nine shows the time^{-n} dependence of capacitance
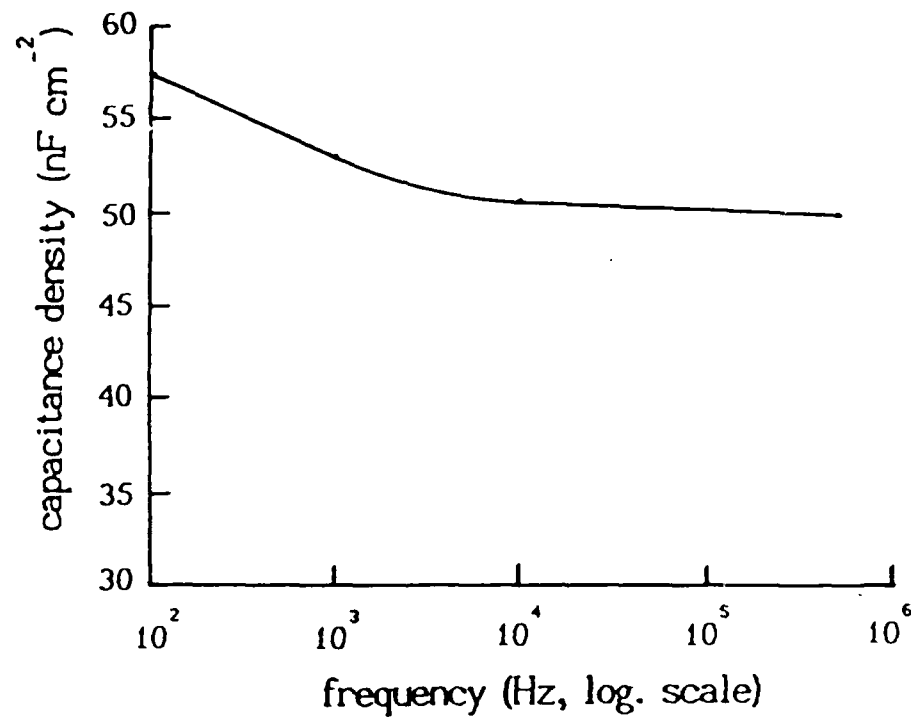
Figure 7 Typical frequency response of C_d for an hard oxide film. V_f was 100V. [5]
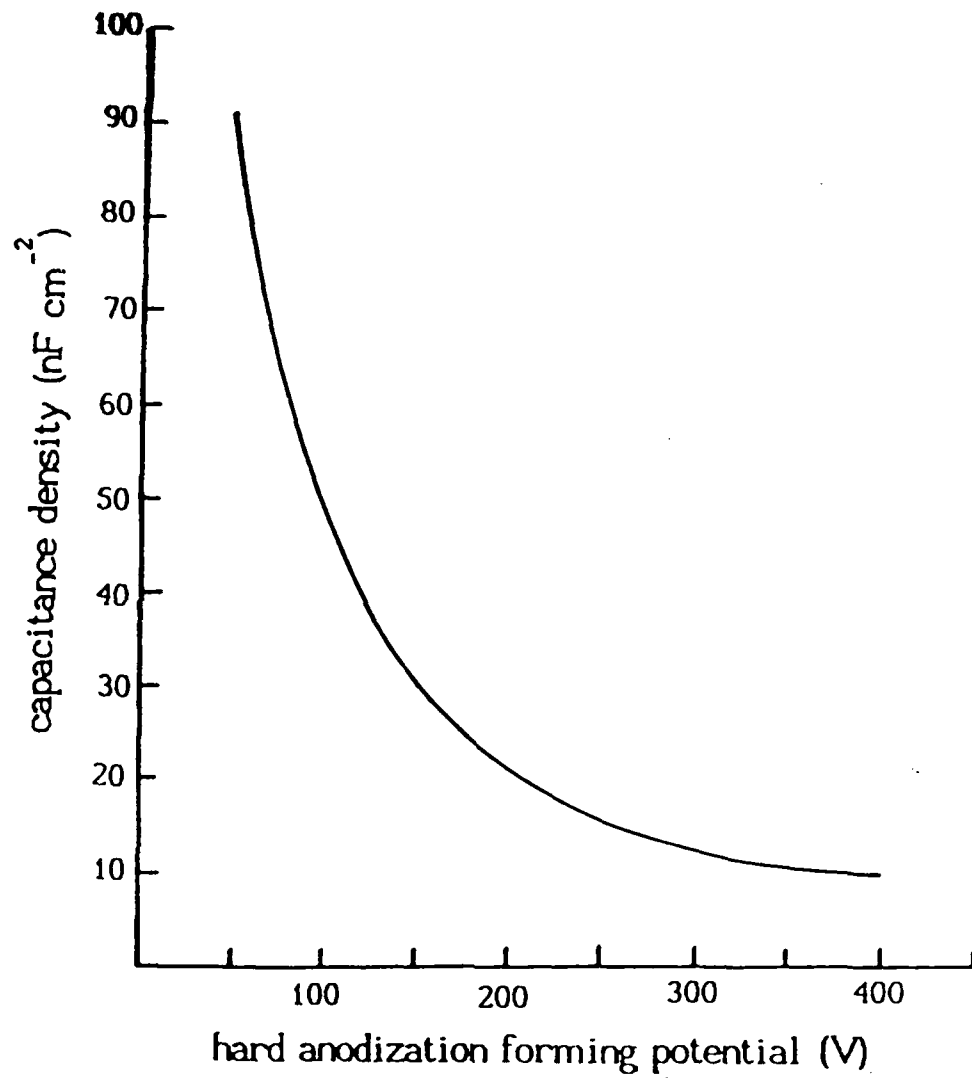
Figure 8 Typical variation of the capacitance density with the anodization's forming voltage measured at 100kHz. [5]

which Birey[27] found was due to an increase in thickness rather than a change in the dielectric constant.
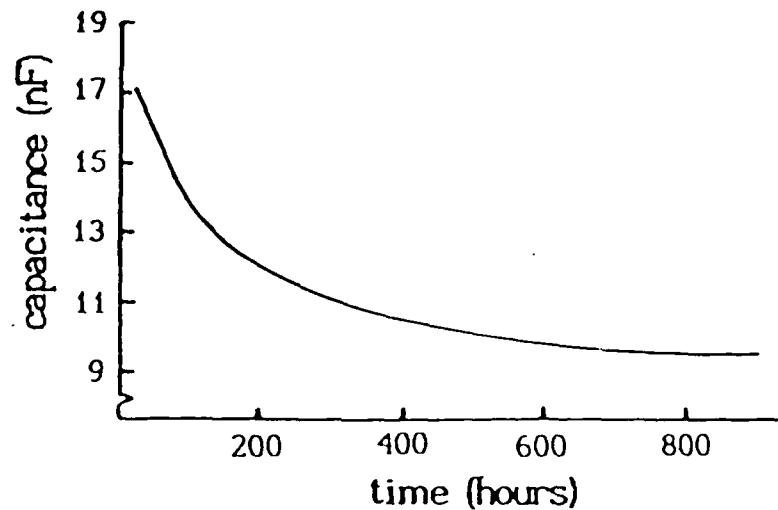
Figure 9   Typical capacitance variation with aging time for a thin, hard oxide film 115Å thick. [27]

The relative permittivity of a conventionally formed hard oxide is between 3.5 and 4.0 for ultrathin films[28] and increases asymptotically toward its bulk value with increasing thickness. Figure Ten below gives an example of this. The bulk value of ϵ_r has been reported to be as low as 7.0 and as high as 15.0 but is generally thought to be between 8.0 and 10.0.
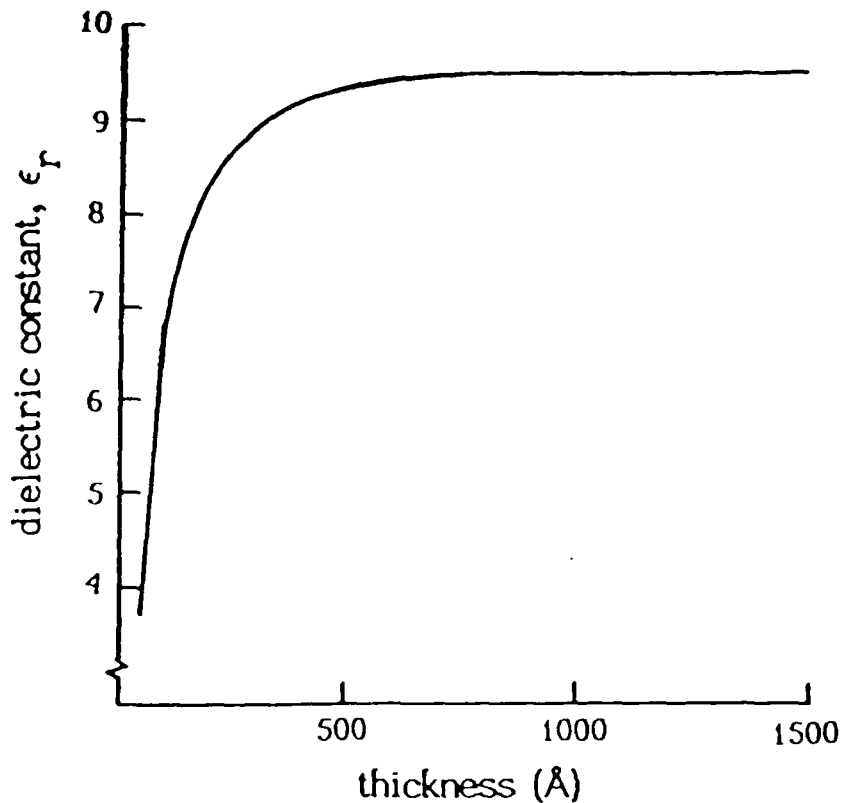
Figure 10 Typical variation of the dielectric constant for barrier Al_2O_3 with oxide thickness. [28]

The observed decrease in ϵ_r for very thin films is thought to arise from the increase in the density of voids. The frequency dependence of ϵ_r for different film thicknesses is shown in Figure 11. An increase in its value can be seen starting at a certain frequency which is inversely proportional to the thickness and becomes more appreciable towards lower thicknesses.
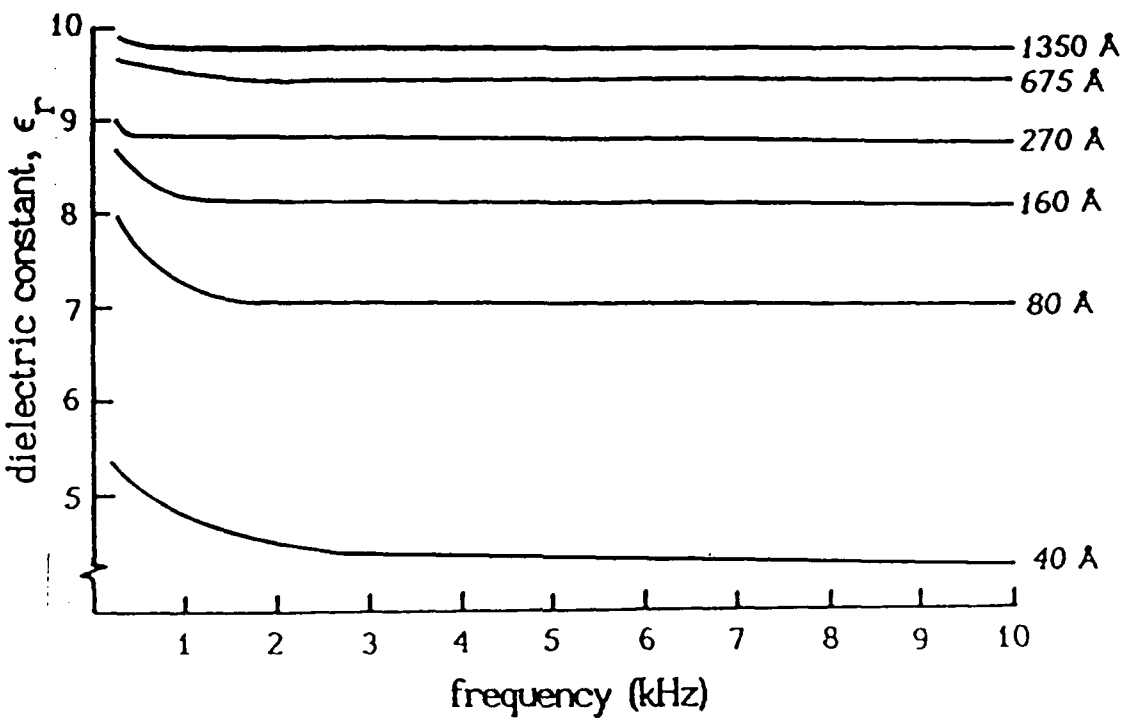
Figure 11   Variation of the dielectric constant
with frequency for several thin, hard oxide
films of Al_2O_3. [28]

Boeva et al. [29] reported that at audio frequencies the dielectric

constant increases sharply with temperature, but this depen-

dence is less pronounced at higher frequencies.

Figure 12 shows how the breakdown voltage varies with the

forming voltage in a conventional anodization.   These data points

can be thought of as points of destructive breakdown as opposed

to Figure 13 which illustrates the relative amount of non-

destructive clearings versus the forming voltage for a given number of tests.
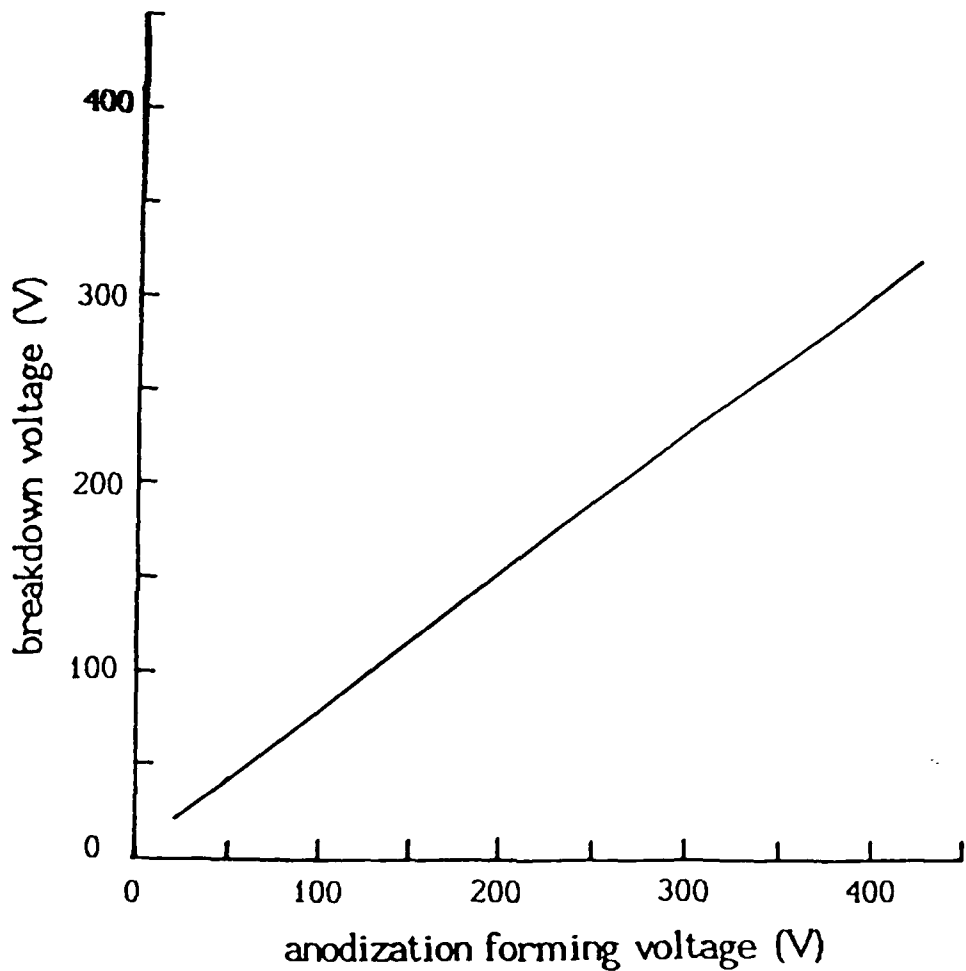
Figure 12   Typical destructive breakdown voltage versus forming potential characteristic. The test voltage dV/dt was 2V/sec. [5]

It has been proposed that the localized partial crystallization of amorphous material is a transformation which immediately precedes an electrical breakdown event in a barrier anodic
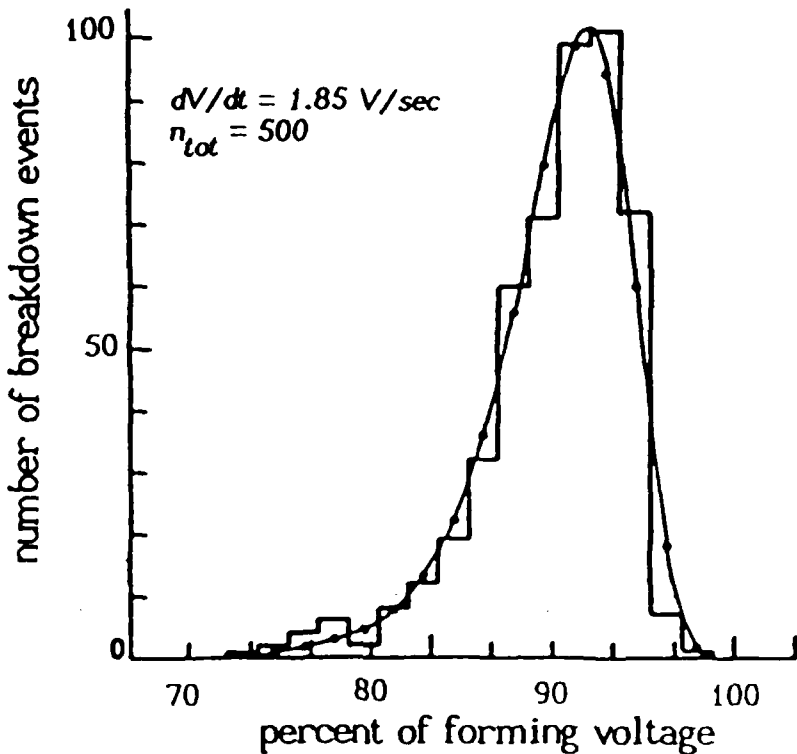
Figure 13 Typical breakdown voltage distribution of hard aluminum oxide. Five hundred tests were performed. [15]

film.[17] De Wit and Crevecoeur[15] found that if the polarity in a breakdown test is reversed, that the breakdown field is lower. They also noted that when the temperature is lowered to -196°C the breakdown field increases by approximately 20%.

When considering dc resistivity (or conductivity) it should be noted that the value obtained is dependent upon the applied field as well as the oxide thickness and this dependence is not linear. If the density of localized states is high, the dominant

process of carrier injection into the insulator is by direct tunneling into the localized states. If the insulator has very few localized states in the forbidden gap, charge carriers are predominantly injected over the contact barrier.[28] Figure 14 shows how the conductivity varies with the applied field for several thin films. Figure 15 shows how conductivity varies with oxide thickness.
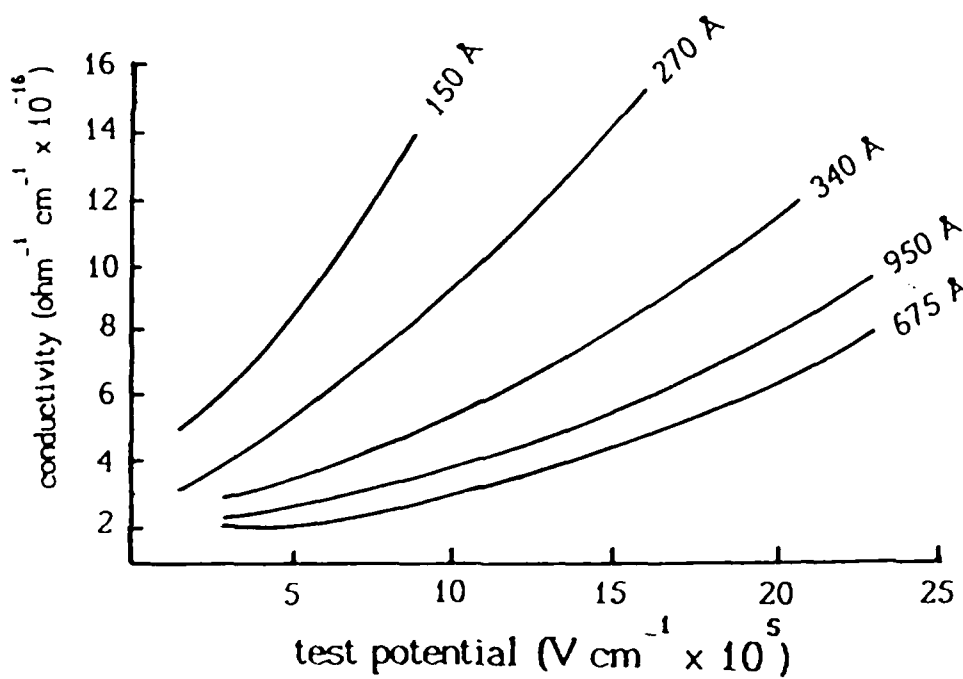
Figure 14 Typical field dependence of the d.c. conductivity for several thin oxide films of alumina. Notice that the conductivity is considerably greater as the test potential approaches the forming potential for each film $(V_f \simeq$ thickness$/15$ Å$/$V). [28]
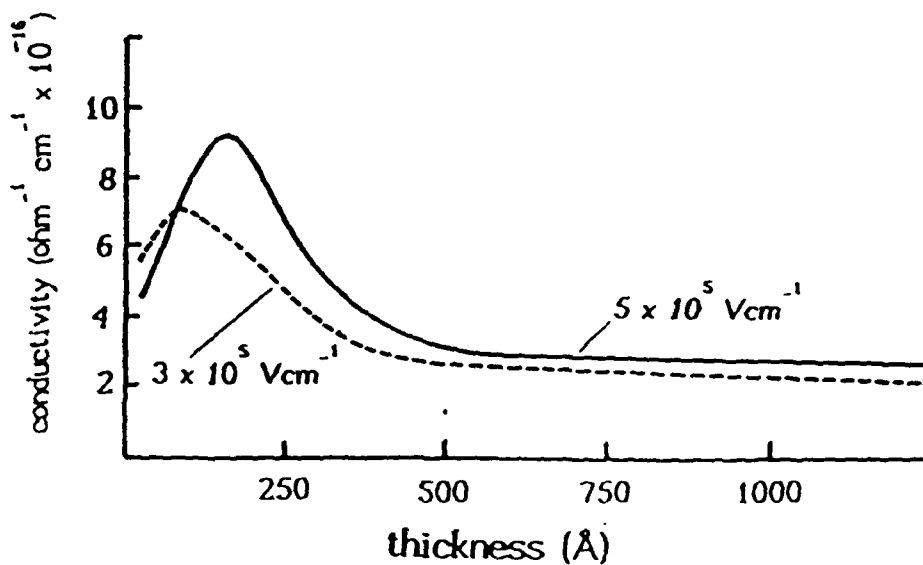
Figure 15   Typical variation of conductivity versus oxide thickness characteristics using two different testing fields. [28]

The dissipation factor (DF) is strongly dependent on the post baking of the Al_2O_3 [29] and is known to increase sharply with increasing temperature at 1kHz.   Figure 16 shows how the DF varies with the forming voltage, and Figure 17 shows its relationship to the applied signal frequency.   Since the thickness of the anodized hard oxide formed in the conventional manner has been shown to increase linearly with the forming voltage, Figure 16 also represents, qualitatively, the variation of the DF with thickness as well.
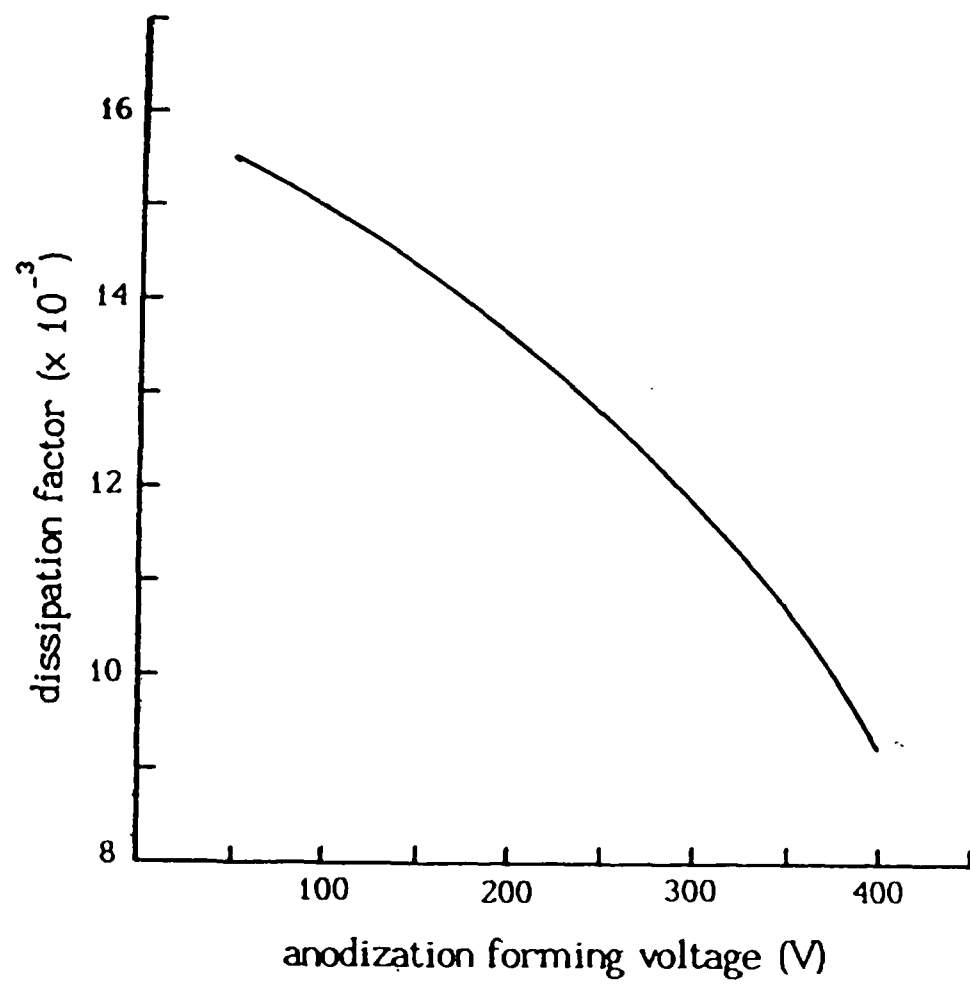
Figure 16 Typical variation of the dissipation factor versus forming potential characteristic tested at frequency of 100kHz[5].
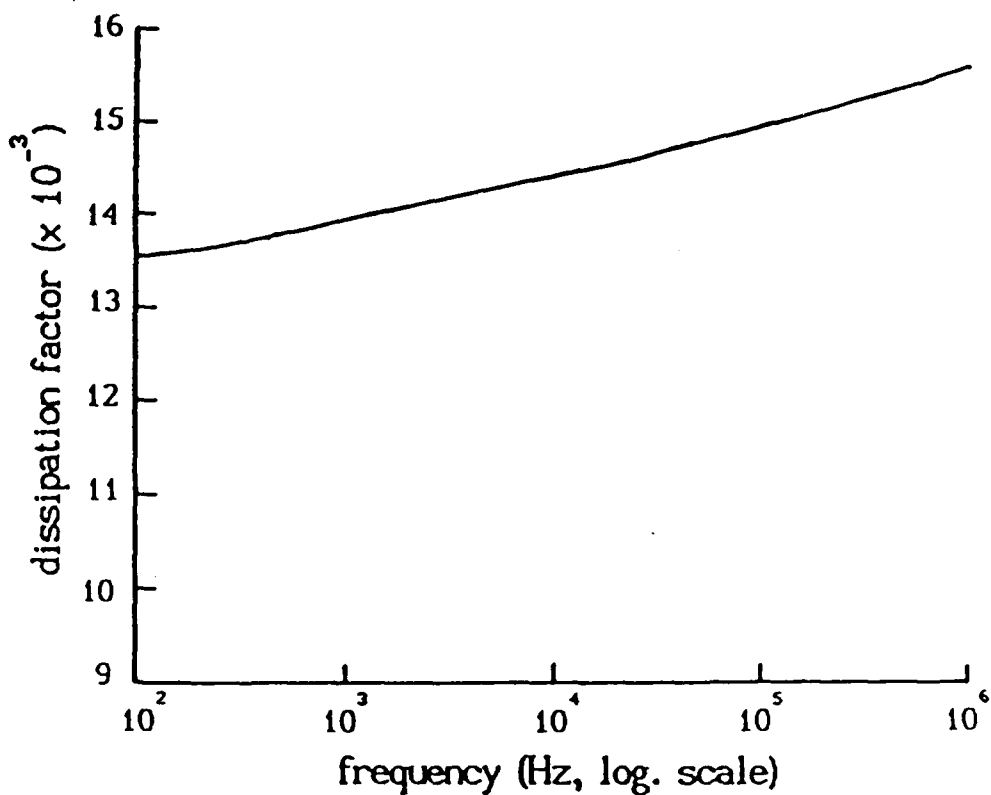
Figure 17 Variation of the dissipation factor
with frequency for a hard oxide film of
alumina anodized with a 100 V forming
voltage.[5]

The increasing value of the DF (or tan δ) with decreas-

ing thickness implies that a polarization mechanism with a

long relaxation time (interfacial polarization) becomes

more effective as the film thickness decreases. Also, the

dependence of the DF on the applied frequency shows that the

contribution of interfacial polarization increases with decreas-

ing frequency especially in thinner oxide films which have a greater density of voids or flaws.[28]

It is known that the contribution of polarization mechanisms with long relaxation times increases at lower frequencies. Furthermore, the interfacial polarization produced in distinct regions separated by voids and/or flaws is expected to contribute more as the film thickness decreases.[28]

II. SOFT/HARD ALUMINUM OXIDE

With the ultimate purpose in mind of storing a large amount of electrical energy (e.g. 10^6 joules) in a multilayered, thin film, solid dielectric capacitor, an unconventional (though not unprecedented) approach to alumina formation was examined. Alumina has a good thermal conductivity which is the primary concern for high frequency pulse-power devices.[1] It is also light weight and inexpensive to fabricate. Though the dielectric properties of both porous and barrier oxides of Al_2O_3 have been documented, little has been written on what shall be referred to as the soft/hard anodization. Merrill and West[24] examined a soft/hard oxide but their electrolytes were aqueous and their anodization procedure followed the conventional course as illustrated in Figure Five. Their soft anodization was carried out in oxalic acid as opposed to sulfuric and their results differ considerably from those observed herein.

In the soft/hard process, as the name implies, an alumi-

nized silicon wafer is first wet anodized to produce a layer of soft alumina and then anodized in a different electrolyte to produce a hard oxide. Presumably, several phases of the Al_2O_3 are present after such an anodization.

If this process could be utilized to create a film with a highly determinable growth pattern, good dielectric and thermal qualities, and low cost in product and man-hours, then it might be a good candidate of which to construct an high energy storage device.

In the following section, breakdown, resistivity, permittivity, capacitance, oxide growth, and humidity effects are discussed.

Procedure

The anodization set-up is the same as in Figure 3. Aluminized silicon wafers were first anodized in a sulfuric acid electrolyte at five to six degrees Centigrade. An ice bath was used to keep the temperature constant. This electrolyte was prepared by diluting the acid volumetrically 1:10 with deionized water. During this step, the current density was maintained at a constant $1.50 mA/cm^2$. This value was calculated by consid-

ering the area on the one side of the wafer facing the cathode and in the electrolyte as being active. In this way, the number of Coulombs used could be easily calculated.

In the second step, these same wafers were anodized in a boric acid solution. This was prepared by mixing powdered H_3BO_3 (3% by weight) with deionized water. In order to lessen the free water content of the electrolyte, the solution was diluted volumetrically 1:20 with ethylene glycol. The pH was adjusted by titration to 5.0 with a small amount of NH_4OH. This pH, though lower than reported in the literature, was found to give better and more controllable results at the 5-6 degree temperature.

During this second step, the voltage across the electrode was held constant. As can be seen in Figure 5, this procedure is somewhat different than the conventional anodization and was chosen because of its controlability and repeatability. It was also noted in the literature that polycrystalline formation was found to begin early during the conventional anodization process. It was hypothesized by this researcher that this formation was due not only to the current density but also to its rate of

change and could be caused to take place later in the anodization if the initial current was made to rise rapidly and then allowed to fall. By following this anodization procedure, the current density did rise extremely rapidly through the reported value needed for enhanced polycrystalline formation in the early part of the anodization.

Presented in Figures 18 and 19 below are sample voltage versus time and sample current versus time characteristics for the 85 wafers (approximately 270 capacitor structures) that were anodized.

Physical Properties

It should be noted that the criterion for stopping the hard anodization step was when $|di/dt|$ fell to less than 0.4mA/min. The current density at this point varied with the applied potential. This criterion was established as the result of an effort to eliminate the crystalline islands that appeared in the oxide when the process was allowed to continue beyond this point. Figures 20, 21, and 22 below illustrate how the utilization of this criterion helped eliminate the polycrystalline islands.
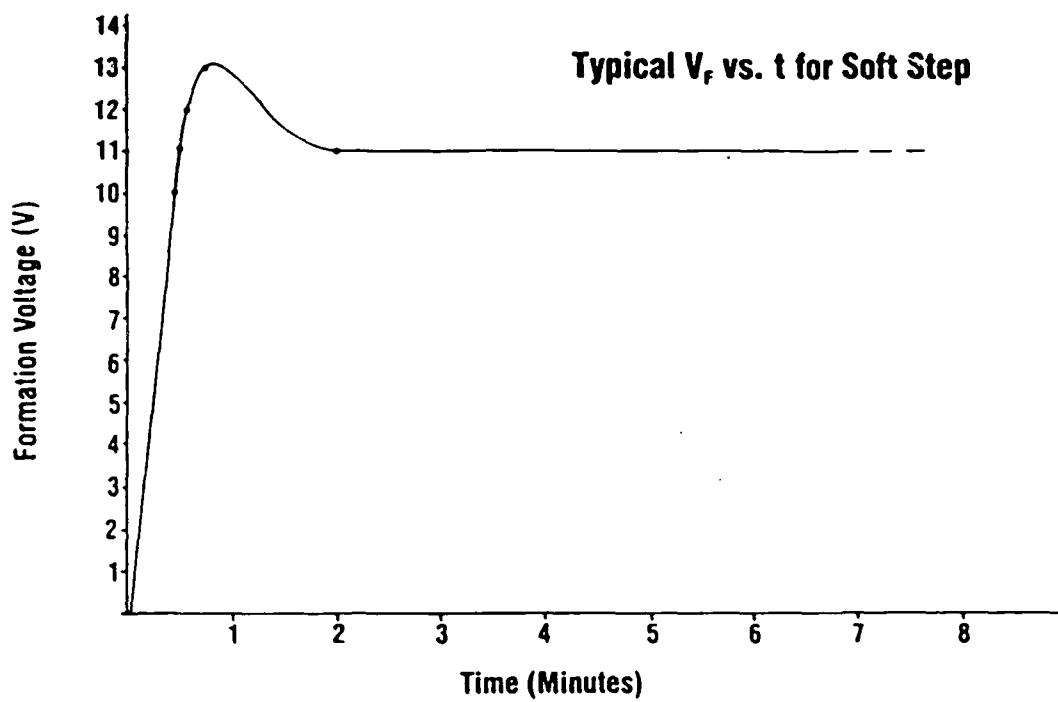
Figure 18 Typical forming voltage character-istic for the porous anodization. Nine minutes of anodization with a constant current density of about 1.5 mA/cm² at 6° centigrade in the sulfuric acid electrolyte produced a 6000 Å thick oxide.
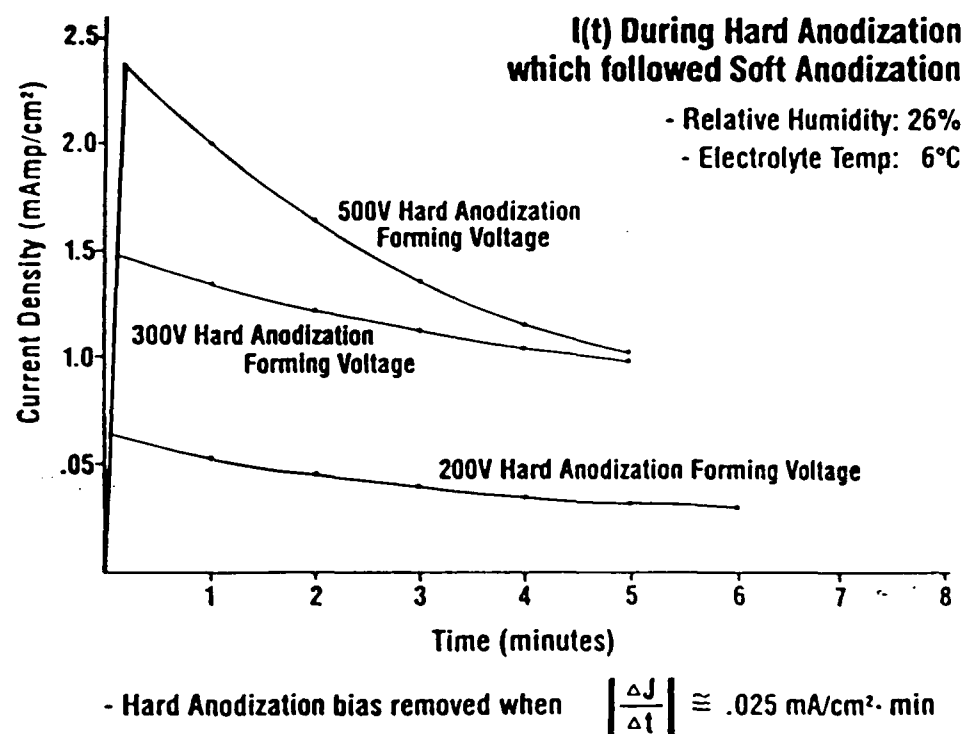
Figure 19 Three typical current density characteristics for the barrier anodization. Because of the size of the sample:

$$|di/dt| = 0.4 \text{ mA/min}$$

corresponds to

$$|dJ/dt| = 0.025 \text{ mA/cm}^2 \text{ min}$$

Elimination of crystalline islands in order to achieve maximum dielectric strength.

Previous soft anodization then 200V forming voltage during hard anodization.

Hard Anodization stopped after 45 minutes.

$$J \cong \frac{.025 \text{ mA}}{\text{cm}^2}$$

Figure 20 This dark field photo shows the large number of polycrystalline islands that form in the oxide when the anodization is greatly 'prolonged' (i.e. allowed to anodize well past the optimum cut - off point. 800x magnification).

Identical conditions as above but hard anodization
stopped after 11 minutes. J $\cong$ .15 mA/cm^2
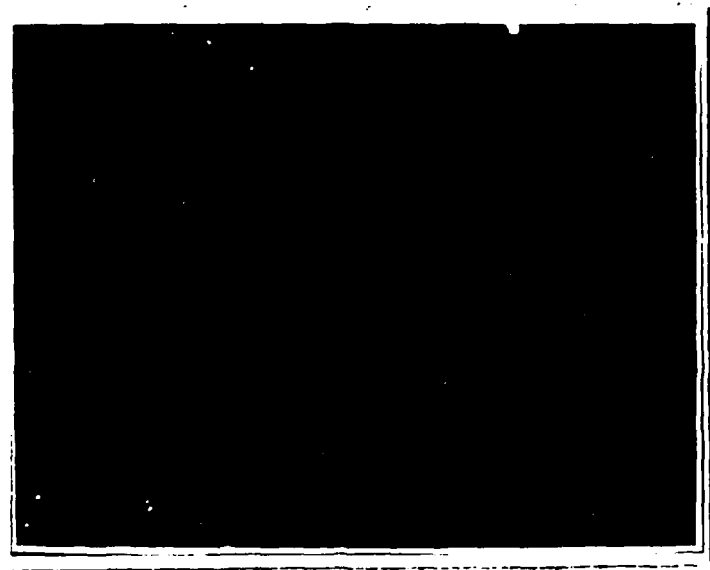
Figure 21 Notice in this figure the reduced number of γ' alumina islands in the otherwise amorphous oxide. This anodization was only slightly prolonged (800x magnification).

**Identical conditions as above
hard anodization stopped when**

$$\left|\frac{di}{dt}\right| = .4mA/min.$$

$$J \cong .3mA/cm^2$$
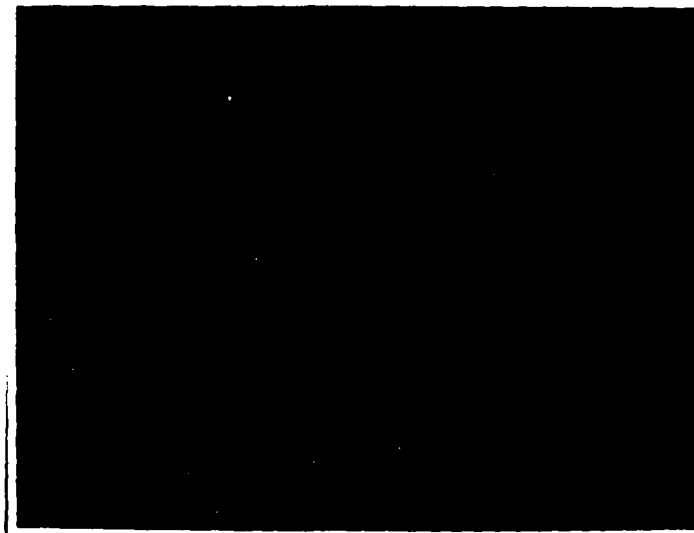
Figure 22   This dark field photo of the oxide film shows that the formation of the undesirable islands can be eliminated using dJ/dt as the cut - off criterion (800x magnification).

It is well known that the dielectric properties of the amorphous oxide are better than those of the polycrystalline film[16]. It was supposed by this researcher that reduction or elimination of the poylycrystalline sites would lead to better, overall dielectric properties. This, indeed, was found to be the case as will be discussed later.

In the process of developing this cut-off criterion, several undesirable conditions were encountered. First, the current density was found to be extremely sensitive to the pH of the electrolyte. When the pH was above 5.2, a high current density (current density increased with pH) promoted the formation of small clear domes on the surface of the oxide. These domes caused a decreased field gradient and lower current density in the local area promoting the formation of sites of polycrystallinity. See Figure 23 below.

Secondly, the absence of a thorough clean of the wafers before aluminizing resulted in weak spots and ruptures in the anodized film. See Figures 24 and 25 below.

Thirdly, prolonged anodization was found to promote the growth of the polycrystalline sites as well as the formation of

Figure 23 When the pH of the hard anodization
electrolyte was raised above 5.2, clear
'domes' of an unknown by-product formed on
the surface. Transformation of the amorphous
alumina to a polycrystalline phase was much
more rapid under the regions covered by these
domes (134x magnification).

Figure 24   A thorough surface clean of the substrate is critical.   The figure above shows one of the results of an improper clean (134x magnification).

Figure 25 The substrate can be seen through this hole in the anodized aluminum. Any surface irregularity will cause field intensifications and thus present sites of more likely breakdown (335x magnification).

ruptures in the oxide (note that these sites result in a short circuit when the counterelectrode is deposited). See Figures 26, 27,and 28 below.

Figure 26 Large, multi - phase crystalline formation resulting from a prolonged anodization (335x magnification).

Figure 27   This defect in the oxide formed near the electrolyte miniscus.   Notice the radial breakdown points (335x magnification).
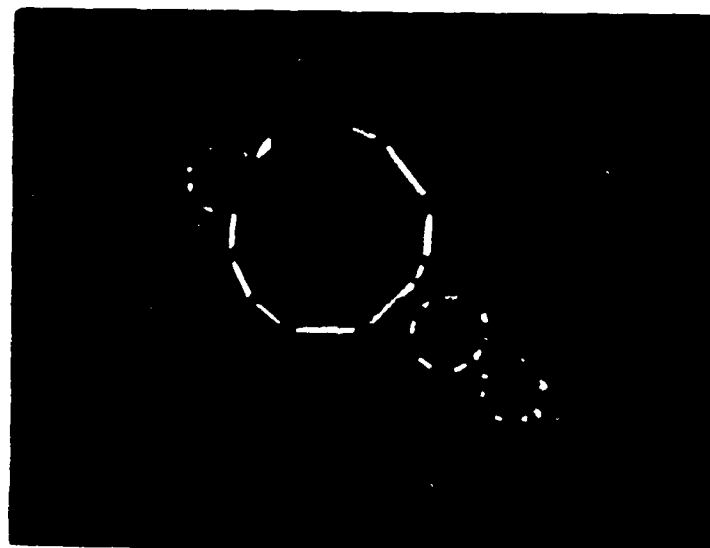
Figure 28 Ruptures in the oxide which expose
the aluminum and would cause a short if a
counter electrode were deposited. The silicon
dioxide substrate can be seen through the
ruptures. These sites occurred during pro-
longed anodizations (134x magnification).

It should be noted that the point of termination of the anodization immediately preceded the point at which the current began to flucuate in its continued slow decline. Some researchers attribute this flucuation to the effects of etching.

In addition to the elimination of the polycrystalline islands, the cloudy film covering typical of higher voltage barrier anodization was also eliminated. Temperature and humidity as well as the pH played important roles in determining the current density during the hard anodization step. Both low temperature and high humidity tended to suppress the current density. The latter observation was noted most readily by comparing the current characteristic of a sample that experenced a pre-hard anodization bake with that of a sample that went straight from the soft anodization to the hard anodization.

After the second anodizaton, the wafers were well rinsed and baked at 225°C for about 40 hours and a counterelectrode was applied in an evaporator using a shadow mask. Figure 29 below shows the resulting capacitor structures.

It was observed that a densification of the porous oxide started at the interface of the initial hard layer and soft oxide.

CAPACITOR STRUCTURE

Aluminum

Oxide

Aluminum

Oxide

$1\mu m$

Substrate

Top View   **Cross Section**
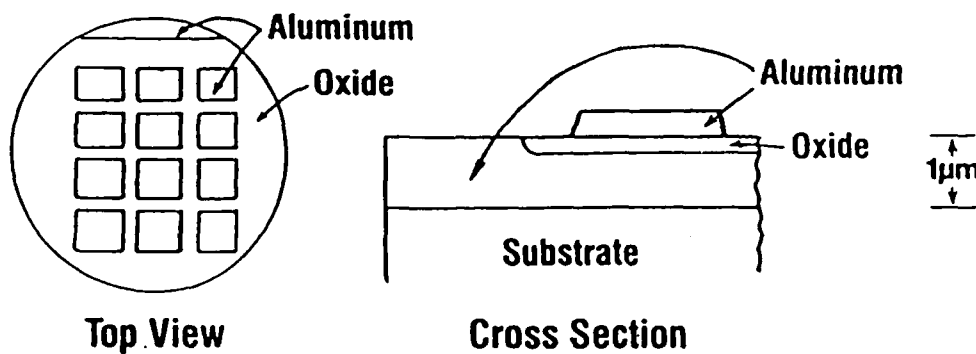
- Post bake at 200° C
- Shadow mask

Figure 29 Capacitor structures were created by using a mechanical shadow mask during an aluminum deposition to create counter electrodes.

In addition to the densification of the porous oxide, the initial hard layer grew thicker but at a much slower rate than the former densification.

The transformation takes place first at the bottom of the soft oxide for the following reason. The soft oxide film formed initially appears as illustrated in Figure 30.

pores

greatest concentration
of aluminum ions
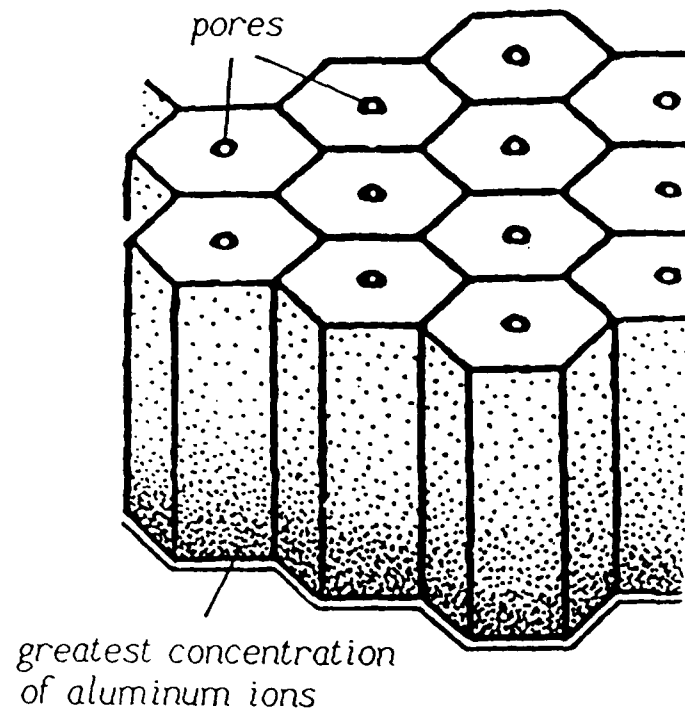
Figure 30   Region of highest concentration of
aluminum ions is first to convert to 'hard'
oxide.

The pores provide avenues for the hard anodization electro-
lyte to access the region of highest Al^{+++} ions which is at the
bottom of the oxide.   Because of these excess ions, this lower
region converts to an hard oxide first.   The transformation
progresses upward as the highest density of Al^{+++} ions shifts.

A forming voltage of 500V was sufficient to densify approx-
imately 3500Å of the soft oxide as well as thicken the initial

hard layer to approximately 1400Å. It was also observed that if the soft anodization was allowed to progress only to its point of maximum potential (usually less than one minute), a hard anodization forming potential of 500V did create at least one micron of hard or hard-like oxide. It should be noted that this is not the same mechanism observed during the sealing of soft oxide pores in a post anodization boil. As discussed in an earlier section, the sealing process is typified by the uniform sealing of the pores caused by the formation of a monohydrate such as boemite or bayerite. In the soft/hard anodization, a definite transformation of certain portions of the soft oxide takes place.

If the forming voltage of the hard anodization is more than sufficient to transform the entire soft oxide film, the layer of initially hard oxide switches from a slow growth (during the soft transformation) to a more rapid growth. In any event, the final thickness of the transformed soft oxide plus the initial hard oxide depends upon more than just the forming voltage of the hard anodization. See Figures 31 through 35 below. An infinite variety of combinatior of soft and hard anodizing

conditions can be put together to form a compound dielectric with varying physical, dielectric, and perhaps optical properties.
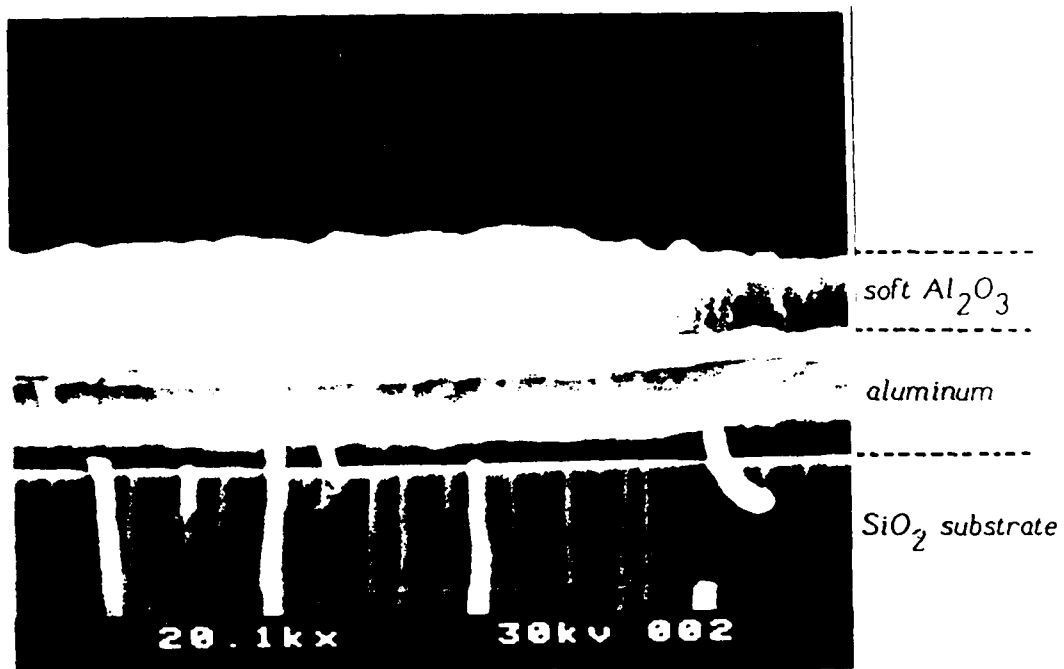
Figure 31   Soft aluminum oxide on aluminum
on a silicon dioxide substrate.

hard Al_2O_3

aluminum

SiO_2 substrate

20 1kx   30kv 006
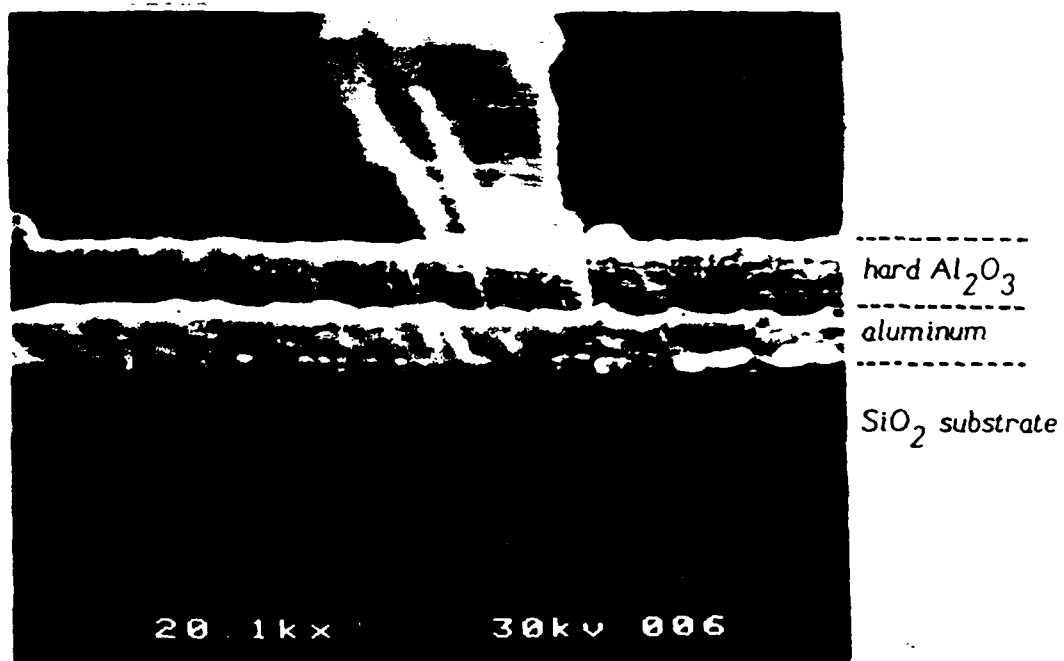
Figure 32   Hard aluminum oxide on aluminum
on a silicon dioxide substrate.

soft Al_2O_3

converted Al_2O_3

hard Al_2O_3

aluminum

SiO_2 substrate
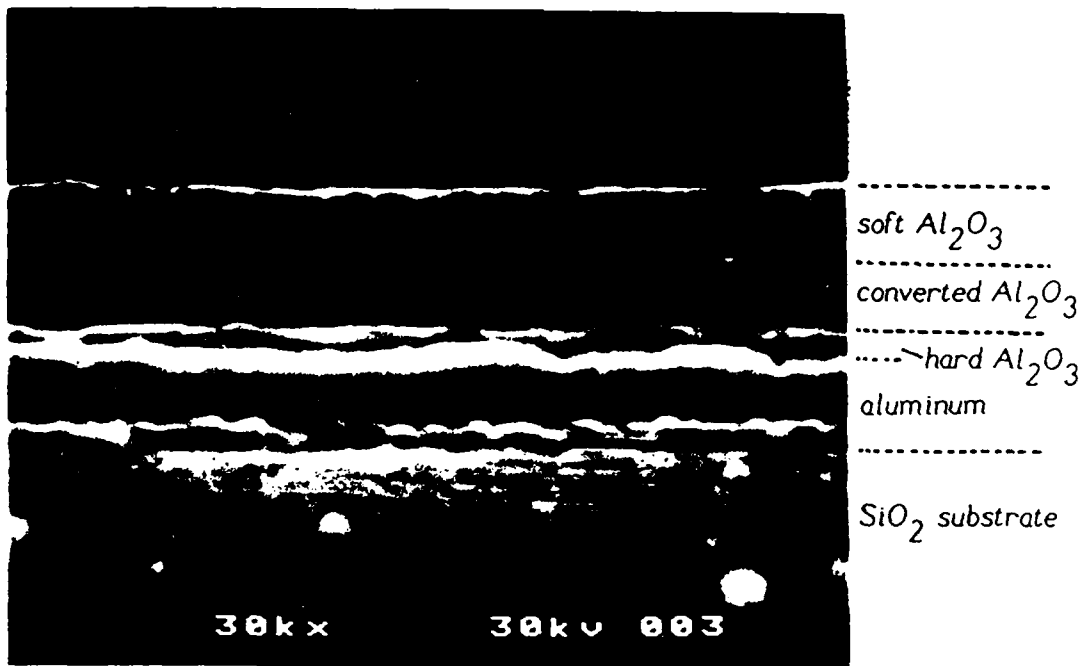
Figure 33 This figure shows the transformation of the originally soft oxide. Now present is a region of soft - turned - hard as well as a thickened layer of hard oxide beneath. This sample had an hard anodization forming voltage of 300 V.
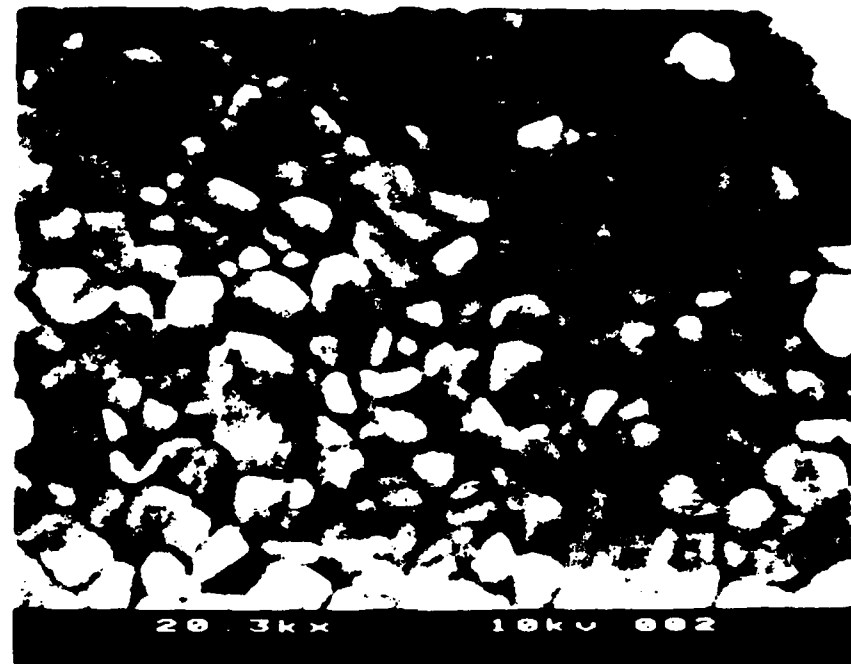
Figure 34 Surface of a partially densified soft/hard Al_2O_3 film.
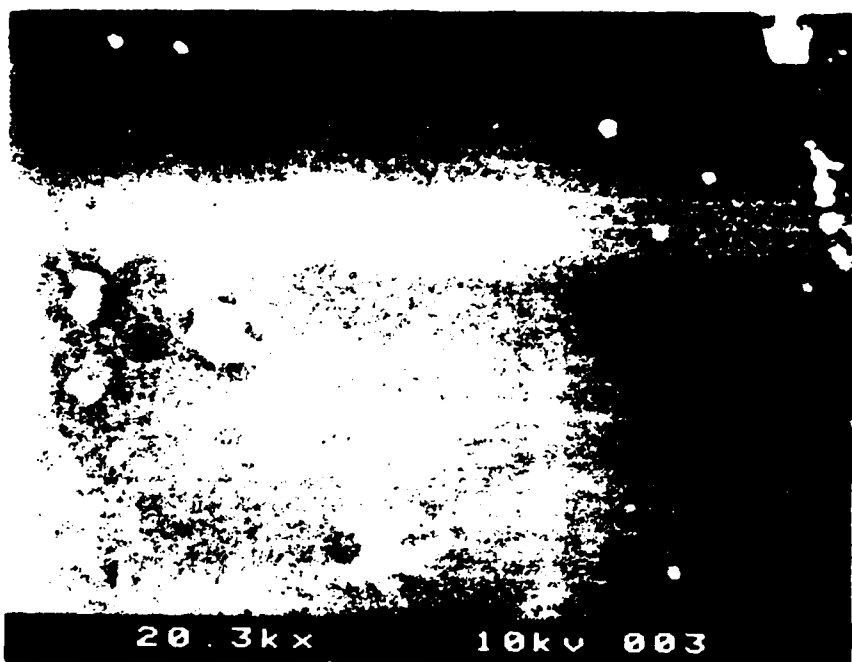
Figure 35 Surface of the completely densified
soft/hard Al_2O_3 film.

A study of the data in Table Three indicates that when equal amounts of charge are utilized in both the soft and the hard steps, the dominant growth mechanism is the barrier type. When the coulombic utilization during the soft step is increased to roughly three and a half times that used in the hard step, the overall growth begins to be more dependent on the growth taking place during the soft step. Since the growth rate (based upon a coulombic utilization) of the combined process is not in close agreement with the growth rates of either the soft or hard alone, it is evident that some sort of transformation of the soft oxide is taking place during the hard anodization as well as the additional growth of some amount of 'purely' hard oxide.

Prolonged anodization in the soft/hard process, that is anodization past the point where $|di/dt| = 0.4mA/min$ in the hard step promoted swelling. Generally, swelling was limited to two times the thickness of the original aluminum and seemed to be determined by the initial soft oxide growth.

It is apparent from the thickness and anodizing current data, that either the current is not 100% efficient in creating the oxide or that at higher current densities, certain phases of

sample	soft J (mA cm^{-2})	soft Vmax (V)	soft anod. time (min.)	soft coulombs (C)	hard voltage (V)	hard Jmax (mA cm^{-2})	hard anod. time (min.)	hard coulombs (C)	thickness (Å)	swell
A	1.5	13.7	9	17.1	-	-	-	-	6000	1.8
B	1.5	13.7	9	17.1	200	.612	6	2.9	6900	1.9
C	1.5	13.7	9	17.1	500	1.480	5	7.2	7300	1.3
D	1.5	12.5	1	1.8	200	.443	4	1.6	3050	1.7
E	1.5	13.1	3	5.4	200	.421	5	1.7	3250	2.0
F	1.5	13.0	5	9.0	200	.450	5	1.9	4700	-
G	1.5	13.2	7	12.6	200	.416	6	2.1	7100	2.0
H	-	-	-	-	500	1.820	10	15.5	4850	1.0

Table Three

Table Three   Representative physical data obtained from the soft/hard anodization of Al_2O_3.

the oxide are formed which require more formation energy. Where the swelling is less than unity, it is probably because of etching during the prolonged anodization.

It was also observed that freckles (see Appendix B) could be eliminated at the Al_2O_3/SiO_2 interface if the oxide was grown all the way through the deposited aluminum. Such an oxide might prove to be useful as an optoelectronic waveguide.

Dielectric Properties

Capacitance and the DF were measured using a General Radio type 716 - B capacitance bridge; an oscilloscope was used as the detector. A probe station was used to measure the resistivity and breakdown field (see Appendix D for the diagram of both of these set ups). To test breakdown, the voltage was ramped at 2V/sec to the point of destructive breakdown. Thickness measurements were made via scanning electron microscope photographs. Table Four is representative of the data obtained.

sample	cap. density ($nF\ cm^{-2}$)	breakdown voltage (V)	resist. @ 5V ($ohm\ cm \times 10^{12}$)	rel. permittivity (ϵ_r)	DF @ 1 kHz (%)
A	18.15	54	.42	12.3	1.3
B	17.40	475	7.00	16.8	0.5
C	20.80	620	8.60	17.2	0.9

Table Four

Table Four Representative dielectric data obtained from the soft/hard anodization of Al_2O_3.

The observed breakdown voltage is up to 2.38 times the hard anodization forming voltage. The breakdown field of the purely soft oxide was 0.83MV/cm . For a 5000Å thick, purely hard oxide the literature reports values between 3.1MV/cm and 6.9MV/cm. For a 7000Å thick soft/hard oxide the breakdown field was found to be 7.14MV/cm. It is well documented that given conventional wet anodization conditions, the breakdown field is considerably reduced as the oxide thickens. The results of Merrill and West on breakdown fields were up to 50% less for this thickness but their estimates on thickness were based on an assumed value for ϵ_r.[24] Odynets et al.[26] obtained a breakdown field of about 6.9MV/cm with a 5000Å thick sample but used a steel ball as the counter electrode. As has been shown in literature[15], contact area influences the breakdown field and it is not clear how large this area is when a steel ball is used.

It is evident that this soft/hard anodization process is be able to create thick oxides with breakdown fields up to twice that which has been reported previously for either hard or other soft/hard oxides. The results obtained also indicate that the

applied field reacts to this soft/hard oxide as though it is purely hard and entirely amorphous.

There is an apparent improvement of up to 100% in the dielectric constant over that which is most often reported in the literature while the losses appear to be in the same range as that reported by others.

As Figure 36 shows, the low frequency DF was much higher than that observed at frequencies greater than 5kHz. Unbaked samples showed very high DF values at low frequencies but decreased rapidly to give similar readings as the baked films at frequencies above 10kHz. DF readings less than 0.005% at 5kHz were obtained in one set of samples. Capacitance increased with frequency. In unbaked samples, the capacitance density showed an initial decline up to 10kHz but then increased with increasing frequency.

Direct current resistance of the films was measured over a range of potentials with the HP 4145A Semiconductor Parameter Analyzer in a reduced-noise environment (HP 16058A Test Fixture). The relative humidity was noted and observations of the increase of resistivity with time were made. Values of up
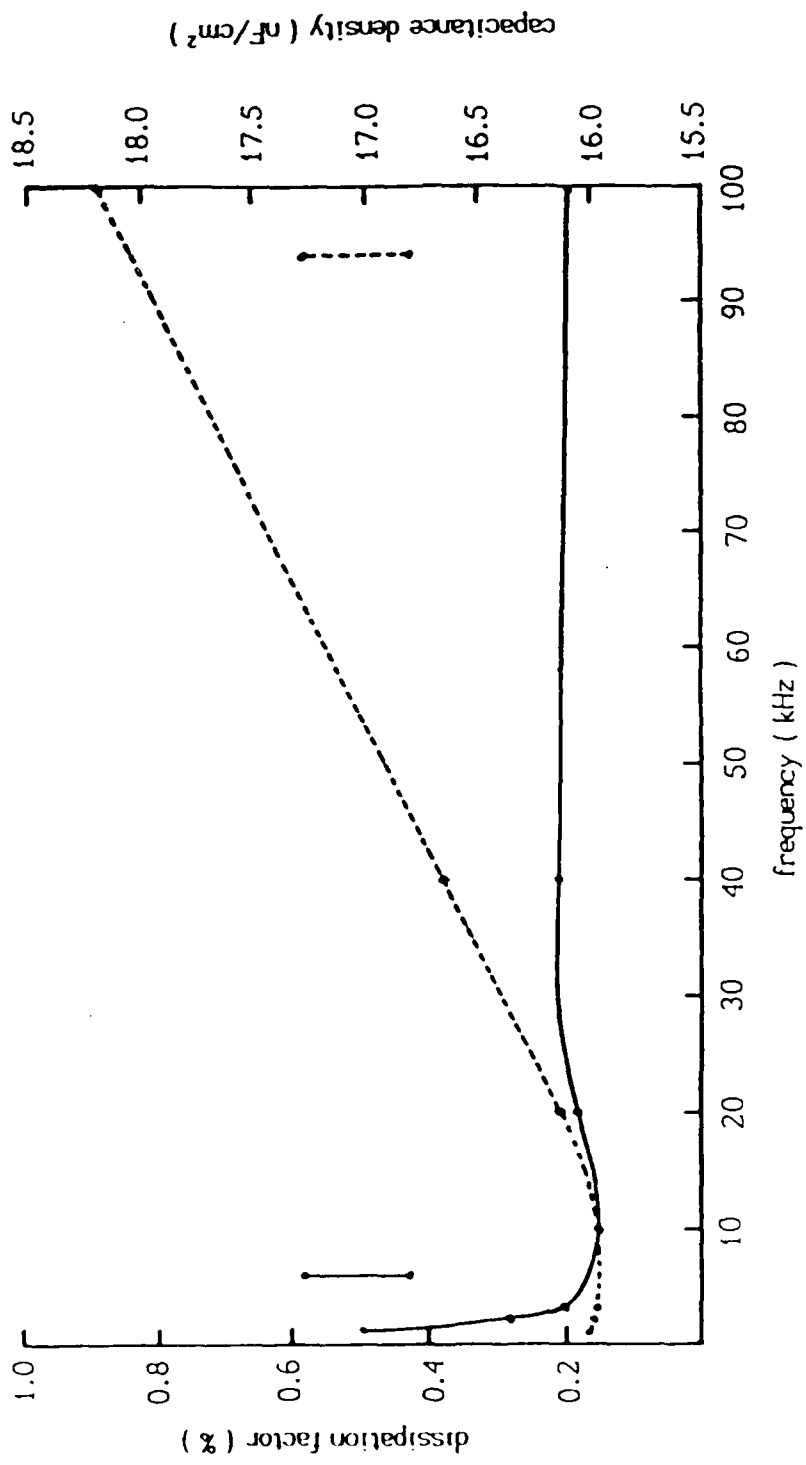
Figure 36 Capacitance density and dissipation factor of soft/hard aluminum oxide versus frequency.

to 1.28×10^{18} ohm-cm at 17% of the forming potential were observed on freshly anodized and baked 41cm^2 size samples. The value of ρ has been reported to be between 10^{11} ohm-cm and 10^{17} ohm-cm [16,17]; however, care should be taken to note at what percent of the forming voltage this measurement is taken. Most resistance measurements in which the applied voltage has been recorded have been made at less than 5% of the forming potential. Since ρ decreases by orders of magnitude as the applied voltage is increased, measurements taken at TTL compatible voltages appear to be much better than those taken at higher levels. It was also confirmed that the post anodization bake does affect the resistivity of the film. See Figures 37a - 37c and Figure 38 below.

Samples that were left exposed to the ambient were affected by the humidity. Figure 39 shows the difference between the DF measured after three months of exposure to the ambient and after a subsequent bake.

The bake at 250°C for four hours brought back the dielectric behaviour obtained after the original post-anodization bake. It was noted, however, that if the baking temperature exceeded

IGATE
(A)

1E-03

decade
/div

1E-12
.0000   100.0
        VGATE   10.00/div   (V)
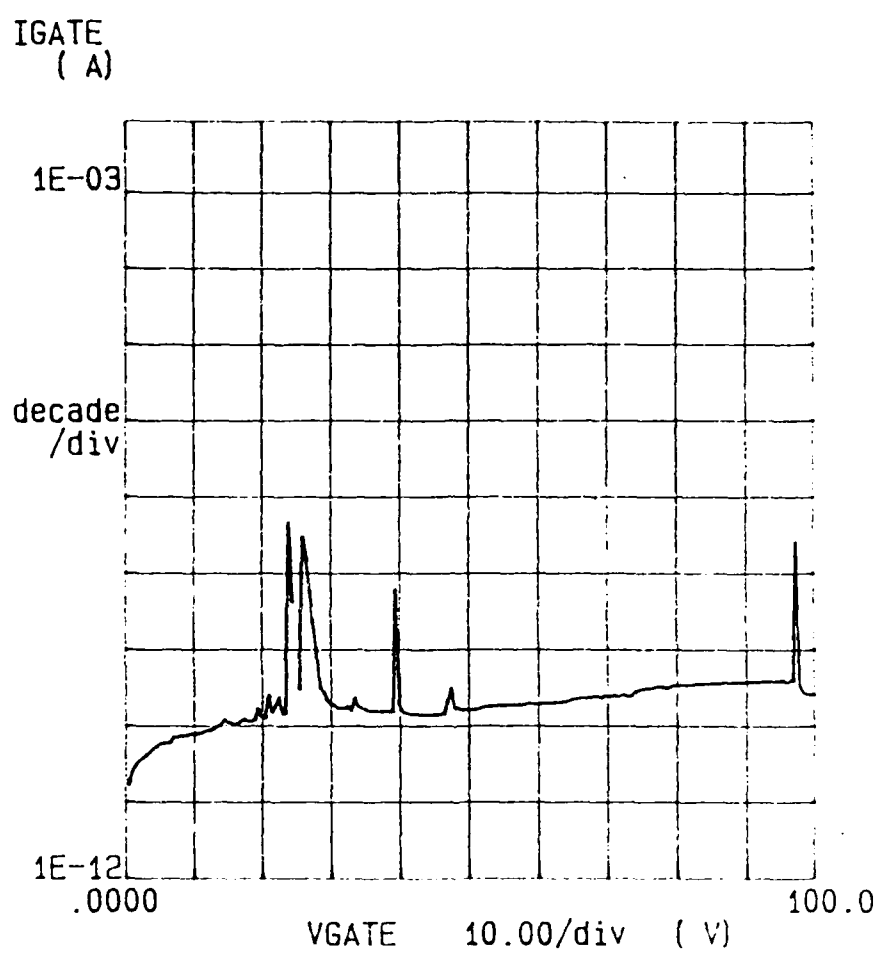
Figure 37a   Leakage current versus testing
voltage performed on a soft/hard anodized
aluminum oxide capacitor.   Notice the spikes
which represent 'healings' of the capacitor.
This procedure is not uncommon in the capaci-
tor fabrication industry.

IGATE
(A)

1E-03

decade
/div

1E-12
.0000

VGATE   10.00/div   (V)
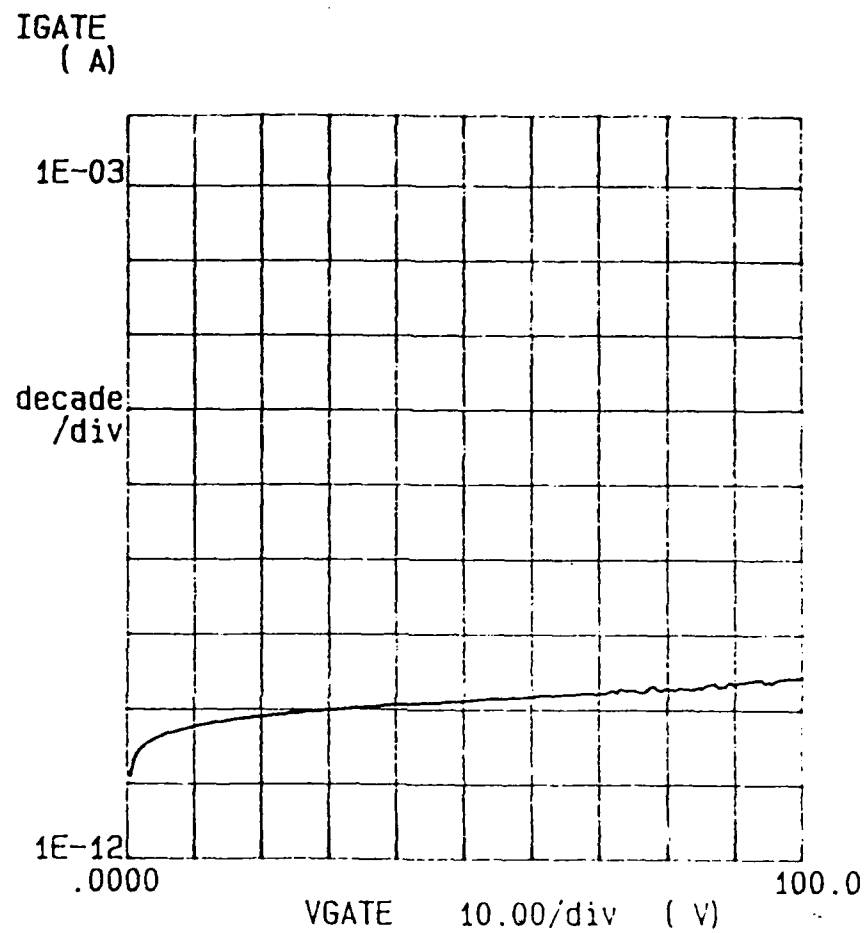
Figure 37b   Same as for Figure 37a but this plot represents the third pass or ramping up of the voltage. Notice that the capacitor has been 'healed' from most of its small defects up to 100V.   The following resistivies were obtained for this $41cm^2$, 8000Å thick capacitor structure:

V_{test} (V)	ρ (ohm-cm)
1.0	2.56×10^{17}
10.0	8.54×10^{16}
50.0	1.28×10^{18}
75.0	9.61×10^{17}
100.0	5.12×10^{17}

IGATE
(A)
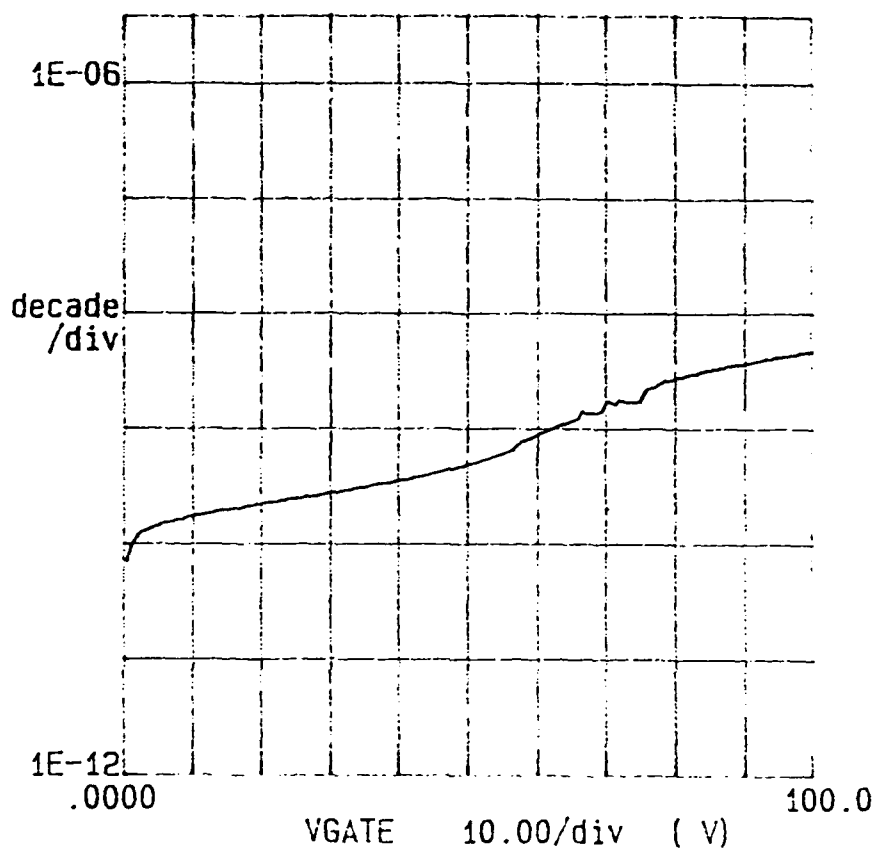
Figure 37c   Leakage current versus testing voltage performed on a soft/hard anodized aluminum oxide capacitor structure.   This sample had been exposed to the ambient for more than four months.   The following resistivities were obtained:

V_{test} (V)	ρ (ohm-cm)
1.0	3.57×10^{15}
10.0	5.33×10^{14}
50.0	3.19×10^{14}
75.0	1.67×10^{14}
100.0	7.60×10^{13}
	accur. ± 0.1
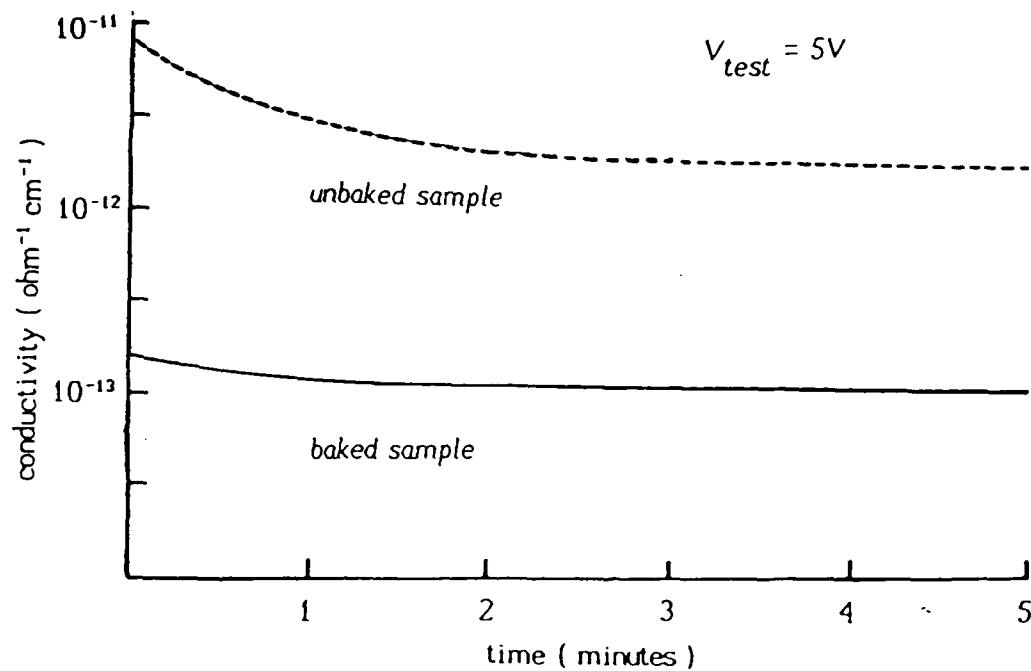
Figure 38 Sample conductivity versus time characteristic for both an unbaked and a baked sample of soft/hard Al_2O_3.
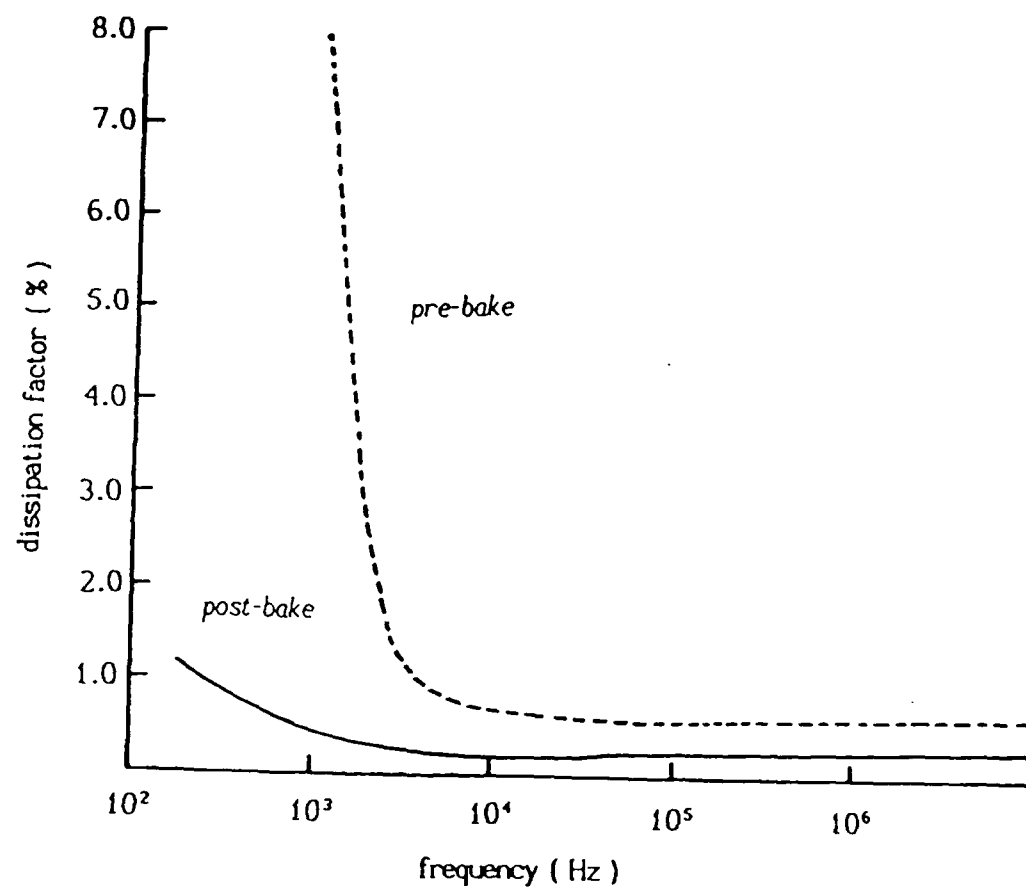
Figure 39 Typical variation of the dissipation factor with frequency for soft/hard oxide exposed to an humid ambient (R.H. > 50%) for three months and after a four hour bake at 250° C.

the substrate temperature during the original aluminum deposition, there was a strong tendency for the aluminum to form hillocks which often pushed through the overlaying oxide. For this reason, the baking time and temperature had to be controlled closely.

Most of the samples that initially behaved like short circuits (when tested for capacitance) could be put through a clearing or healing process one or more times and would then give results similar to other capacitor structures. This process consisted simply of applying a very gradually increasing dc voltage across the plates until the current was observed to jump very high momentarily and then drop to a very low level (in the nA range).

In summarization of the soft/hard anodization process, it is apparent that a wide range of physical and electrical characteristics are obtainable. Improved dielectric properties were observed in conjunction with both the soft/hard process itself and with the reduction/elimination of the polycrystalline islands in the film. It also appears that certain conditions of the process can be set in order to enhance some electrical and

perhaps optical properties. Instability with exposure to the ambient can be resolved by way of a sealing of the film.

III. THIN FILM MULTILAYER CAPACITOR

Energy Density

The theoretical energy density of a multilayered, parallel plate, MIM capacitor can be determined by the following equation:

$$E_d = E/Vol$$
$$= (C \times V^2)/(2 \times Vol)$$
$$= (\epsilon_r \times \epsilon_o \times A \times V^2)/(2 \times t_i \times (A \times t))$$
$$= (\epsilon_r \times \epsilon_o \times V^2)/(2 \times t_i \times t)$$

where $t = t_i + t_m$

t_i = thickness of the dielectric

t_m = thickness of the metal

ϵ_r = relative permittivity of the dielectric

ϵ_o = permittivity of free space

V = voltage across the capacitor plates

Vol = volume of the cell

73

To increase the energy storage capacity, it is clear that a high value for ϵ_r and V and a minimum t are desirable. A very small value for t, however, may be impractical if it means having to form too many layers and thus necessitate too many man-hours to be cost effective in production. Nevertheless, by substituting in values for these parameters that have been brought out in this thesis, E_d could be as much as 32.8 MJ/m^3 (32.8 J/cm^3). If we assume an average mass density of 3.3 g/cm^3 for the MIM system, we could conceivably store one megajoule of energy in a 1.07 ft^3 volume weighing about 100 kg (about 220 lbm). This is approximately a 200 fold increase over the 40 J/kg capacitors currently available.

Fabrication and Testing

In order to achieve a multilevel capacitor (MLC) device, three approaches were tried. They will be referred to as the Anode Rotation approach, the Mask approach, and the Hard/Soft/Hard (HSH) approach. The first of these three processes was successful in creating a multilevel capacitor; the second was unsuccessful and the third appeared heading for

success but requires further study. Each of these will be discussed in detail.

Anode Rotation

A very simple way to create the comb structure necessary for a MLC is illustrated in Figure 40.

The most important initial question to be answered was whether or not the soft/hard anodization would create a dielectric film over the entire wafer surface and remain short - free. In other words, could we create a wafer sized capacitor structure?

Several two - level MLC structures were created and one three - level MLC. Each level corresponds to a layer of dielectric material. In order to be able to test each dielectric layer on the three - level MLC, the rotation used was 90^0 rather than 180^0 as was shown in Figure 40. Each level in the three - level MLC underwent a different set of anodization conditions in order to test the flexibility of the process.

The sample's first S/H anodization is illustrated in Figures 41 and 42 below.

MULTILAYERED, THIN FILM CAPACITOR

Test Design
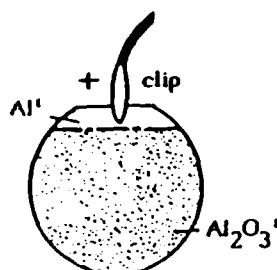
Step 1 — *Anodize an aluminized wafer in either an hard or soft/hard process to optimum thickness.*
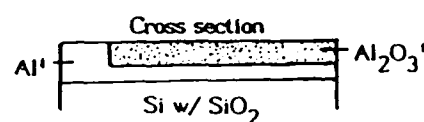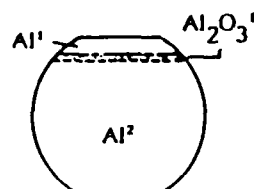
Step 2 — *Aluminize wafer so that the whole wafer is covered except for area that the shadow mask has been covering.*
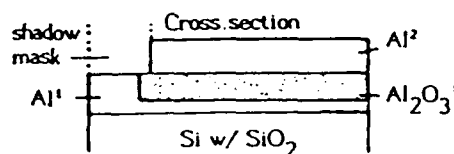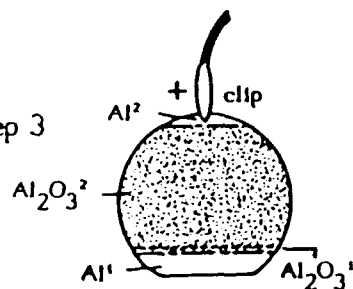
Step 3 — *Rotate the wafer 180° and anodize as in step one.*
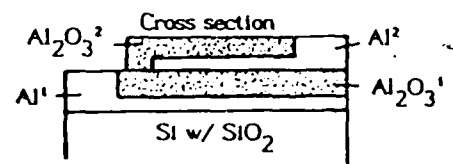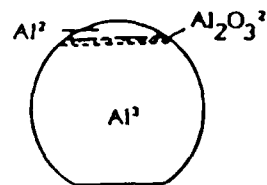
Step 4 — *Repeat step two but with the opposite electrode masked off.*
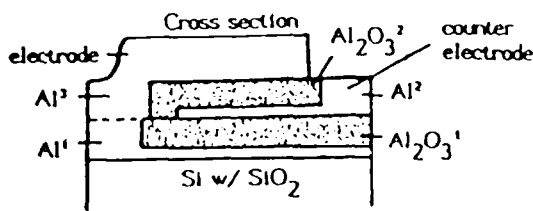
Step 5 — *Repeat steps one through four...*

Figure 40 Process design for creating a multilevel capacitor structure called the Anode Rotation technique.
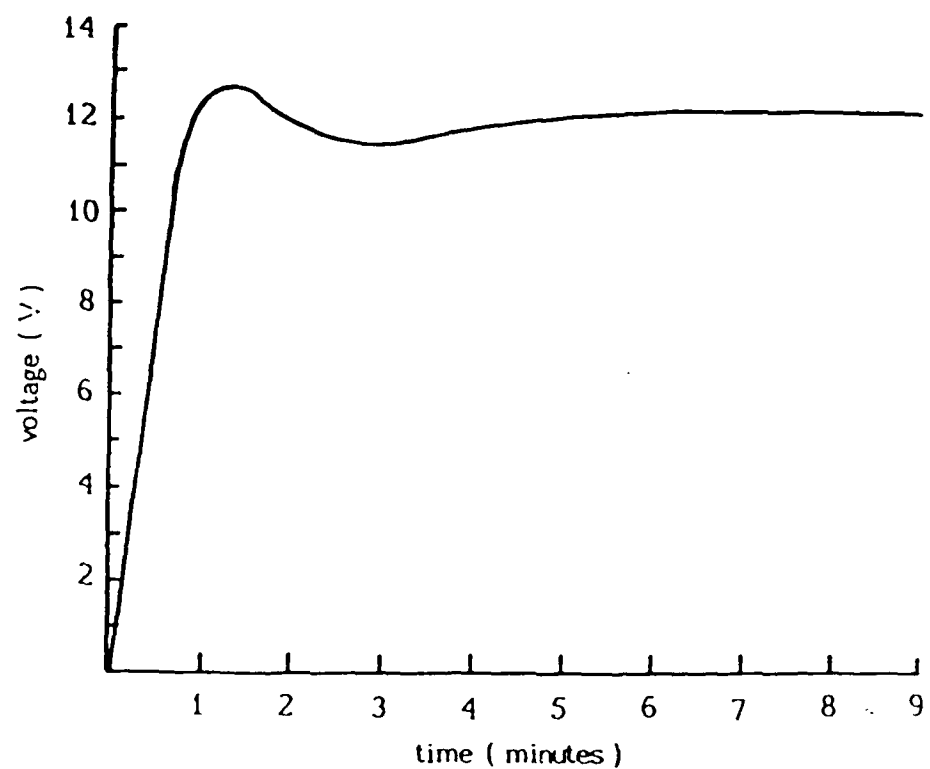
Figure 41 Voltage versus time characteristic
for level one soft anodization. $J = 1.5mA/cm^2$
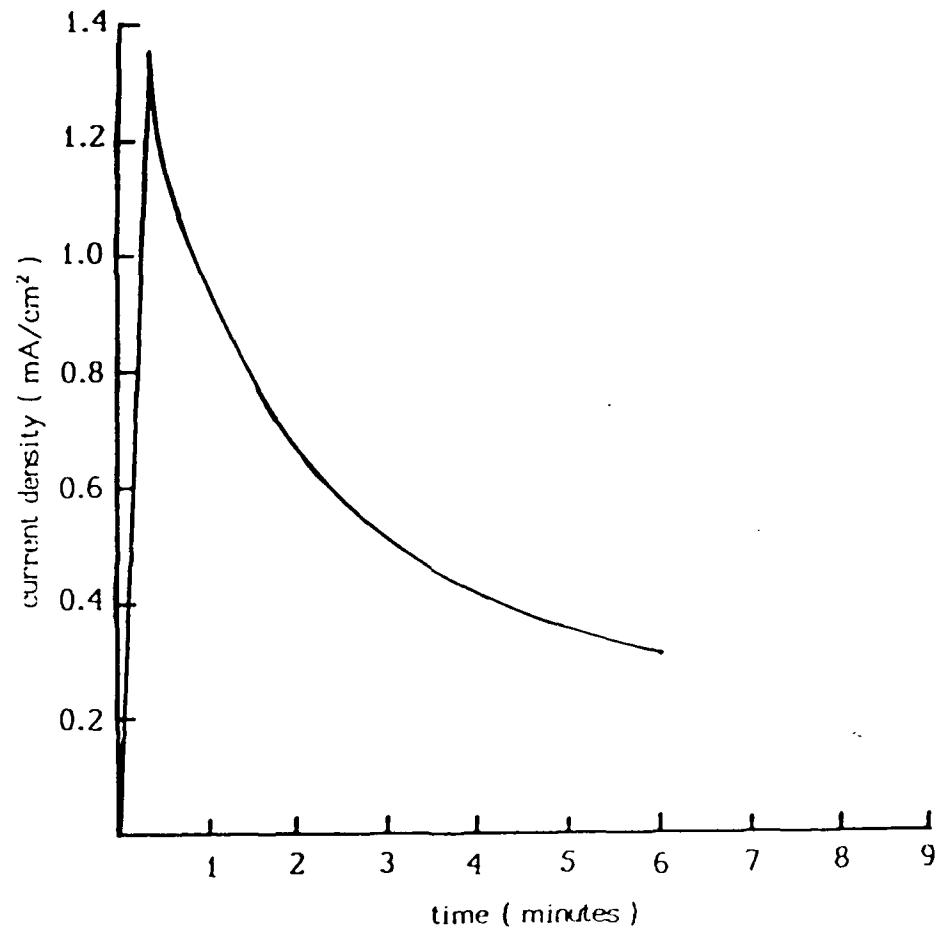
Figure 42   Current density versus time characteristic for level one hard anodization. $V_f = 200V$.

The wafer went through a 20 minute bake at 130°C between the soft and hard anodizations in order to eliminate most of the trapped water. Notice in the Figure above how this, coupled with the higher pH dramatically affected the current density.

A shadow mask was used to cover part of the wafer during the aluminum deposition. This prevented electrode/counter electrode contact and thus a short.

Prior to the deposition of the counter electrode, the sample did not receive a bake. Consequently, its initial DF at 1kHz was unacceptably high. This was corrected in a bake after the electrode deposition. It was found that the whole wafer did behave as a capacitor with a capacitance density of $16764pF/cm^2$ (477nF for the whole wafer).

It should be noted that during the hard anodization, the aluminum above the meniscus was observed to have some arcing at only 130V. It was found that such arcing did not cause shorting of the MLC; however, if the voltage was raised to 200V, some arcing below the meniscus was observed. Some of these latter samples did show shorts in their MLC structure during capacitance testing.

Figure 43 and Figure 44 illustrate the second dielectric level's anodization.
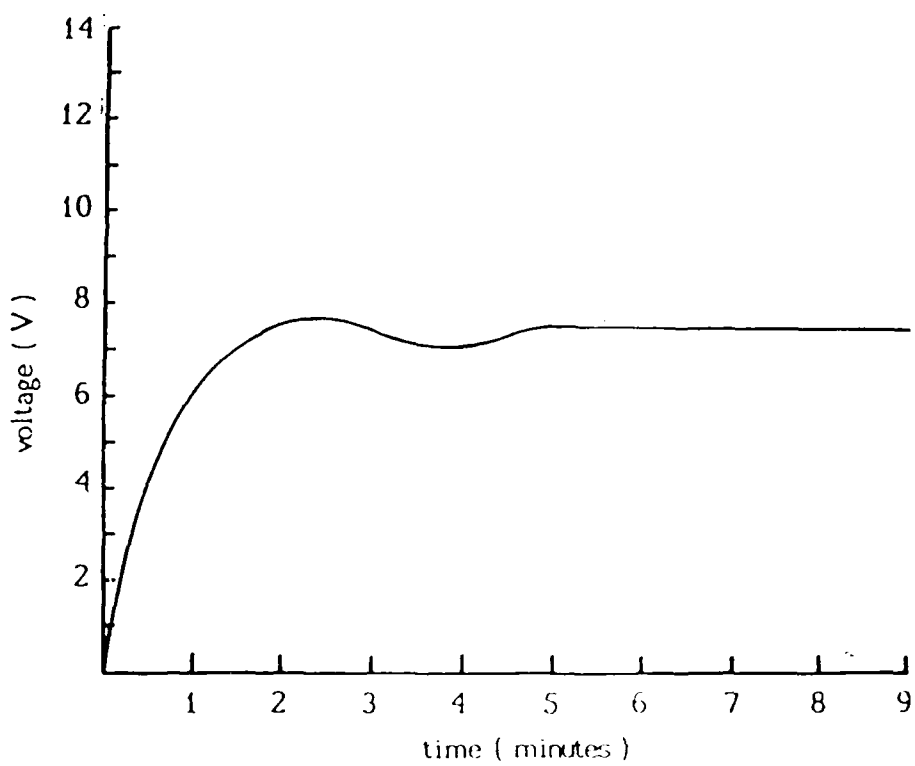
Figure 43 Voltage versus time characteristic for level two soft anodization. $J = 1.5mA/cm^2$
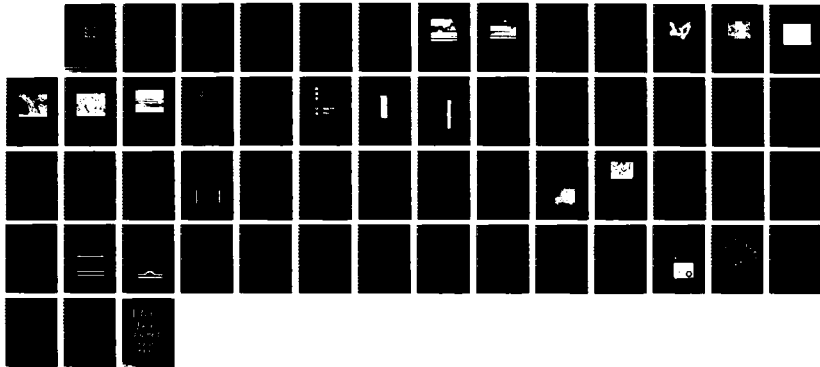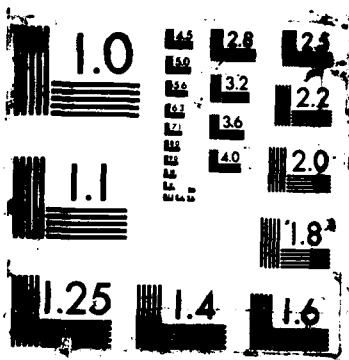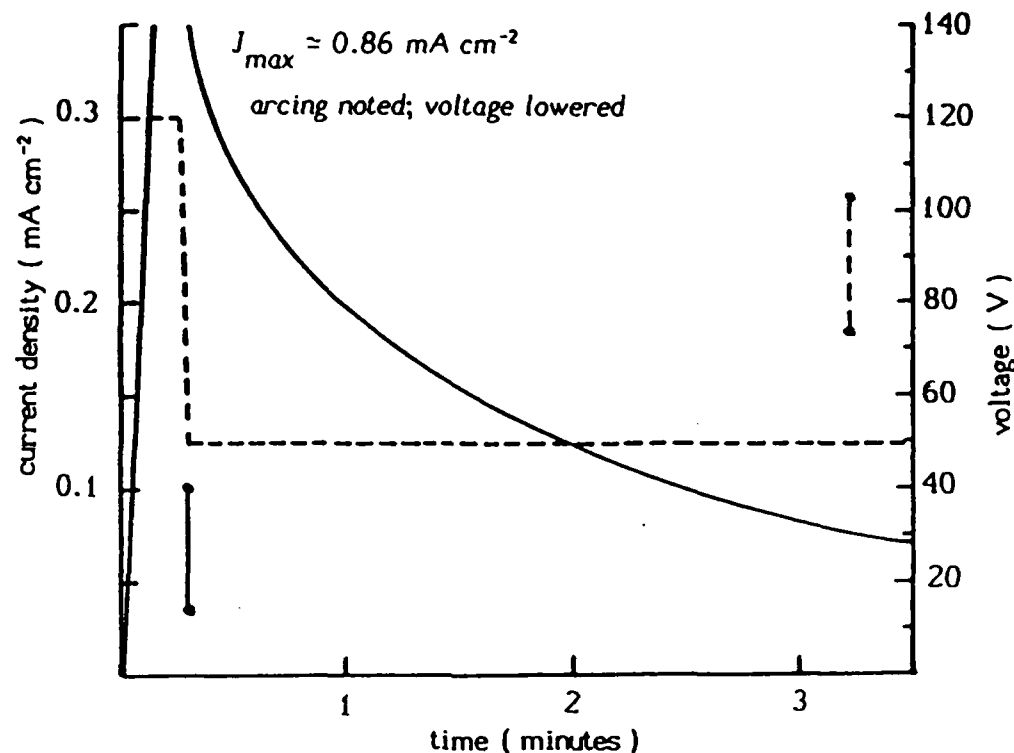
Figure 44 Current density and voltage versus time characteristic of level two hard anodization. Current density characteristic is semi-quantitative for values between maximum and minimums.

In later anodizations, it was discovered that most or all of this arcing could be eliminated if the hard anodization forming voltage was stepped as is shown in Figure 45.

Capacitance density tests done on level one showed that C_d had fallen to about $11.8nF/cm^2$ after the second level's soft anodization. After the hard anodization (2nd level), the first
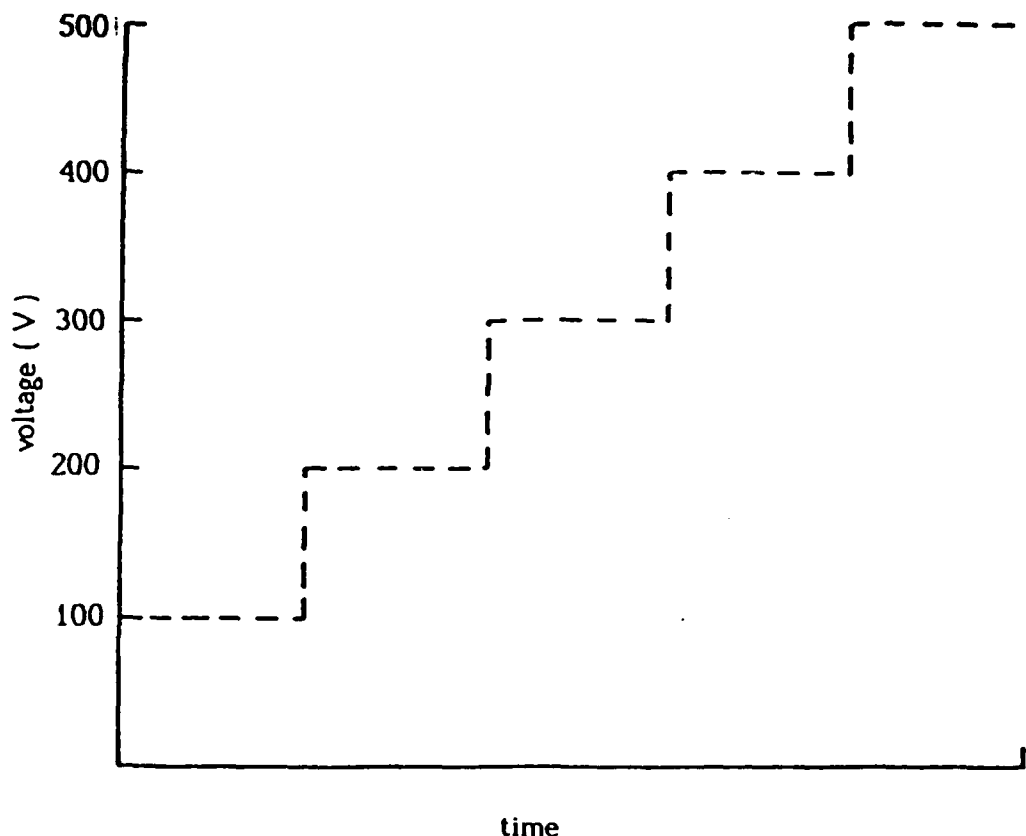
Figure 45 Arcing during the hard anodization
on upper levels was minimized and in some
cases eliminated when the voltage was stepped
to the desired maximum.

level's C_d had fallen to about $11.6nF/cm^2$. This seems to

indicate that undesired anodization and/or swelling of the

sublevel is taking place primarily during the subsequent level's

soft anodization.

After depositon of the electrode, C_{d_t} (C_d for the two - level

device) was found to be approximately $94.3nF/cm^2$. C_{d_1} (C_d of

the first level) did not change drastically during the aluminum

depostion. Because dielectric levels one and two were different thicknesses, there was some question as to whether or not the individual capacitances of each level would simply sum together to give the overall capacitance. However, this was the case as C_{d_1} and C_{d_2} did sum together to give this structure's C_{d_t} (note $C_{d_2} = 83 \text{nF/cm}^2$). Based upon the SEM obtained value for the thickness of dielectric film number two of 7500Å, the relative permittivity, $\epsilon_r \simeq 70$. An increased surface area probably contributes to this high value.

Figure 46 and 47 show the S/H characteristics of level three. Note the low current density during the soft anodization. The voltage did not rise as in the other soft anodizations because the etch rate was somewhat larger than the growth rate. The hard anodization forming voltage was stepped up with each increase being up to the point just below arcing.

Figures 48 and 49 are cross sectional views of the three level device. Note the balls of aluminum on the surface in Figure 48 which developed during the breakdown tests.

C_{d_3} was measured to be 30.16 nF/cm^2; $C_{d_{23}}$ was measured to be 91.2 nF/cm^2. $C_t = C_{d_{123}}$ was calculated to be

102.4 nF/cm^2. It is again evident that further anodization takes place on lower levels while upper dielectric layers are being formed.
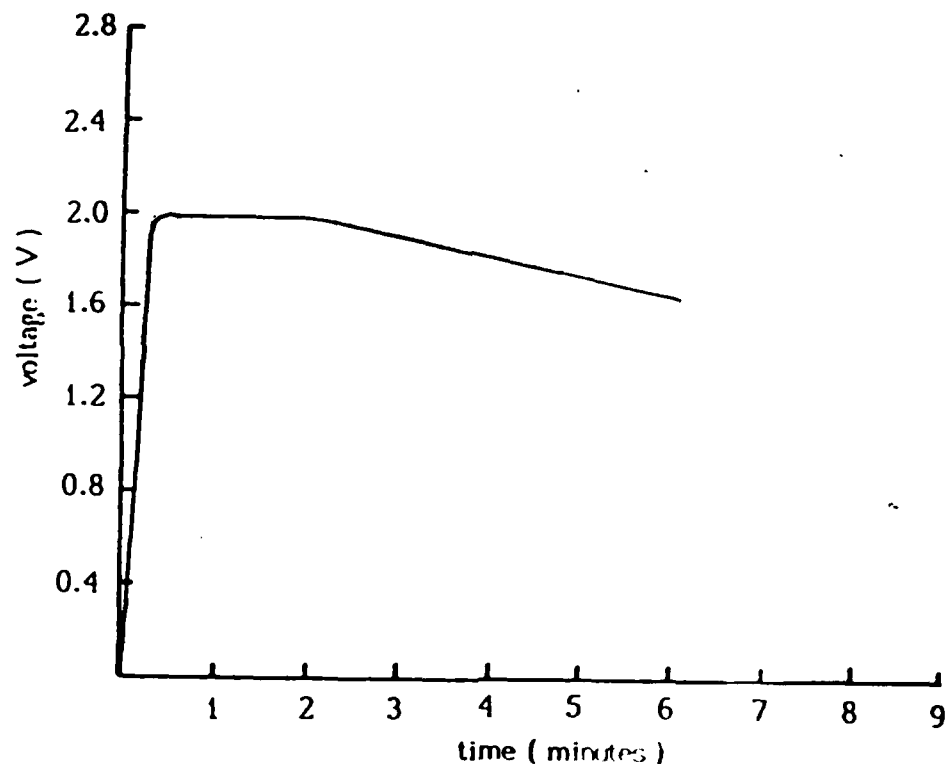
Figure 46   Voltage versus time characteristic for level three soft anodization. J=1.5mA/cm²
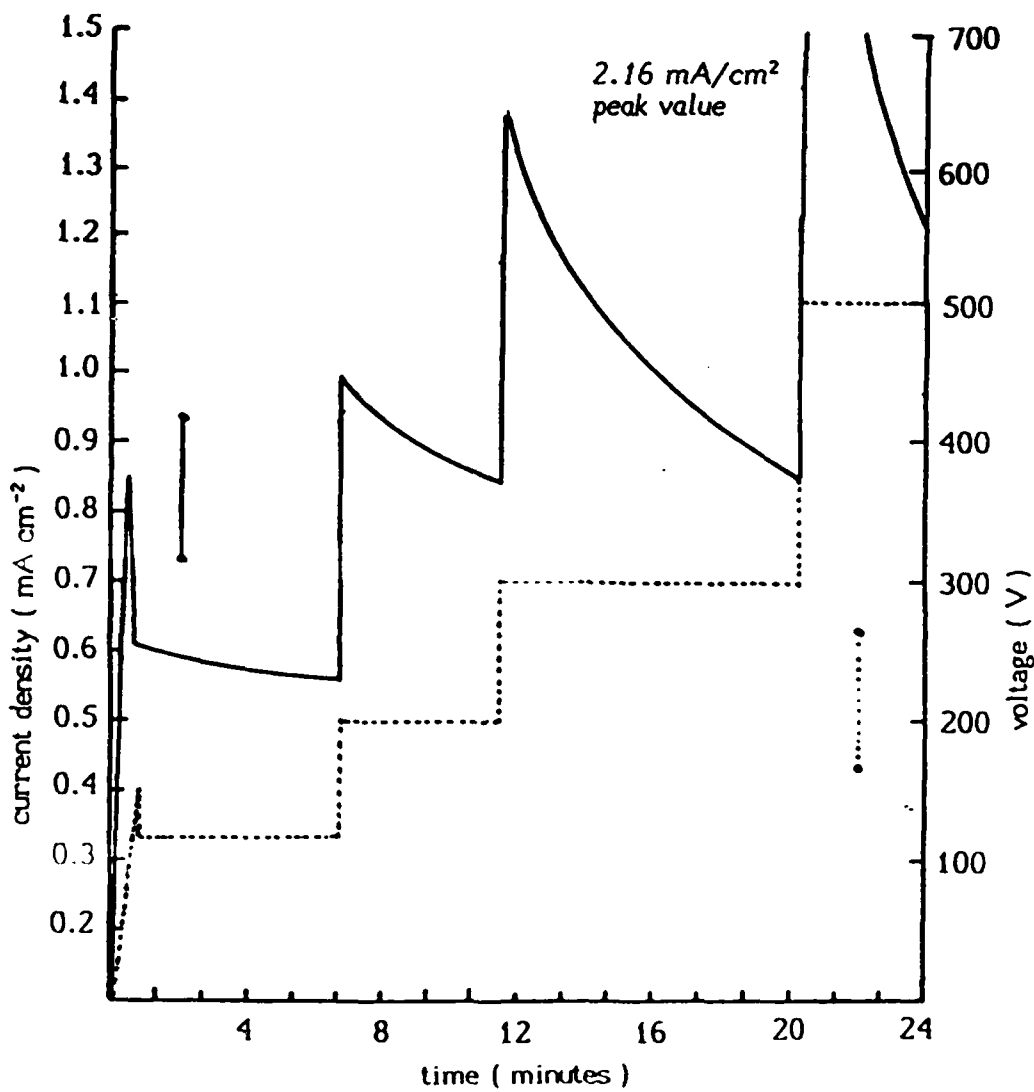
Figure 47   Current density and voltage versus
time characteristic of level three hard anodi-
zation.   Current characteristic is semi-quanti-
tative for values between maximums and
minimums.
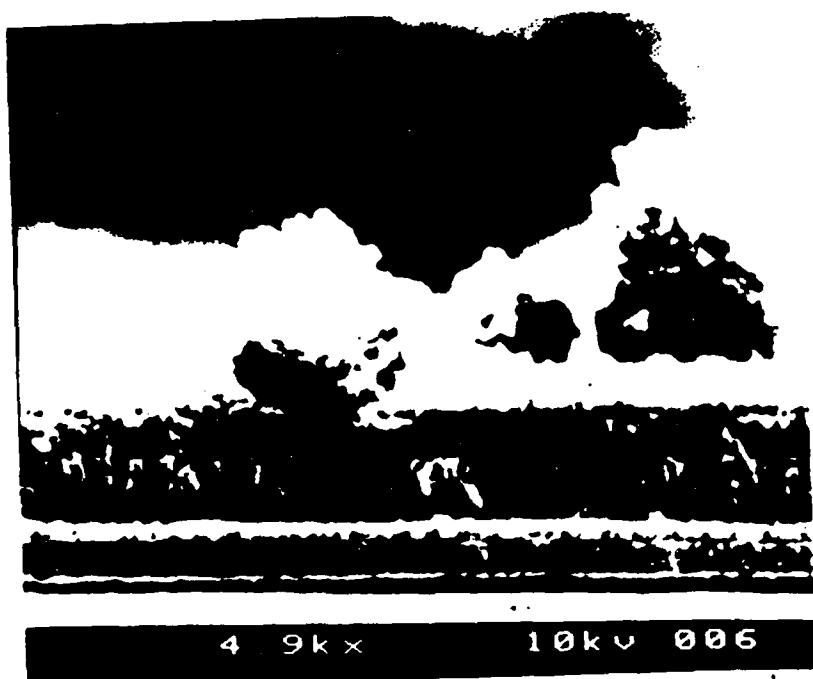
Figure 48   SEM cross sectional photo of
three dielectric level capacitor. The aluminum
layers appear very granular possibly due to the
submerging of the sample in liquid nitrogen
before cleaving.   Notice the puffy balls of
aluminum on the surface as a result of break-
down.

Figure 49 SEM cross sectional photo of successful three level MLC.

Breakdown tests were performed on the individual layers starting with layer two since it had the lowest forming voltage then layer three and finally, layer one. Layer one was found to be shorted before a breakdown test could be performed on it; this was possibly the result of breakdown in layer two. Table Five shows the results of these tests.

Table Five

test	dielectric layer	maximum forming voltage	breakdown voltage
1	2	*	90-100**
2	3	514	620
3	3	514	520
4	3	514	560
5	3	514	600
6	1	200	***

* See Figure 45. The maximum forming voltage is probably closer to 50V but is not easily defined for this anodization.
** Voltage readings became erratic above 90V
*** V_b not determinable. See discussion.

Table Five Breakdown tests performed on the S/H, three dielectric level capacitor. Test were performed on each level individually. The dV/dt = 2V/sec.

At the point of breakdown, arcing was widely distributed (see Figures 50a - f) as if some substance trapped in the porous structure of the upper part of the film had vaporized. If, indeed, a dielectric by-product of the bath was trapped in the film, this could help explain the high dielectric constant. C_d and the DF of the structure varied with frequency in virtually the exact same manner as the individual layers did.

The Anode Rotation method was successful in forming a multilevel capacitor. However, the fabrication of MLCs with even more layers using this method will have to overcome at least two pitfalls. They are:

1. If anodization at lower levels is continuing via leakage current, there may be problems with swelling, loss of capacitance, polycrystalline formation, and even breakdown.

2. Each successive level appears to become increasingly roughened on the surface. This causes localized field magnifications. A polishing etch is highly recommended. An etchant such as $H_3PO_4(5\%) + CrO_3(2\%) + H_2O$ used at $85^{\circ}C$ is reported to remove surface protrusions and has a very controllable etch rate at this temperature of 2.7 Å/sec. Using this etchant between aluminum depositions would make the topology more uniformly smooth and promote a more even oxide formation.
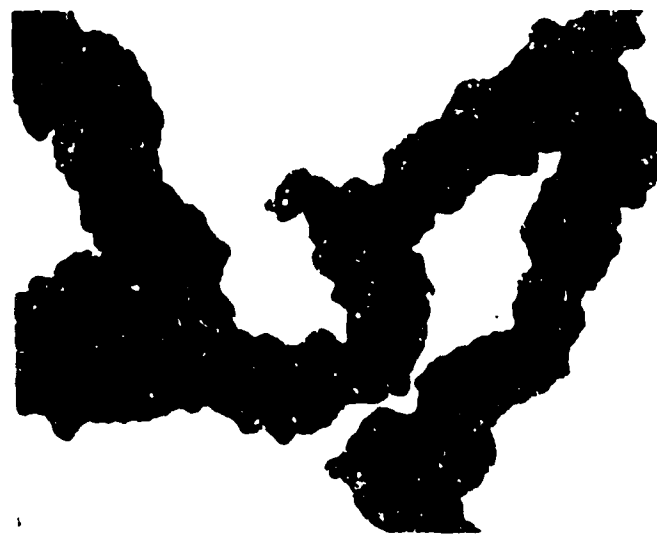
Figure 50a   Dispersed dielectric breakdown observed in the third level of the MLC (200x magnification).
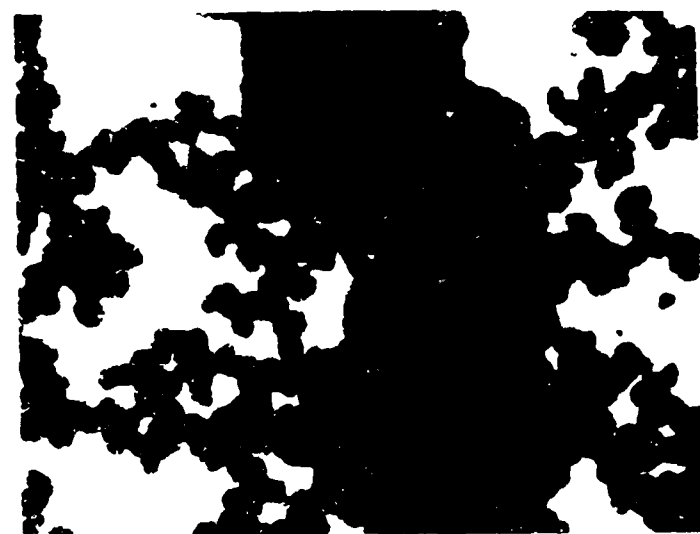
Figure 50b Note large darker regions of breakdown where cratering has proceded to the lower aluminum electrode. Vaporization and even ionization of the aluminum gas takes place in these regions. See Appendix A for a description of the pinch effect which is probably the main contributor to the breakdown phenomenon (200x magnification).

0.20kx   10kv 010
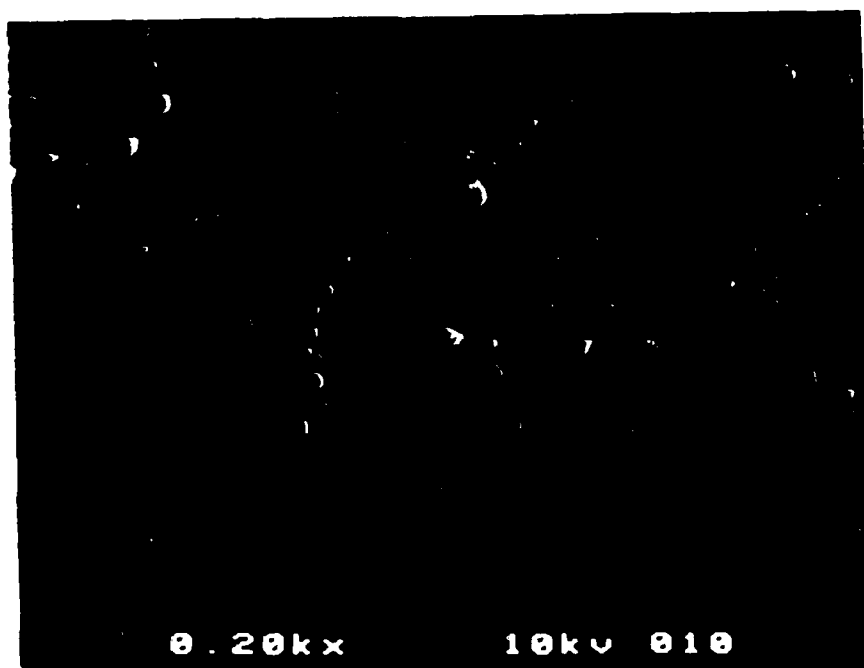
Figure 50c   SEM photo of the distributed
breakdown on the top of the third level.
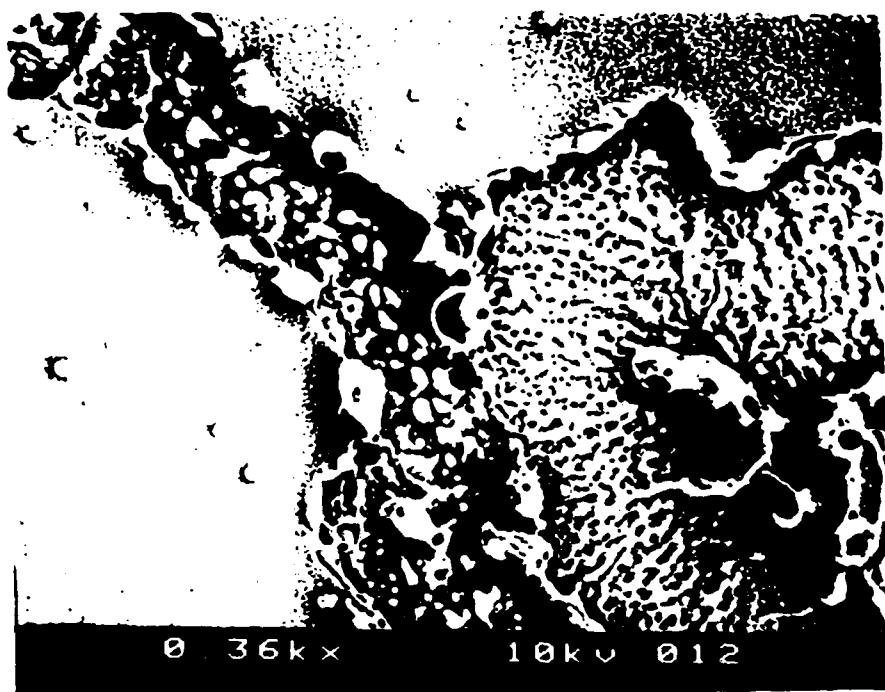
Figure 50d SEM photo -- same as Figure 50c
but with greater magnification.

Figure 50e   SEM photo -- same as Figure 50c
but with greater magnification.   This photo
seems to indicate that the porous surface of
the third level may have contained some
anodization by-product.
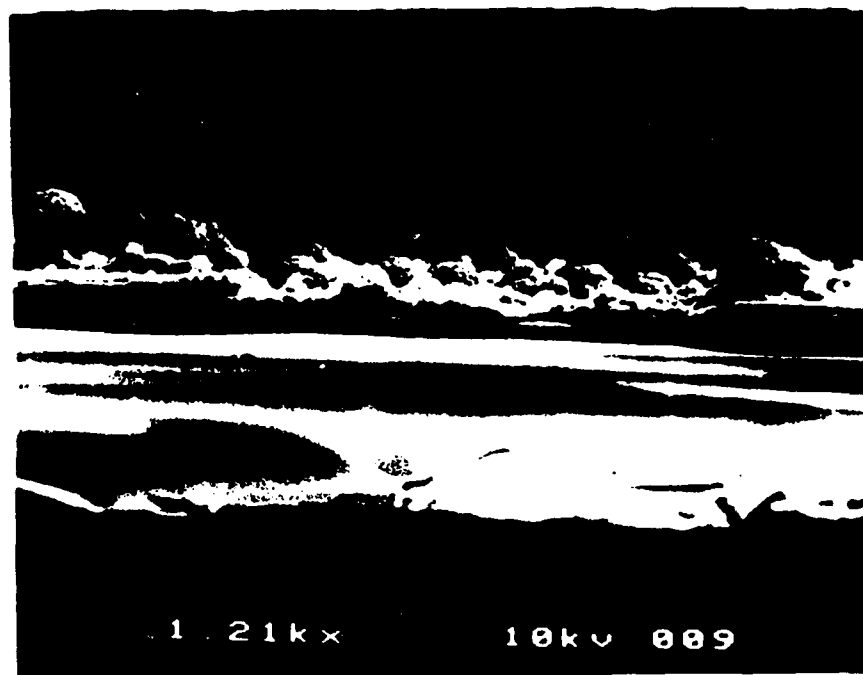
Figure 50f SEM photo -- this cross sectional view shows the site of the breakdown of level two which may have caused the failure in level one. Note the aluminum and the breakdown by-products on the surface.

Mask Approach

Another approach to creating the comb structure involves the use of conventional microelectronic, photolithographic processes. A cross sectional view of the desired device is shown in Figure 51.
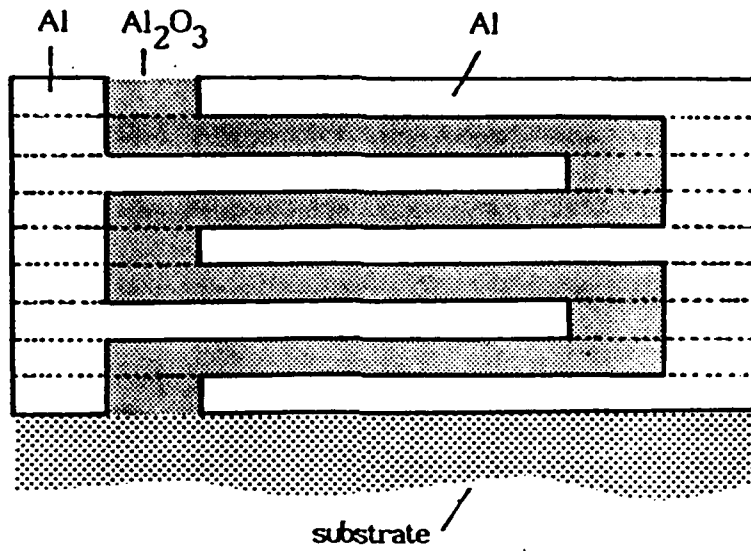
Figure 51 Cross sectional view of comb-like
structure which provides the two necessary
electrodes and an increased surface area
capacitor.

Two masks were developed to produce the above structure.
They are shown in Figures 52 and 53. Mask B is rotated 180^0
each time it is used. The process proceeds as follows:

1. As with the Anode Rotation approach, this process begins
with an aluminized silicon wafer which, previous to aluminizing
has undergone a thermal oxidation (i.e. about 8000Å of SiO_2
lies between the Si substrate and the deposited aluminum).

2. Mask A is applied to the wafer using positive photoresist
in the conventional manner.

3. The wafer is soft anodized such that the entire thickness of the aluminum film is converted to porous Al_2O_3 except where the photoresist pads are located.

4. Now that a dielectric isolation of the pads exists, a hard anodization is performed up to a forming voltage necessary to densify all of the soft alumina. Under normal conditions, without the previous isolation, the photoresist lifts off from the aluminum at low voltages.

5. The photoresist pads are then removed with acetone; the wafer is rinsed and baked as has previously been described, and is ready for another film of aluminum.

6. One micron of aluminum is deposited on the wafer.

7. Mask B is applied and is aligned using the surface protrusions caused by the lower level's alignment marks. A similar anodization procedure is used as in steps 3 - 5.

8. Repeat step 6.

9. Repeat steps 2 - 5.

10. Repeat step 6.

11. Rotate mask B 180^0 and repeat steps 3 - 5.

12. Repeat steps 2 - 11 as desired.
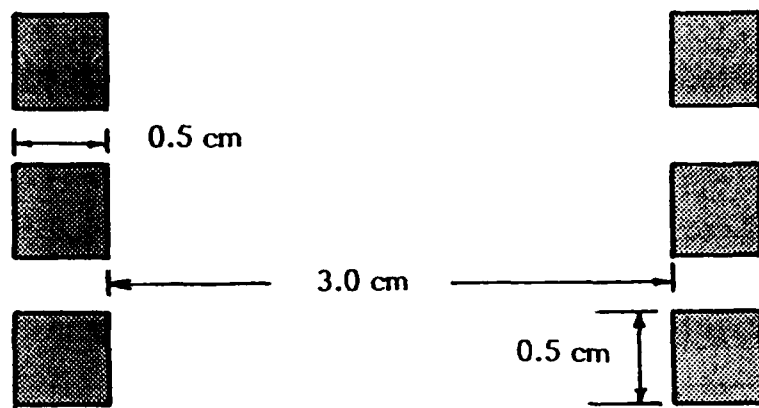
Figure 52 Mask A for mask approach creation of a MLC.
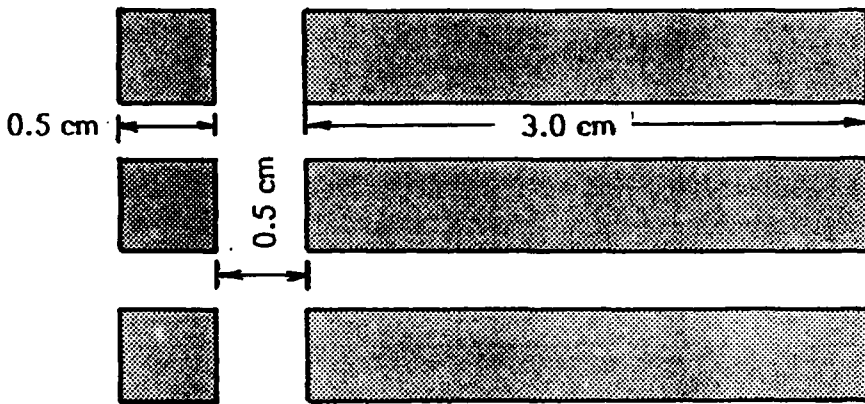
Figure 53 Mask B for mask approach creation of a MLC.

Figures 54 and 55 illustrate the problem encountered at the offset. The photoresist cap caused a field intensification at its edge. This resulted in a much more rapid localized growth of the oxide. The growth was rapid enough in this case to cut off a necessary part of the electrode.

Figure 54 This top view shows the rapid oxide growth at the edge of the photo resist mask which caused a punch-through effect.
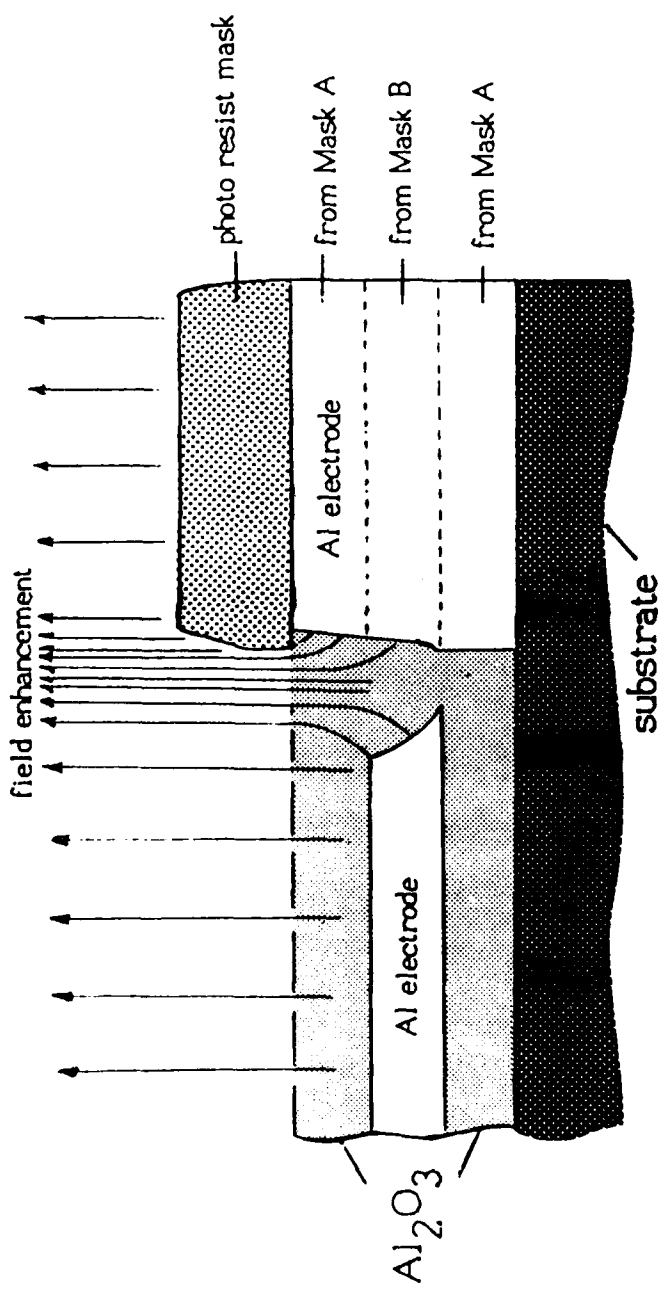
Figure 55 The field is enhanced significantly at the edge of the photo resist mask. As a result, the oxide grows much more quickly in this region and cuts through the electrode as is shown in this cross section.

A proposed solution to this problem is shown in Figure 56. By staggering the thickness of the anodized film and reducing the current density (and growth rate), a slightly altered form of the comb structure should be realizable.
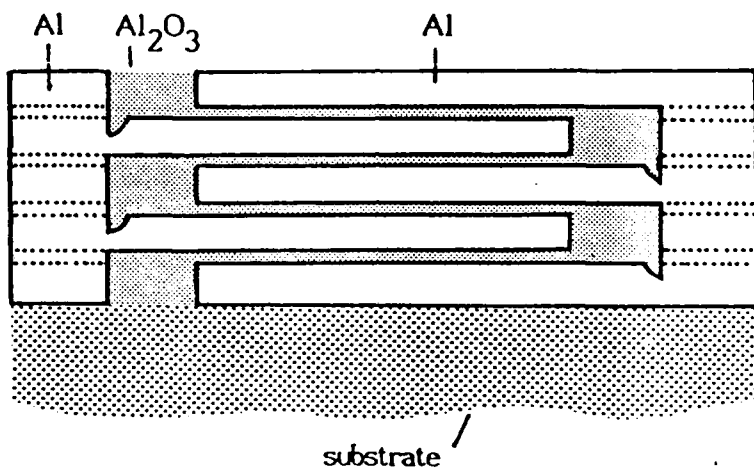
Figure 56 Cross sectional view of proposed method to create comb structure via photo resist masking. Note that the thickness of the successive layers is staggered.

Hard/Soft/Hard Approach

In order to grow a thick, porous oxide within a reasonable amount of time, a higher current density must be used. However, because of the pinch effect (see Appendix B) caused by localized field enhancements, the soft oxide growth can be

unevenly distributed across the surface being anodized. To provide a barrier other than the SiO_2 (or what would be a sublevel Al_2O_3 dielectric if upper levels were being anodized) a thin layer (e.g. 1000Å) of hard alumina is formed on the surface of the aluminum.

Next, another layer of aluminum is deposited and the wafer is soft anodized with a current density of 2.5 mA/cm^2. The soft oxide growth stops at the previously formed hard oxide layer. If the hard oxide has weak spots, the porous oxide will 'punch through' and can form a soft oxide column through the aluminum beneath in an extremely short time.

Thirdly, the wafer goes through a hard anodization with the desired forming voltage. Another film of aluminum is deposited and the whole process is repeated for each layer; the Anode Rotation technique is utilized to create the electrodes.

This HSH approach was used to create two wafer scale capacitor structures each with two levels of dielectric film. Problems with aluminum deposition prevented the depositon of the top electrode and subsequent testing. Preliminary capacitance tests made on the first level of dielectric revealed a

capacitance density of $9.2 nF/cm^2$. These tests indicate that the HSH process is capable of producing MLC devices. The advantage of producing thicker, hard, amorphous films repeatedly may make this or a similar process more viable.

IV. CONCLUSION

The soft/hard anodization of aluminum is capable of produ-
cing alumina with a wider range of thickness while maintain-
ing the dielectric appearance of amorphous hard oxide. The
anodization procedure itself was altered to eliminate the
constant current density during the hard anodization. This led
to the reduction and elimination of the formation of the dielec-
trically weaker polycrystalline Al_2O_3. These oxide films are
able to withstand very high fields, show an increased relative
permittivity and have desirable high frequency performance.
Densification of the previously formed soft oxide during the hard
anodization can be controlled to produce films that range from
almost purely soft oxide to almost purely hard oxide.

The fabrication of a multilayered capacitor using the
soft/hard anodization was successful in creating a three -
dielectric level capacitor structure and demonstrated the wide
range of flexibility possible in the process itself. With some

adjustments, such as using a thicker thermal SiO_2 on the substrate to prevent leakage anodization and utilizing the $CrO_3 +$ H_3PO_4 etch to smooth the surface of the oxide, the creation of MLCs with many layers appears to be possible.

The possibilities for use of the soft/hard oxide as described in this report are extensive. The microelectronics industry might be able to produce devices requiring capacitors with less real estate or passivation layers with less leakage current. The capacitor fabrication industry might produce aluminum, rolled-foil capacitors with enhanced properties and there are, perhaps, some power conditioning applications even in spacecraft.

APPENDICES

APPENDIX A

Although a capacitor is basically an energy storage device, it is used in many other applications such as coupling and decoupling of electronic circuits, impedance level control, filtering, and switching control. In this appendix, the basic parameters describing the behavior of a thin film aluminum oxide capacitor are examined.

Resistance

Electrical insulating materials should not carry current at all when under the action of a direct current voltage. However, all electrical insulating materials do carry a certain very weak current. Thus, the resistivity of these materials has a finite, though extremely high value. The higher the resistivity of the dielectric, the better its quality. When the dielectric is used in a capacitor structure, it can be modeled as having a series and a parallel resistance as the Figure A1 illustrates.
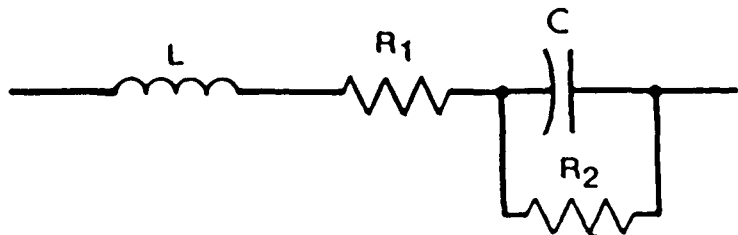
Figure A1 Equivalent circuit for a capacitor showing series and parallel resistances. [33]

When a high frequency AC signal is applied to the above circuit, the parallel resistance tends to influence the signal less. Under DC conditions, the overall resistance is the series combination of the parallel and series resistances. Considering the bulk of the dielectric, its resistance can also be classified as either surface resistance or volume resistance. The primary concern in a capacitive device is the volume resistance. For a body with a constant cross section α and a length τ, the volume resistance can be found from the formula:

$$R_v = \rho \times (\tau/\alpha)$$

The value of ρ, the volume resistivity, however, has been found to vary greatly according to how the dielectric material is dried.[9] See Figure A2 below.
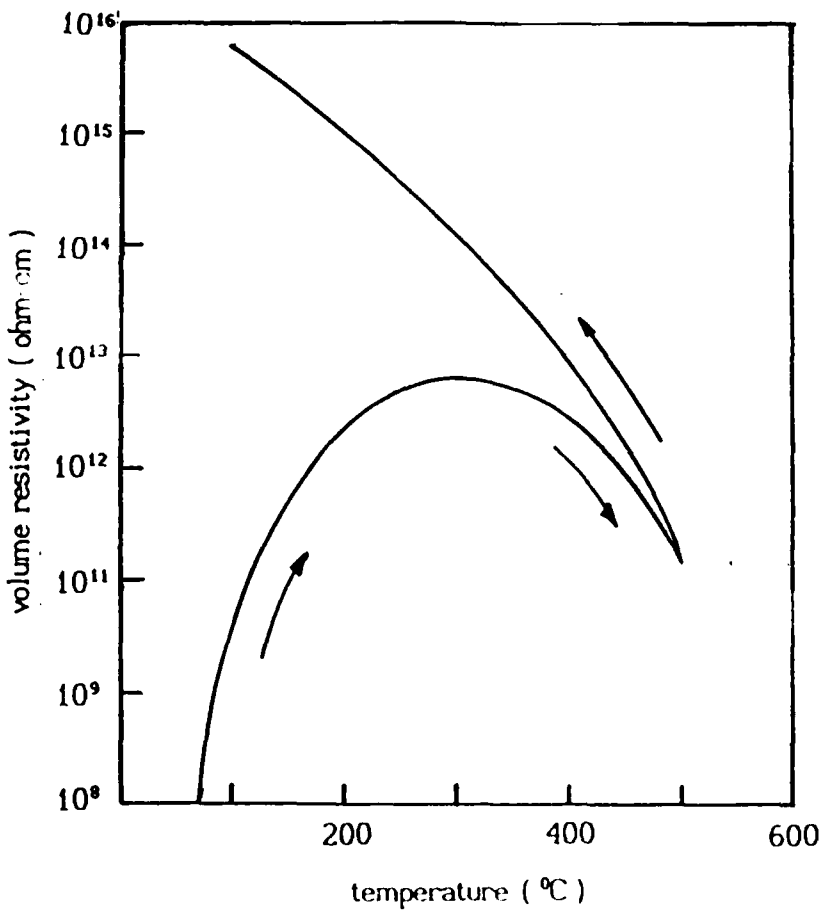
Figure A2 The drying or baking of the dielectric material has a profound effect on its resistivity. This figure is for a sample polar dielectric oxide. [9]

ρ has also been found to be voltage dependent, decreasing as the applied voltage is increased. When measuring the DC resis-

tance of a given dielectric, it is necessary to maintain definite temperatures, humidity and applied voltage. The AC resistance can be determined by applying a square wave input to the capacitor and observing its time constant.

Polarization

The most important property of a dielectric is its ability to be polarized. The action of an external electric field brings the charges of the molecules of the dielectric into a certain ordered arrangement in space as shown in Figure A3 below.
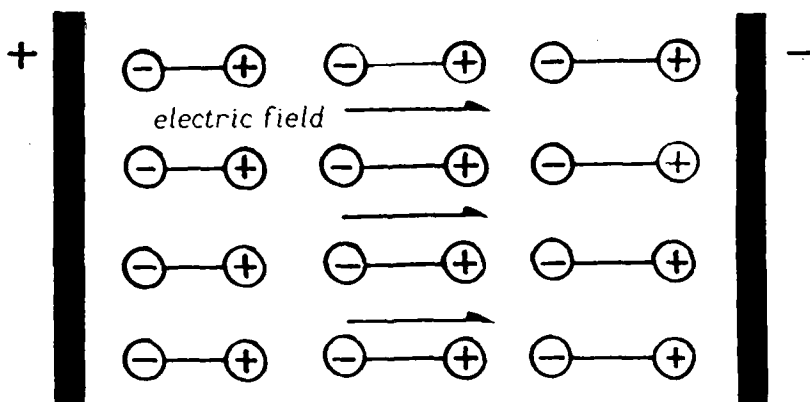
Figure A3   Arrangement of charges in a polarized dielectric shown schematically.

The polarization is equal to the limit of the ratio of the electric moment of a certain volume of a dielectric to this

volume when the latter approaches zero. It can also be shown that the polarization is equal to the surface density of the bound charges in the dielectric.

Permittivity

The parameter of a dielectric that determines its ability to form a capacitance (energy storage) is the permittivity, ϵ. When the capacitance is measured, the permittivity can be determined from the equation:

$$C = \epsilon_o \times \epsilon_r \times A \times (N-1)/\tau$$

where ϵ_o is the permittivity of free space, ϵ_r is the relative permittivity of the dielectric, A is the cross sectional area orthogonal to the electric field, N is the number of plates, and τ is the thickness of the dielectric between the conducting plates. Polar dielectrics have permittivities that are dependent upon frequency, temperature, and humidity. Figure A4 below shows an example of this variation with frequency.
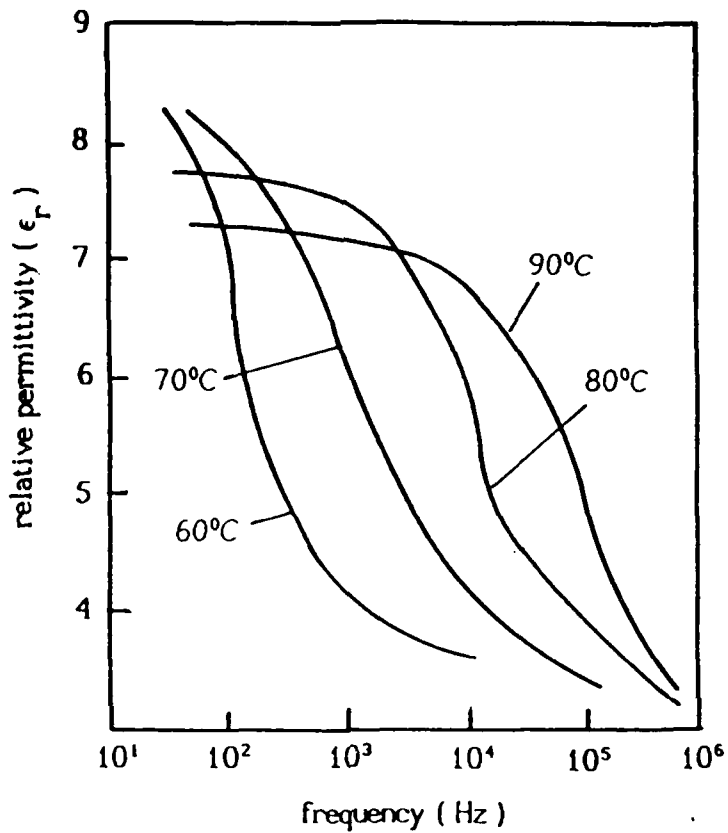
Figure A4 Typical variation of the dielectric constant with frequency and temperature for a polar dielectric. [9]

Loss Tangent

When an electric field acts on any matter, it dissipates some of its energy into heat energy. This is commonly termed as the expense or loss of power. In an ideal capacitor, the current should lead the voltage by $90°$. In reality, this is not so. The phase difference is less than $90°$ by some angle δ. The

angle δ is called the dielectric loss angle. The tangent of this angle is equal to the ratio between the active and reactive currents or the ratio of the active power to the reactive power. All other conditions being equal, the dielectric losses generally increase with this angle. The values of tan δ (very closely associated with and often substituted for the power factor) for good dielectrics are on the order of thousandths and even tenths of thousandths. This loss factor has been shown to be dependent upon frequency and temperature as well as post-baking. Figure A5 illustrates the temperature dependence for two dielectrics containing Al_2O_3.

Absorption

Dielectric absorption produces a residual charge in a capacitor which is first charged and then shorted. Absorption can be quantitatively estimated by the absorption coefficient equal to the ratio of the residual voltage measured in definite conditions, to the initial voltage. Table A1 below gives some examples.
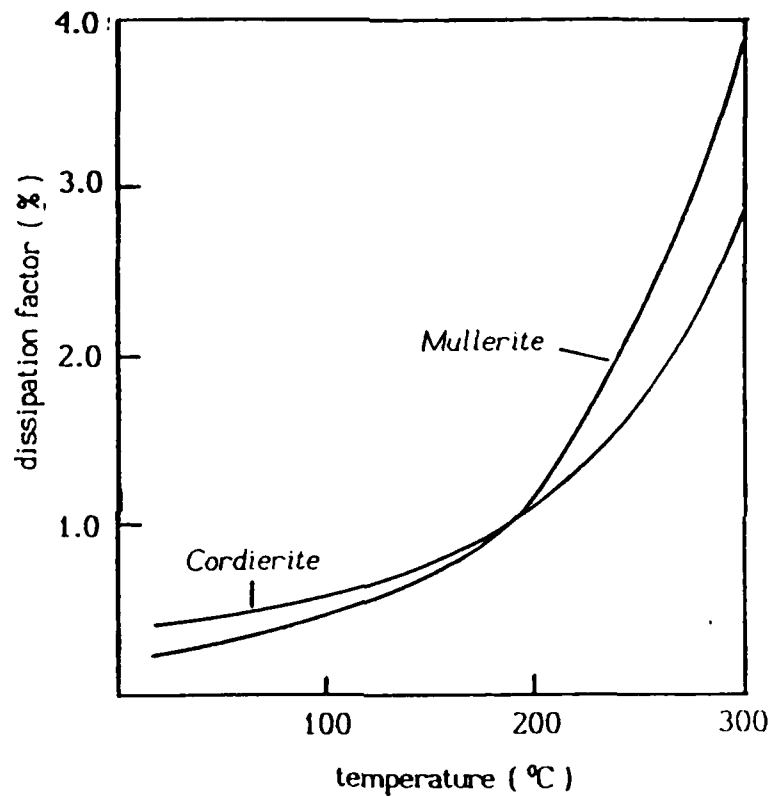
Figure A5 The value of the dissipation factor of Mullerite and Cordierite measured at 1 MHz. [9]

Table A1

types of capacitors	κ_{abs} (%) $t_1 = 15$ min $t_3 = 3$ min $t_2 = 5$ s	κ_{abs} (%) $t_1 = 24$ hr $t_3 = 5 - 10$ hr $t_2 = 5$ s
Film:		
(a) with nonpolar (polystyrene) film	0.02 - 0.10	0.10 - 0.20
(b) with polar (polyethyleneterephthalate) film	0.2 - 0.8	1.7 - 2.5
Mica	2 - 5	18 - 20
Paper	0.6 - 2	30 - 32
Metallized-paper	2 - 5	39 - 41
Oxide:		
(a) aluminum oxide	5 - 6	15
(b) tantalum oxide	2 - 5	9 - 10
Ceramic:		
(a) from ceramics with $\epsilon_r = 150$	5	20 - 22
(b) from ceramics with $\epsilon_r = 900$	15	46 - 47

Table A1 The values of the absorption coefficient κ_{abs} for various types of capacitors. 9

Breakdown

The two main kinds of dielectric breakdown are electric and electrothermal. An electric breakdown developes as a result of interaction of free charged particles accelerated by an electric field with the particles of the dielectric. It is distinguished by a short time of developement. Electrothermal breakdown incorporates the heat of the dielectric losses. Figures A6 and A7 show the results of both kinds of breakdown in thin film aluminum oxide.
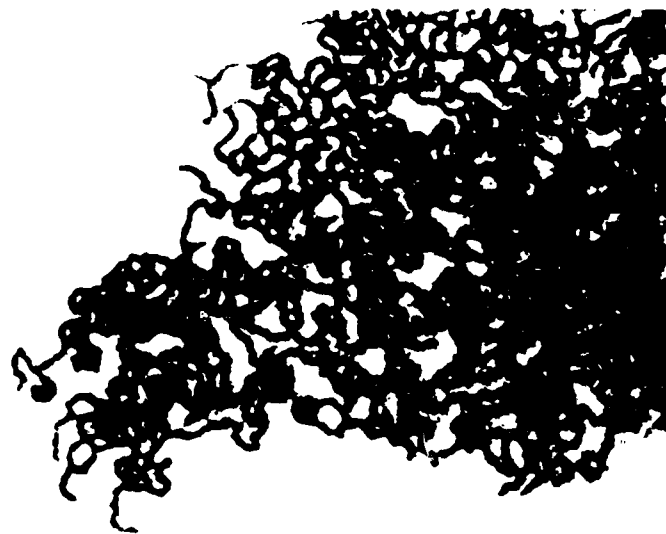
Figure A6 Electric breakdown in this thin film of aluminum oxide was characterized by its quick developement.
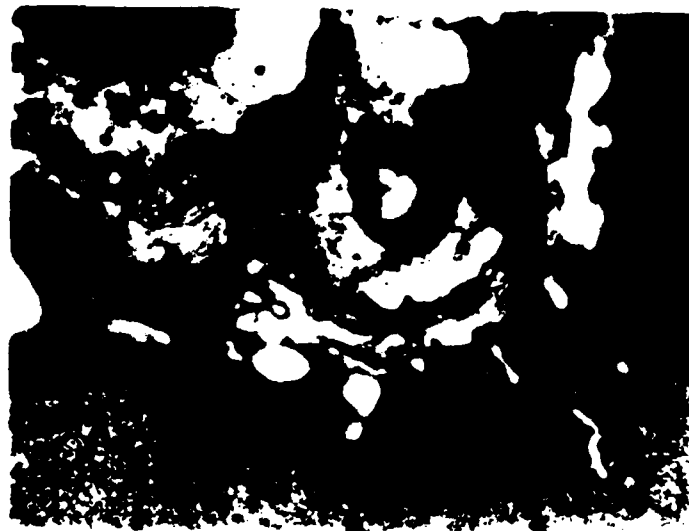
Figure A7   Electrothermal breakdown in an
anodized thin film dielectric incorporates the
heat of the dielectric losses.

DeWit et al.[15] demonstated that the breakdown field is inde-

pendent of the oxide thickness which implies that breakdown,

although somewhat dependent on the contact material is really a

surface phenomenon and not a volume phenomenon.   Breakdown

is completely determined by the introduction of an ion from the

surface into the volume of the oxide.   Once this has occurred,

ionic conduction at that spot starts up which may lead to a

breakdown either by heating, as described by Ridley,[30] or by the

buildup of space charge followed by electron injection, as

suggested by Shousha.[31]   If breakdown occurs in another location, the remaining charge carriers are swept away.

O'Dwyer,[32] however, showed that a dependence of the breakdown field upon the inverse of the square root of the film thickness can be obtained; Klein and Gafni deduced that such a field goes as the reciprocal of the logarithm of the film thickness.[15] It is evident that the basic mechanism of dielectric breakdown is not fully understood.

Thermal Conductivity

In multilevel thin film capacitor design (utilized in pulsed-power applications) perhaps the most important parameter to consider is the thermal conductivity of the materials. Table A2 gives some sample values while Figures A9 and A9 show the dependency of this parameter upon temperature for several oxides and for several alumina ceramics respectively.

Table A2

material	λ, W/K-m
Air (in small clearances)	0.025
Varnished cloth	0.13
Paper-based laminate	0.35
Fused quartz SiO_2	1.25
Porcelain	1.6
Titanium dioxide TiO_2	6.5
Crystalline quartz	12.5
Aluminum oxide Al_2O_3	30
Germanium	55
Silicon	80
Beryllium oxide BeO	218
Aluminum	226
Copper	390

Table A2 The thermal conductivity of several types of materials including Al_2O_3. [9]
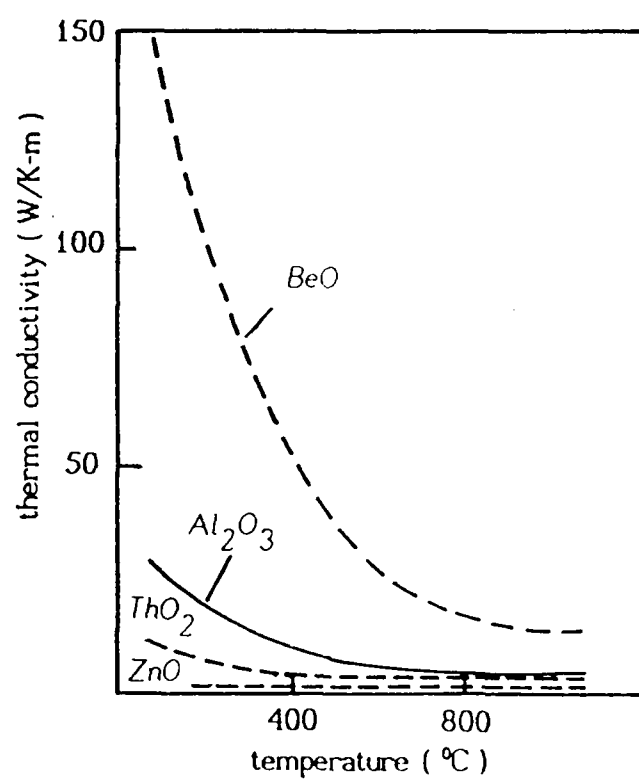
Figure A8   Thermal conductivity versus temperature for several oxides. [9]
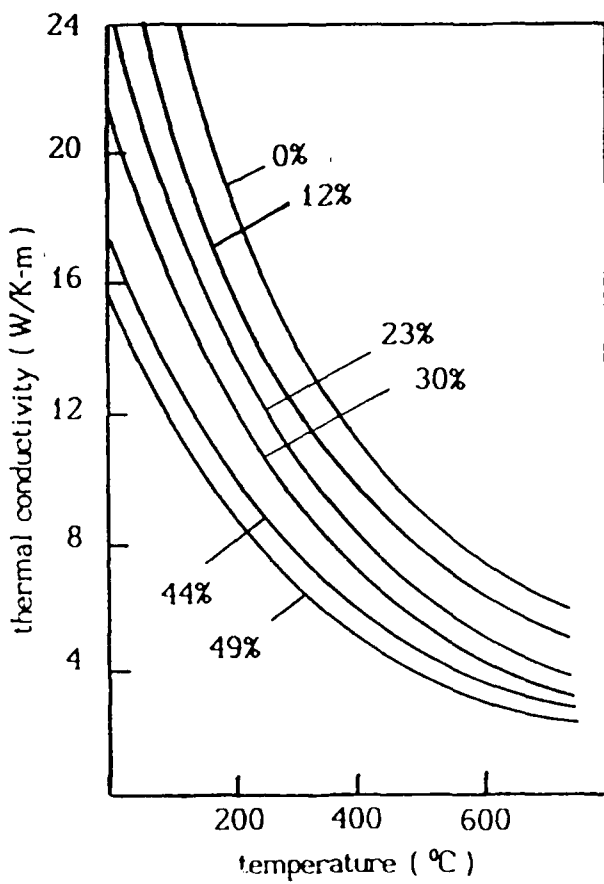
Figure A9 Thermal conductivity versus temperature for alumina ceramics with various porosities indicated in per cent. [9]

Appendix B

Proposal on the Growth Dynamics of Wet Anodized Alumina

If we were to assume the ideal case of an uniform electric field between the anode and cathode, the field lines would all be parallel and would appear as in Figure B1 below.

positive aluminum anode
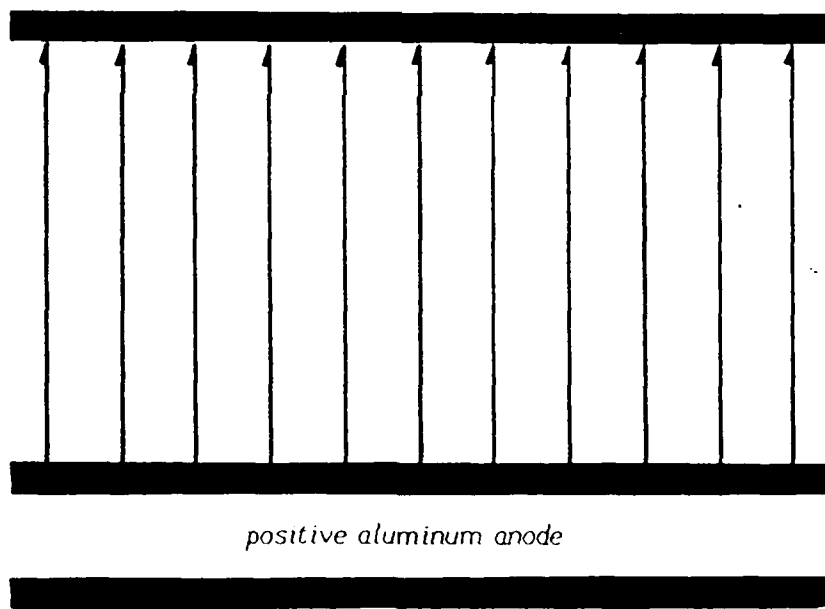
Figure B1   Electric field lines indicating an uniform field strength given a smooth surface on the anode and the cathode.

Under more real circumstances, the surface of both the anode and cathode are not perfectly smooth. Thus the field lines between them are not of a uniform density nor parallel near their surfaces. If we examine the surface of the aluminum anode closely, the 'terrain' has many hillocks and 'valleys' These points of topological deformation present regions where the electric field intensity will be greater than in areas where the surface is smooth. Figure B2 shows this.

intensity and direction of ionic current

aluminum anode
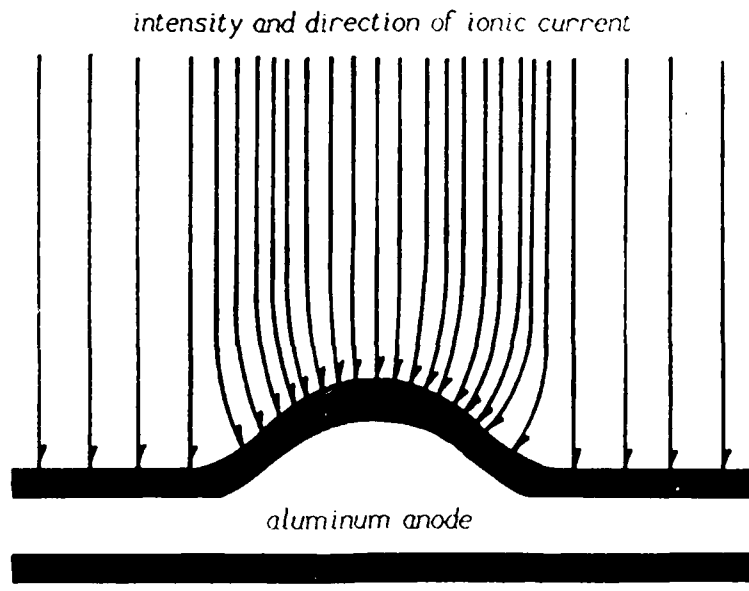
Figure B2   Localized intensification of the electric field causes an increase in ionic transport.

Under these conditions, the aluminum oxide will first begin to form and grow at these points of more intense field concentration. As the first incremental layers are formed, the majority of the formation voltage is across this dielectric. This puts the thin but growing oxide in a state of imminent electric (as opposed to electrothermal) breakdown which would occur if the voltage gradient did not decrease as the oxide thickness increased. Nevertheless, the electrodynamics which are characteristic of the pre-electric breakdown state take place within the newly formed alumina. Research by V. Kuchin permitted the establishing of the following pattern during pre-electric breakdown.[9]

The prebreakdown current passing through a dielectric forms a magnetic field whose electrodynamic effect is to compress the current (pinch effect) into a thin pinch, producing therewith a radial electric field with an intensity of hundreds of kV/m which causes the ions to move in a radial direction. At the maximum compression of the pinch, the current density along its axis exceeds by several orders of magnitude the mean current density. Since the energy of the ions in the growing

dielectric under these conditions is much greater than that of the electrolyte ions, oxide growth under the initial point of oxidation takes place faster than under the surrounding surface area. Figure B3 below illustrates this process. Note that although the electric field lines in the electrolyte find new points of maximum intensity as the anodization progresses, the thickness of the alumina formed under them does not catch up with that growing under the point of initial oxidation.

electrolyte

Al_2O_3

magnetic field

Al
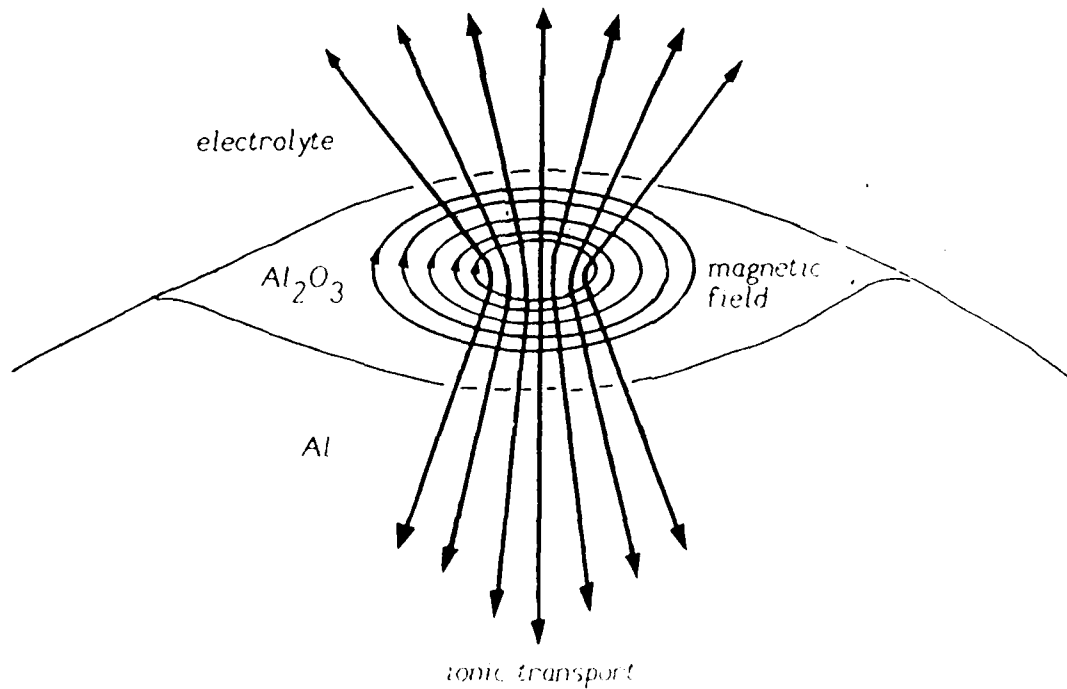
ionic transport

Figure B3 Pinch effect of the magnetic field causes an intensification of the ionic transport and a radial/vertical growth pattern.

There is a swelling from oxide growth at the oxide/electrolyte interface but primarily, the oxide growth is in a radial fashion proceding away from the electrolyte. This growth pattern, when anodizing a thin film of aluminum which has been deposited on a dielectric substrate, will isolate small portions (or 'freckles') of the aluminum as the anodization terminates. See Figure B4.

arrows indicate direction of growth

Al freckle Al_2O_3 Al freckle
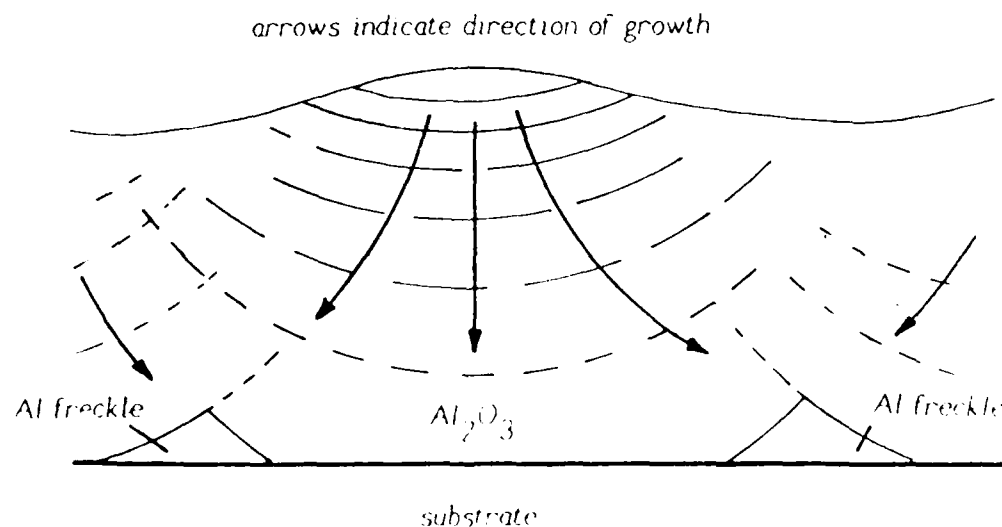
substrate

Figure B4   Growth pattern of oxide isolates islands of aluminum at the surface of the substrate. These are referred to as freckles.

These freckles may be eliminated if the impedance of the substrate is weak enough to allow a 'finishing' leakage current through its bulk.

Appendix C

The following Appendix is presented in tabular form. The data contained herein are pertinent to the fabrication of any anodized, thin film capacitor for use in pulsed power applications.

density	3.97 g/cm^3
molecular mass	101.9602
oxygen content by mass	47.07
melting point	2319.7±8 °K
boiling point	3253 °K
heat of fusion	108.86 μJ/kg-mole
heat of evaporation	485.669 μJ/kg-mole
heat of formation	1675.557 μJ/kg-mole (-)
heat of combustion	
$\alpha - Al_2O_3$	1670.952 μJ/kg-mole
$\gamma - Al_2O_3$	1611.248 μJ/kg-mole
heat of decompositon	
$\alpha - Al_2O_3$	1117.038 mJ/mole of O_2
$\gamma - Al_2O_3$	1059.679 mJ/mole of O_2^2
standard entropy	51.02 mJ/kg-mole deg
hardness	9 conventional units
magnetic susceptibility $\times$ 10^9	- 0.098 m^3/kg
work function ϕ	7.75 $\times$ 10^{19}
width of forbidden band	4.0 - 5.75 ($\times 10^{19}$ J)
refractive index	
barrier anodized	1.62 1.67

temperature ^0K	specific resistivity of single crystal alumina ohm - cm
287	1×10^{16}
473	3×10^{14}
673	3×10^{12}
873	4×10^{10}
1073	3.5×10^8
1273	5×10^6
1373	1×10^6
1873	8.1×10^4
1998	4.25×10^4
2083	2.9×10^4
2148	2.2×10^4

temperature ^0K	thermal conductivity λ, W/m -deg
373	30.27
873	9.127
1273	6.154
1473	5.526
1673	5.485
1873	6.071

temperature ^0K	linear coefficient of thermal expansion $\alpha * 10^6/deg$
373	7.1
773	9.7
1273	14.2

temperature ^0K	free energy of formation $\mu J/kg$ mole
298	1580.098
1000	1406.765
1500	1281.161
2000	1168.117

temperature ^{0}K	modulus of normal elasticity GN/m^2
473	372.67
673	362.86
873	353.05
1073	338.34
1273	315.79
1473	269.69
1673	201.04
1773	147.11

temperature ^{0}K	tensile strength σ MN/m^2
293	259.70
573	231.28
1078	235.20
1323	233.24
1403	216.58
1473	127.40
1583	44.10
1673	29.40
1733	10.78

temperature ^{0}K	compressive strength σ_{comp}, MN/m^2
293	2940
673	1470
873	1372
1073	1274
1273	882
1373	588
1473	490
1673	245
1773	98
1873	49

temperature °K	specific heat capacity C_p, J/kg - deg
10	.419
25	2.093
50	18.422
100	132.303
150	328.664
200	509.115
298.16	774.977

temperature °C	oxide	dissociation pressure N/m^2
1727	Al_2O_3	2.63×10^{-3}
2000	$\alpha - Al_2O_3$	$< 133 \times 10^{-50}$
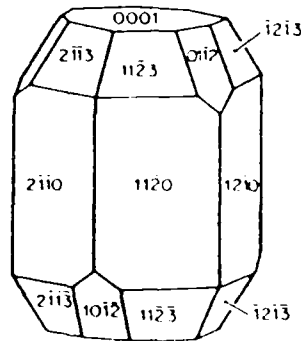
Crystal of aluminum oxide (forms present; hexagonal prism (1120); rhombohedron (0112); hexagonal bipyramid (1123) and pinacoid (0001).

CRYSTAL STRUCTURE

		lattice constants, nm			
		a	b	c	c/a
α - Al_2O_3	Hexagonal	.4758		1.2991	2.72
β - Al_2O_3	Hexagonal	.564		2.265	4.02
γ - Al_2O_3	Cubic	.790			2.07
θ - Al_2O_3	Monoclinic	.57	.290	1.18	
χ - Al_2O_3	Cubic	.795			

crystal lattice energy   15520.468 μJ/kg-mole

APPENDIX D

Shown schematically below are the set-ups for the anodization procedure, the measurement of capacitance and DF, and the measurement of resistivity.

Hewlett - Packard
3311A Function Generator

Tecktronix
5440 Oscilloscope

General Radio
Type 716 - B
Capacitance Bridge
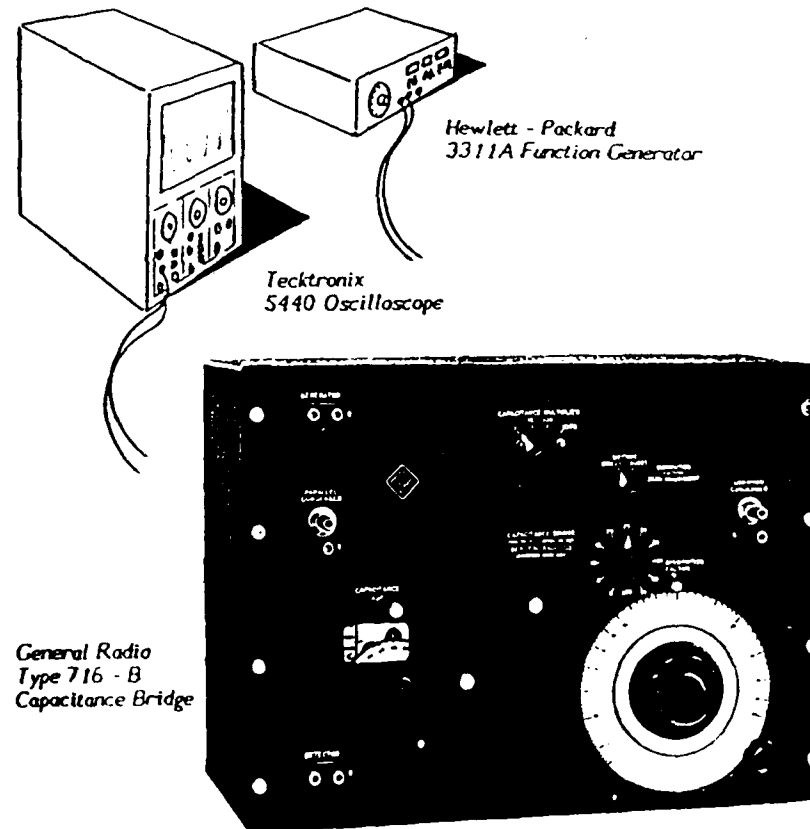
Set up for measuring the capacitance
and dissipation factor.

Fluke 8010A
Digital Multimeter

Keithley 179 TRMS
Digital Multimeter

Ephortec 3KV
Power Supply
for constant voltage, hard
anodization

Hewlett - Packard
6218B Power Supply
for constant current, soft
anodization

Set up for performing the
wet anodization.

Corning PC 101
Hot Plate/Stirrer

Hewlett - Packard
16058A Test Fixture

Rucker & Kolls Probes

Hewlett - Packard
7475A Plotter

Hewlett - Packard
4145A Semiconductor Parameter
Analyzer

Set up for measuring the resistivity
of the dielectric between two capacitor
plates.

Bibliography

1. W.J. Sarjeant, "Critical Pulse Power Components", technical paper #819092, Los Alamos National Laboratory

2. O.J. Murphy, The Electrochemical Society Meeting, Toronto Canada, May, 12 - 17, 1985, p.66

3. J.H. Thorington, Jr., "An Improved Interconnect Structure for Integrated Circuits", Master's Thesis, Auburn University, June 6, 1986

4. C.J. Dell'Oca, Thin Solid Films, Vol. 26, pp.371-380, Elsevier Sequoia S.A., Lausanne, Switzerland (1975)

5. S. Ahmad and R. Singh, "High Quality Dielectric Film For Distributed RC Filters and Amorphous Semiconductors", April 18, 1980, Thin Solid Films, 74 (1980) 165 - 171

6. W.C. Cochran, "Electroplating Engineering Handbook", 4th Edition, New York, Reinhold Pub. Corp., pp.396 - 399 (1984)

7. U.R. Evans, "The Corrosion and Oxidation of Metals: Scientific Principals and Practical Applications", New York, St. Martin Press, pp.241 - 249 (1960)

8. A.F.A.B. El-Safti and H.L. Hartnagel, Int. J. Electronics, Vol. 44, No. 6, pp.561 - 571 (1978)

9. B. Tareev, "Physics of Dielectric Materials", (1975)

10. C.J. Dell'Oca and A.J. Learn, Thin Solid Films, Vol. 8, R47 - R50, Elsevier Sequoia S.A., Lausanne, Switzerland (1971)-

11. R.A. Wodehouse, "Electroplating Engineering Handbook", 3rd Edition, New York, Reinhold Pub. Corp., pp.456 - 464

12. T.S. Wu, T. Shiramatsu, and S.H. Jwo, IEEE Proceedings of the 31st Electronics Components Conference, pp.145 - 148 (1981)

13. M.G. Mier and E.A. Buvinger, "A Comparative Study of Anodized, Evaporated, and Sputtered Aluminum Oxide Thin Films", J. of Vacuum Science and Technology, Vol. 6, No. 4, pp.727 - 730 (1969)

14. G.A. Huchins and C.T. Chen, J. Electrochem. Soc., Vol. 133, No. 7, pp.1332 - 1337, (1986)

15. H.J. deWit, Ch. Wijenberg, and C. Crevecoeur, J. Electrochem. Soc., Vol. 123, No. 10, pp.1479 - 1486, (1976)

16. K.S. Chari and B. Mathur, Thin Solid Films, 81 (1981) 271 - 278

17. D.J. Sharp, J.K.G. Panitz, R.M. Merrill, and D.M. Haaland, Thin Solid Films, 111 (1984) 227 - 234

18. R.K. Nigan, R.C. Saini, R. Kapoor, Indian J. Chem., Sect. A, 17A(4), 340 - 3 (1979)

19. K. Kobayashi, K. Shimizu, and H.Nishibe, J. Electrochem. Soc., Vol. 133, No. 7, pp.140 - 141 (1985)

20. W.J. Bernard and P.G. Russell, J. Electrochem. Soc., 127(6), 1256 - 61 (1980)

21. R.S. Alwitt and H. Takei, "Passivity of Metals and Semi conductors", M. Froment, Editor, pp741 - 746, Elsevier, Amsterdam, (1983)

22. R.S. Alwitt, Paper 46, The Electrochemical Society Meeting, Toronto, Canada, May 12 - 17, 1985

23. T.A. Libsch and O.F. Devereux, J. Electrochem. Soc., Vol. 122, No. 12, pp.1654 - 1660

24. R.C. Merrill and R.A. West, Abstract 1, The Electrochem. Soc. Extended Abstracts, Spring Meeting, Pittsburgh, PA, April 15 - 18, 1963

25. S.M. Gubanski and A. Krowinski, IEE Conf. Publ., 177 (Int. Conf. Dielectr. Mater., Meas. Appl., 3rd), 298 - 301 (1979)

26. L.L. Odynets, F.S. Platonov, and E.M. Prokopchuk, Radio- tekh. Elektron., 16, 1739 (1971); Radio Eng. Elektron. Phys. (Engl. Transl.), 16, 1576 (1971)

27. H. Birey, J. Appl. Phys., Vol. 48, No. 12, pp.5209 - 5211 (1977)

28. A. Akseli, Thin Solid Films, 80 (1981) 395 - 401

29. T.V. Boeva, S.N. Koikov, A.Yu. Polonskii, M.N. Rozova, Vses. Konf. "Fiz. Dielektr. Perspekt. Ee Razvit.", Meeting Date 1973, Vol. 2, 58 - 9

30. B.K. Ridley, J. Appl. Phys., 46, 998 (1975)

31. A.N.M. Shousha, J. Non-Cryst. Solids, 17, 108 (1975)

32. J.J. O'Dwyer, "The Theory of Electrical Conduction and Breakdown in Solid Dielectrics", Clarendon Press, Oxford (1973)

33. G.V. Samsonov, "The Oxide Handbook", IFI/Plenum (1973)

34. H.W. Ott, "Noise Reduction Techniques in Electronic Systems", Wiley, (1976)

END

DATE
FILMED

FEB.
1988